NOTICE

The quality of this microform is heavily dependent upon the quality of the original thesis submitted for microfilming. Every effort has been made to ensure the highest quality of reproduction possible.

If pages are missing, contact the university which granted the degree.

Some pages may have indistinct print especially if the original pages were typed with a poor typewriter ribbon or if the university sent us an inferior photocopy.

Previously copyrighted materials (journal articles, published tests, etc.) are not filmed.

Reproduction in full or in part of this microform is governed by the Canadian Copyright Act, R.S.C. 1970, c. C-30.

AVIS

La qualité de cette microforme dépend grandement de la qualité de la thèse soumise au microfilmage. Nous avons tout fait pour assurer une qualité supérieure de reproduction.

S'il manque des pages, veuillez communiquer avec l'université qui a conféré le grade.

La qualité d'impression de certaines pages peut laisser à désirer, surtout si les pages originales ont été dactylographiées à l'aide d'un ruban usé ou si l'université nous a fait parvenir une photocopie de qualité inférieure.

Les documents qui font déjà l'objet d'un droit d'auteur (articles de revue, tests publiés, etc.) ne sont pas microfilmés.

La reproduction, même partielle, de cette microforme est soumise à la Loi canadienne sur le droit d'auteur, SRC 1970, c. C-30.

THE UNIVERSITY OF ALBERTA

Analysis of the Equivalent Tissue Air Ratio Method of Photon Dose Computation

BY

Larry Yakiwczuk

A THESIS

SUBMITTED TO THE FACULTY OF GRADUATE STUDIES AND RESEARCH IN

PARTIAL FULFILLMENT OF THE REQUIREMENTS FOR THE DEGREE OF

Master of Science

DEPARTMENT OF Physics

EDMONTON, ALBERTA

FALL 1987

ISBN 0-315-40968-1

THE UNIVERSITY OF ALBERTA

RELEASE FORM

NAME OF AUTHOR: Larry Yakiwczuk

TITLE OF THESIS: Analysis of the Equivalent Tissue Air Ratio Method of Photon Dose Computation

DEGREE: Master of Science

YEAR GRANTED: 1987

Permission is hereby granted to THE UNIVERSITY OF ALBERTA LIBRARY to reproduce single copies of this thesis and to lend or sell such copies for private, scholarly or scientific research purposes only.

The author reserves other publication rights, and neither the thesis nor extracts from it may be printed or otherwise reproduced without the author's written permission.

Larry Yakiwczuk

(Student's signature)

4328-29 st

Edmonton Alberta

DATE: October 10/87

THE UNIVERSITY OF ALBERTA

FACULTY OF GRADUATE STUDIES AND RESEARCH

The undersigned certify that they have read, and recommend to the Faculty of Graduate Studies and Research for acceptance, a thesis entitled:

Analysis of the Equivalent Tissue Air Ratio Method of Photon Dose Computation

Submitted by Larry Yakiwczuk in partial fulfillment of the requirements for the degree of Master of Science.

.....
(Supervisor)

.....

.....

.....

.....

DATE: October 10/87

Dedication

Remember:

No matter where you go,

There you are.

B.B.

Abstract

This thesis is a critique of the Equivalent Tissue Air Ratio method of dose calculation for megavoltage photons incident on a heterogeneous medium. It is an overview in which the major physical and computational assumptions of the method are highlighted and studied in detail. This method accounts for the influence of tissue density inhomogeneity, as identified by x-ray computed tomography, on the primary and scatter components of the incident photon radiation. It is used routinely on many computerized systems developed for planning the radiation therapy of cancer patients.

Chapter 1 presents a clear definition of the dose calculation problem, followed by the introduction of some important terms and concepts used in radiation dosimetry. Chapter 2 focuses on the Simple Ratio of TAR's method since it is an important precursor to the Equivalent Tissue Air Ratio method which is explained in detail in Chapter 3. Chapter 4 deals with all of the assumptions highlighted in Chapter 3. Their implications in terms of dose accuracy are examined by comparison with measured dose data for Cobalt-60, 6-MV, and 15-MV x-rays which are incident on lung phantoms of various configurations. The influence of the following on dose accuracy was investigated:

1) Dominance of Compton interactions.

2) Dominance of primary and first scatter components.

3) Electronic equilibrium.

4) Primary depth scaling for the scatter component.

5) Tissue attenuation in determining the weights.

6) Two dimensional simplifications.

7) Effect of the reference depth on the weights.

8) Resolution of the scatter grid.

The thesis concludes with a brief summary as well as some suggestions for future research. It is concluded that the Equivalent Tissue Air Ratio method of dose calculation correctly predicts the Inhomogeneity Correction Factors within lung-like inhomogeneities for Cobalt-60 radiation. At higher energies (15-MV x-rays) the results are less accurate for situations of electronic disequilibrium.

Acknowledgements

The author would like to thank Dr. Marc R. Sontag for first developing this method of dose calculation, and thus making all subsequent work possible. Thanks are also extended to N.J. Schroeder who contributed much of the computer code used during this project. The author is also deeply indebted to all the people who have worked on, and are working on, the Alberta Treatment Planning system at the Cross Cancer Institute. A special note of thanks goes out to the author's supervisor, Dr. J.J. Battista, who inspired this project, and who's excellent editorial abilities made this thesis what it is.

Funding for this project was provided, in part by the Alberta Heritage Fund for Medical Research and the Department of Physics.

Table of Contents

Table of Figures

1. Introduction

1.1 Introduction

In 1896 Grubbe and Despeignes [23] pioneered cancer treatment using recently discovered x-rays on inoperable carcinomas. In the 91 years that followed the technique of radiation therapy has developed considerably. Today radiotherapy is one of the three most effective forms of cancer therapy, replacing or complimenting both surgery and chemotherapy. External radiation therapy is particularly suited for therapy of localized tumors whose location can be accurately determined through imaging. In Alberta, about 55% of cancer patients receive radiation during the course of their disease.

The most common form of radiotherapy is applied with external photon beams. Other forms of radiotherapy include the use of internally placed (interstitial or intracavitary) sources, as well as external particle beam therapy. In the latter, a beam of particles such as electrons, protons, heavy nuclei, or mesons are used instead of the conventional photons to improve dose localization or biological effect.

Unfortunately, external photon therapy is not without its complications. These complications may involve short term effects such as erythema (skin reddening) or the long

term residual effects such as lung fibrosis. Most of these complications result from the inevitable irradiation of healthy tissue surrounding the diseased volume.

Since both healthy and diseased tissues are exposed to the radiation, it is very important that the dose be maximized in the cancerous tissue. It is the function of the treatment planner to determine the energy, combination, and orientation of the radiation beams that will deliver the desired dose to the tumor while minimizing the dose to the healthy tissue. The planner achieves this by modeling both the patient anatomy and the physics of the radiation penetration. The accuracy of the delivered dose should be kept within 5 % of the prescribed value [4], which corresponds to 2-3% in the accuracy required of the dose computation step.

1.2 Computed Tomography (CT) Imaging

It would be ideal if all patients were composed of water-equivalent tissue, because then the patient could be modeled simply by relying on radiation measurements made in a simple water tank. This is not the case and before any attempt can be made to correct the dose for tissue inhomogeneities, their size, position, and material composition must be accurately known [14]. Furthermore all of this information must be acquired from the patient

through non-destructive imaging techniques. The most common method of obtaining this information is through X-ray Computed Tomography (CT). The CT scan produces a two dimensional image of a transverse slice (typically 1 cm. thick) through the patient. The scan yields information about the different x-ray attenuation properties of the tissues in the slice. The images that are produced are composed of many individual pixels (e.g. 256 x 256) whose numerical value is directly related to the linear attenuation coefficient (cm^{-1}) at the x-ray energy used for the scan. However it is possible to convert these attenuation values to relative electron densities [2] for a wide range of tissues. Electron densities are more suitable for dose computation at megavoltage photon energies because Compton and Coulomb interactions are the major effects causing dose deposition. These numerical images (or matrices) are " naturally " suited for numerical analysis by a computer and can be stacked together to provide a complete three dimensional model of the patient.

The use of CT scans in treatment planning has many advantages [5]. Many cancer institutions have access to a CT scanner which is used for diagnostic purposes. The advantage of CT is the high spatial resolution (0.1 cm.) of the images in a well defined plane. In general, this resolution is greater than that which is needed for dose computations. A side benefit of the good resolution is a very well defined

patient surface contour. The contour can usually be determined to within one pixel because of the high contrast at the air-tissue interface. The greatest advantage is the tissue density resolution (0.5%). Thus CT scans provide the true geometry and density of tissues to be transversed by the therapy beams.

There are also some disadvantages in using CT scans. The "donut" design of the CT scanner sometimes makes it difficult to place the patient in the exact treatment configuration for the scan. Another problem discussed above involves the conversion CT numbers to relative electron densities. However this problem can be overcome through auxiliary calibration procedures [2] with an accuracy sufficient for dose computations.

1.3 Magnetic Resonance Imaging (MRI)

Another type of diagnostic imaging system with potential application to radiotherapy planning is the process of magnetic resonance imaging. This process relies on the fact that certain atoms (principally hydrogen) have magnetic dipoles that can be aligned with a pulse of external magnetic field [24]. When the field is removed, the dipoles emit a small electromagnetic signal as they relax back to an equilibrium state. If this is done in the presence of an additional magnetic field gradient, these

signals can be localized to a tissue volume and manipulated to form an image.

The main advantage of this type of imaging is that different nuclei of biological interest can be imaged. Also the images are not restricted to predefined planes through the patient. The data may be obtained to image directly any plane through the patient (ie. true three dimensional volume information has been recorded). With x-ray CT, similar versatility can only be achieved by post-scan manipulation of a stack of slices.

This system appears to be ideal for diagnosis. For treatment planning, there are drawbacks. Availability is one of the major stumbling blocks since capital and operating costs are high. Furthermore the time required per image is considerably longer (minutes instead of seconds) than for a CT scan, because of the dipole relaxation times. Finally, the quantitative data obtained (proton density, relaxation times) are not appropriate for accurate megavoltage dose computations, where electron density distributions are required.

1.4 Sources of Photon Radiation

There are two types of sources available for the production of external photon radiation beams; a radioactive source and x-rays produced by accelerated electron bombarding a target. The most common radio-isotope is Cobalt-60, which releases two characteristic gamma rays (1.17 and 1.33 MeV) that are useful for radiotherapy. The linear accelerator uses high voltage to accelerate electrons towards a tungsten target. As the electrons decelerate in the target, they produce bremmsstrahlung radiation. The radiation produced here is different than that produced by a radioactive source in that it is a continuous spectrum of photons instead of discrete monoenergetic photons. This makes the " output " of a linear accelerator a little more difficult to specify and model mathematically. The radiation spectrum must be approximated by numerous monoenergetic levels whose combined effect will give the desired effect (e.g. depth dose penetration). In the simplest approximation a single equivalent or effective energy is used to represent the spectrum. This simple energy is determined from measurements of the beam penetration (i.e. half value layer).

1.5 Interactions of Photons With Tissue

When a photon interacts with a medium it can happen by one of three major processes; Photoelectric effect, Compton scattering, or pair production [6].

If the photon interacts by the photoelectric effect, the atomic " collision " will eject a bound electron. This photoelectron will have an energy equal to the incident photon less the binding energy of the electron, and it is responsible for the dose deposition. After the interaction, the remaining atom is left in an excited state, and fluorescence x-rays and Auger electrons are emitted during de-excitation.

A Compton interaction results in an electron as well as the incident photon being scattered. The energy of the incident photon is divided between the scattered photon and the recoil electron, which is responsible for dose deposition. Compton scattering is assumed to occur with electrons for which the binding energy is small compared to the energy of the incident photon. The Compton interaction is the most important type of interaction in tissue-like materials for megavoltage photon beams (Section 4.3.1).

The third type of interaction is pair production. This type of interaction is only possible if the incident photon energy is greater than the threshold energy of 1.02 Mev. If this is the case, then the strong field of the nucleus may cause the incident photon to disappear, and an electron positron pair to be created. This is an example of electromagnetic energy being changed into mass. The resulting charged particles then travel away from the interaction site, each depositing dose along their path.

The relative importance of these three types of interactions is energy and tissue dependent. In water, the photoelectric effect dominates up to energies of about 30 kev. Compton interaction are dominant between the energies of 30 kev and 30 Mev. Above 50 Mev, pair production is the dominant process. Care must be taken in the intervening energies because more than one process may be active.

1.6 Dose Deposition Mechanism

When a beam of radiation passes through matter, energy from that beam is transferred to the medium by charged particles set in motion. This energy transfer occurs in a two stage process. The first stage is the interaction of a photon with the atoms of the medium. The photon does not usually interact with the nucleus (except in pair production) but rather, with the surrounding orbital

electrons. This results in high energy electrons being liberated from the atom and this transfer of energy is referred to as the KERMA (Kinetic Energy Released per unit Mass) step. The electron then travels through the medium during which the second stage of the energy transfer takes place. In this stage the high energy electron transfers its energy to other parts of the medium through numerous Coulomb collisions. These collisions result in ionizations and excitations of the host material along the charged particle tracks. Thus all of the energy deposited in the medium is not deposited at the original interaction site, but is dispersed through a small volume around the interaction site. If a small enough volume were monitored around a single interaction site, a substantial amount of energy would be deposited beyond this volume. Hence we have a situation in which energy is both leaving and entering small volumes at the same time. If the amount of energy leaving is equal to the amount entering, then charge particle equilibrium is said to be established. Since the bulk of the charged particles are electrons (set in motion by photons), this is loosely referred to as electronic equilibrium.

Under most conditions of irradiation, electronic equilibrium is indeed present. This greatly simplifies dose computations since this reduces the problem to one of photon transport in which the electron energy can be assumed to be absorbed " on the spot ". However, equilibrium is generally

not present at interfaces between materials of different density and electron scattering properties, and at field boundaries (e.g. the build up region). For these situations, more complex calculations are needed, and have been developed [8][9][10].

1.7 Dose in a Homogeneous Medium

1.7.1 Tissue Air Ratio (TAR)

The tissue air ratio is defined as a ratio between two doses [7] and is related to the total dose due to primary and scattered photons. The first dose (DT) is to a small volume of tissue, located at a point (P) in an all-water medium at a given depth (d). The other dose (D'A) is to the same volume of tissue located at the same distance from the source, but located in air (Figure 1-1). The term small volume means the minimum volume required to establish electronic equilibrium at the point of measurement. Assuming a beam of circular cross-section, the Tissue Air Ratio (TAR) is defined as:

$$TAR(d,r,E) = DT / D'A \qquad (1\text{-}1)$$

The TAR is functionally dependent on the depth (d) within the medium, the beam size (r) at the depth of measurement, and the incident energy (E).

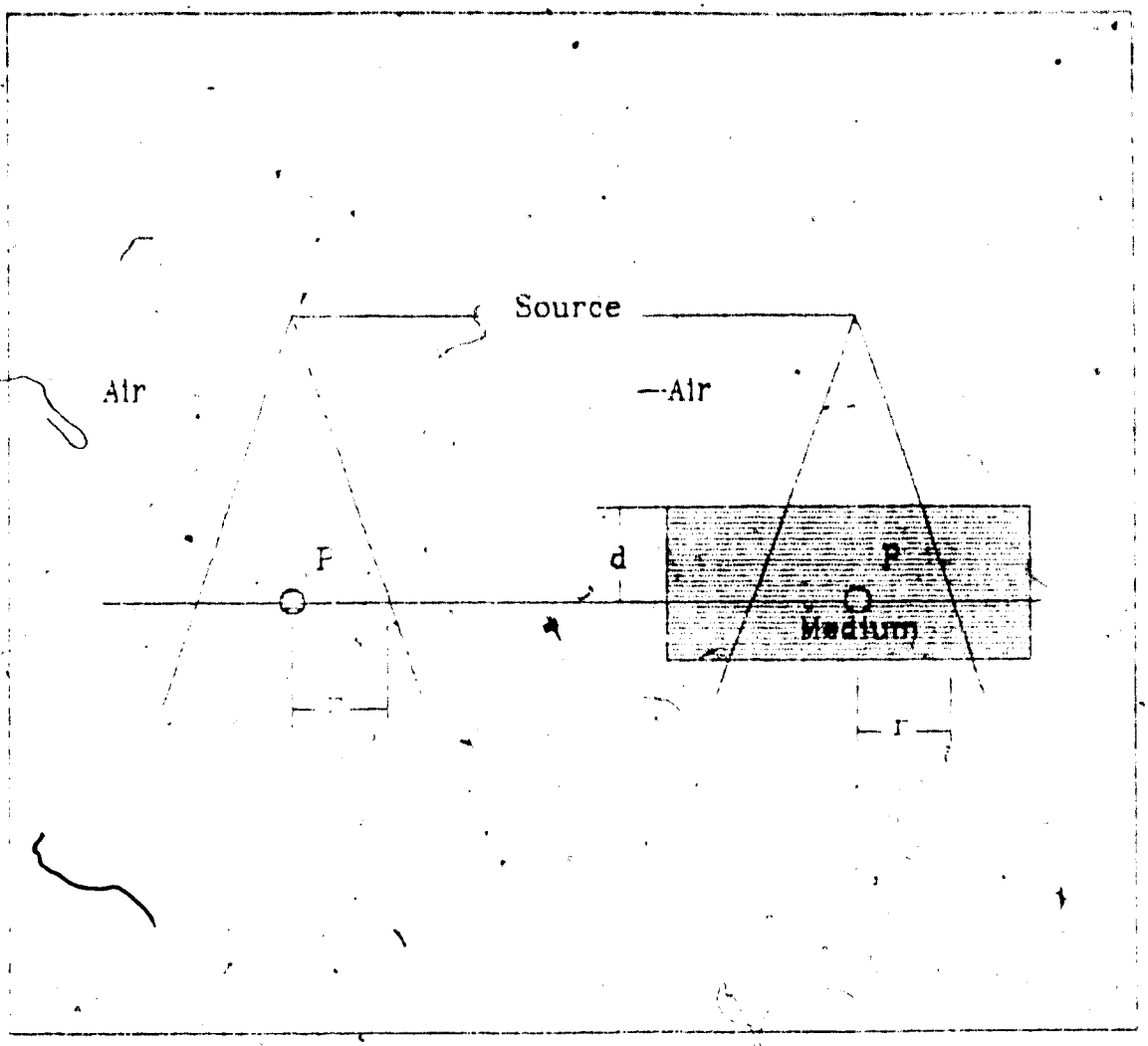

Figure 1-1

The Tissue Air Ratio of two doses. One dose is to a small volume of tissue located at point P in an all water medium. The other dose is to the same volume located in air.

1.7.2 Primary Tissue Air Ratio

A useful quantity derived from tissue air ratios is the zero-area TAR. This represents the primary component of the radiation field since it refers to a narrow pencil beam (sufficiently wide to achieve lateral electronic equilibrium). This quantity is determined through a semi-empirical approach. Tissue air ratios are measured for decreasing beam sizes and are then extrapolated to give the TAR for a beam of "zero" radius.

1.7.3 Scatter Air Ratio (SAR)

A tissue air ratio can be considered to be composed of two separate and independent parts. One component represents the dose due to the primary photon radiation of the beam and is the zero-area tissue air ratio just defined. The other component describes the scattered photon radiation and is called the Scatter Air Ratio (SAR).

$$TAR(d,r) = TAR(d,0) + SAR(d,r) \qquad (1\text{-}2)$$

Scatter air ratios cannot easily be measured directly but can easily be calculated by a subtraction method:

$$SAR(d,r) = TAR(d,r) - TAR(d,0) \qquad (1\text{-}3)$$

Since the SAR is derived from a Tissue Air Ratio, it has similar functional dependence on depth, field size, and energy. The scatter air ratio is a very useful quantity when dealing exclusively with scattered radiation. Graphs of TAR's and SAR's will be presented in Section 4.3.2.

1.8 Dose in a Heterogeneous Medium

1.8.1 The Problem

The real problem is to calculate the radiation dose at any point within an inhomogeneous 3-dimensional patient irradiated with an external photon beam. In principle this is a simple problem since the photon interactions are well known, but in practice it is actually a very complex situation which may never be solved in closed analytic form because of multiple competitive interactions. However, approximate numerical solutions have been developed, including the various ratios of Equivalent TAR's methods, investigated in this thesis.

1.8.2 The Semi-Empirical Approach

Most methods of dose calculation rely on a semi-empirical approach. Most of the data used to calculate radiation doses to patients is based on measurements collected in water phantoms (e.g. TAR values). The

radiation dose is measured in these phantoms as a function of several variables such as depth of measurement, beam radius, and energy of the incident beam. These data are then arranged in tables that can be "looked up" by the computational algorithms. By using these data, very accurate dose predictions can be made for regions that have near water density.

Most dose algorithms yield an Inhomogeneity Correction Factor (ICF). This correction factor is a ratio of doses, and we have seen that doses are related to Tissue Air Ratios. Thus most correction factors can be considered as some type of ratio of TAR's. Many of the dose algorithms use this fact and modify the TAR's in some way to give a more accurate dose prediction in a heterogeneous medium.

1.8.3 Inhomogeneity Correction Factor (ICF).

The inhomogeneity correction factor connects the dose distribution between a homogeneous (all water) medium to the dose in the inhomogeneous medium (Figure 1-2). The correction factor is a simple ratio of these two doses.

$$ICF(X,Y,Z) = \frac{\text{Dose in inhomogeneous medium}}{\text{Dose in homogeneous medium}} \qquad (1\text{-}4)$$

Each correction factor is for a single point of calculation at (X,Y,Z) and has to be recalculated for every point that

is irradiated within the medium in order to yield a complete dose distribution.

The reason for linking to the dose in an all-water medium is that the radiation data base upon which most methods of dose calculation are based is measured in a homogeneous water medium. Furthermore the dose distribution in water is a good first order representation of the actual dose distribution, since most tissues are water-like in density, with the notable exceptions of lung and bone.

1.8.4 The Batho Method

The Batho method [1] [15] uses an exponential power law of the TAR's in an attempt to correct for both primary and scattered radiation. It takes into account the thickness as well as the proximity of the inhomogeneity.

Within the inhomogeneity, the correction factor is given by:

$$ICF = [\ TAR(d2,r)\ ]^{E-1} \qquad (1\text{-}5)$$

Beyond the inhomogeneity, a different form is used:

$$ICF = [\ TAR(d2,r) / TAR(d1,r)\ ]^{E-1} \qquad (1\text{-}6)$$

where,

E The electron density of the inhomogeneity relative to water.

d1 Distance from calculation point to bottom of inhomogeneity.

d2 Distance from calculation point to top of inhomogeneity.

The above factors are for a single layered inhomogeneity but they can be compounded to take into account multiple layered inhomogeneities.

This method is limited in that it assumes that for each beam ray, the inhomogeneity is momentarily flat topped and is as wide as the beam. Thus it does not accurately account for the lateral size and shape of the inhomogeneity. The method also assumes that backscatter does not contribute significantly to the dose.

1.8.5 Pixel Based Algorithms

With the advent of CT scans a number of pixel based algorithms have been developed to calculate the radiation dose within a patient. These algorithms make use of the inhomogeneity density information contained within each pixel of the CT scan. These algorithms tend to be numerically complex and require considerable computer resources.

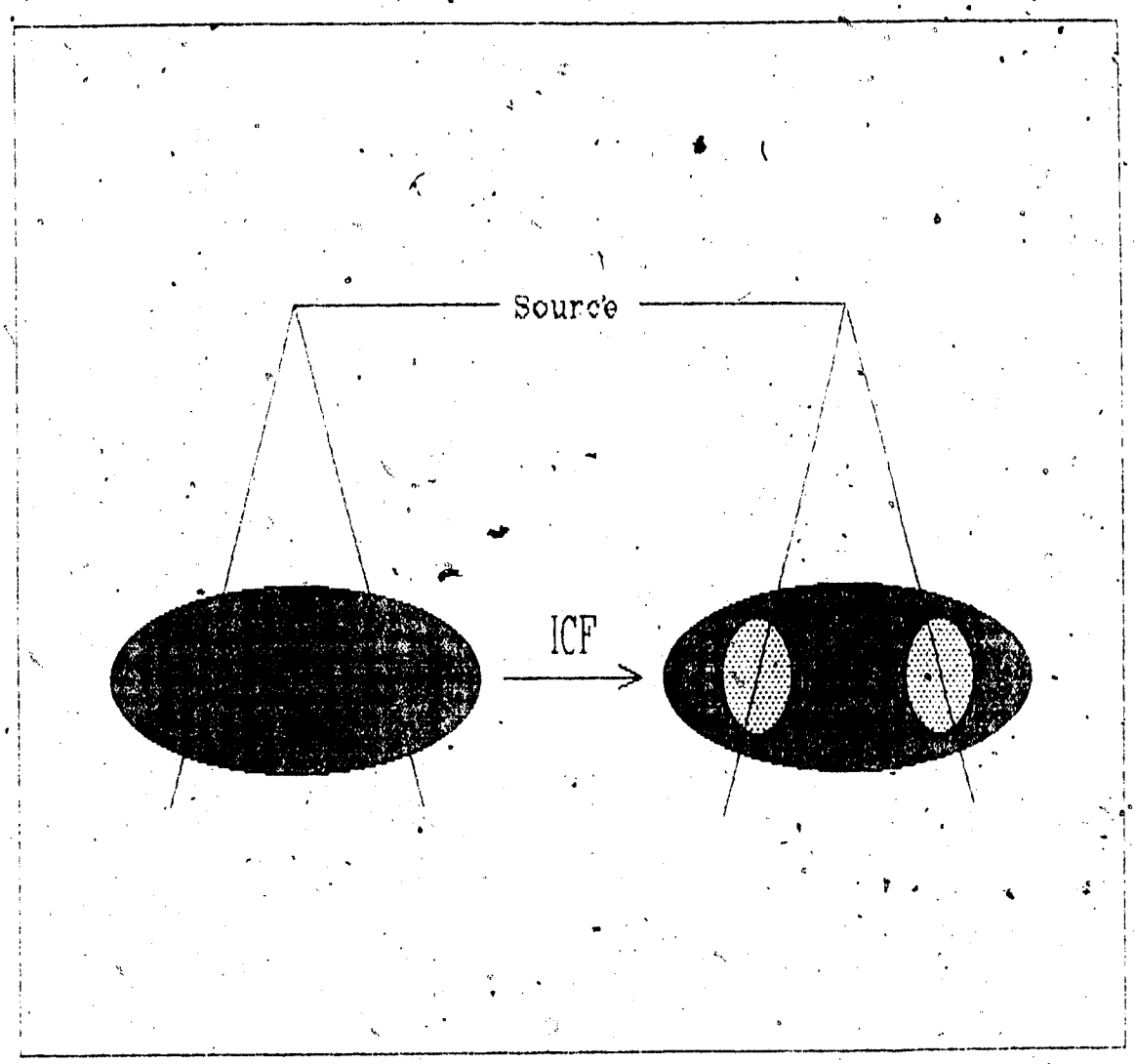

Figure 1-2

The Inhomogeneity Correction Factor (ICF) connects the dose between a homogeneous water medium and the dose in an inhomogeneous medium.

1.8.6 Simple Ratio of Tissue Air Ratios

This is one of the simplest of the inhomogeneity corrections. Only the path travelled by the primary photon is examined and the depth of the calculation point used in the tissue air ratio is a radiological depth instead of the normal geometric depth. The radiological depth can be considered to be an equivalent water depth and is equal to the line integral of the relative electron densities along the path traveled by the primary photon. Thus the correction factor is a ratio of two tissue air ratios [4].

$$ICF = TAR(d',r) \,/\, TAR(d,r) \qquad (1\text{-}7)$$

- d' The radiological depth.
- d The geometric depth.
- r The beam radius.

This method is very well suited to pixel based calculations because the good resolution of the image allows for a rapid and accurate calculation of the radiological depth by simple pixel value summation along the beam rays.

This form of correction is usually called a primary correction because it properly accounts for the change in the primary component of the radiation. However, this method incompletely corrects for the scatter component of the

radiation because the method does not sense the three dimensional density neighborhood around the calculation point. A complete explanation of this method and its limitations will be discussed in Chapter 2.

1.8.7 Equivalent Tissue Air Ratio Method

This method developed by Sontag [12] [13] [16] uses the premise that for each point in a heterogeneous medium there exists an equivalent water environment. This premise assumes that Compton interactions dominate, and that electronic equilibrium is present.

In determining this equivalent water environment certain parameters must be density-scaled. The depth of the calculation point is scaled as in the ratio of TAR's method (ie. the radiological depth is used instead of the geometric depth). However the beam radius is also scaled in an attempt to account for the scattered radiation by considering an equivalent field size. This gives an inhomogeneity correction factor of the following form:

$$ICF(x,y,z) = TAR(dEQ,rEQ) / TAR(d,r) \qquad (1\text{-}8)$$

dEQ The radiological depth.

rEQ The scaled beam radius.

This method attempts to sense the three dimensional neighborhood around each point of calculation. This is done by using multiple CT slices as a three dimensional model of the patient.

This method has many advantages. Among them is the fact that there is improved agreement with experimental data when compared with simpler methods. Another advantage is the use of three dimensional matrix data instead of a two dimensional vectoral description of a patient. Also this method is currently commercially available on many treatment planning systems used clinically.

There are also a number of disadvantages, among them being the numerous physical and computational assumptions, many of which initially appear to be ill-founded. These assumptions as well as a complete explanation of the method will be presented in Chapters 3 and 4.

1.8.8 Delta Volume Method

This method developed by Wong [19] uses the premise that the majority of the dose is due to the primary radiation, the first scatter component, and an identifiable portion of the second scatter component. The dose at the calculation point is given by,

$$DOSE(x,y,z) = D0 + D1 + DM \qquad (1\text{-}9)$$

D0 Dose due to primary radiation.

D1 Dose due to first scattered radiation and limited second scattered radiation.

DM Dose due to the multiple scatter component of the radiation.

The method thus relies on the knowledge that the multiple scatter component is small, and can be estimated from empirical data. The method takes into account the first scatter and a portion of the second scattered radiation (limited to a 45 degree forward scattering cone) and ray traces the path of these scattered photons. It assumes that the energy of second scattered photons reaching the calculation point is the same as that of the first scattered photons.

This method does have a number of drawbacks. The use of an empirical data base for the multiple scatter component requires very precise measurements of low level radiation. However, the major problem of this method is the "ray tracing" computational burden. Because three dimensional volumes are used, an extremely large number of ray traces must be done, and even with modern computer technology the time required by this algorithm is still excessive.

1.8.9 Convolution

This method uses the concept of dose spread functions [8] [10]. The dose spread function represents the dose deposited in different volumes (voxels) surrounding a single voxel in which photons interact. These kernals are then spatially convolved with the KERMA to produce a dose distribution. This is an elegant solution and an easy task for a homogeneous medium. However, if heterogeneities are introduced the complexity increases and approximations are necessary. One way of dealing with these inhomogeneities is to distort the dose spread arrays prior to convolution . Presently there is much research being carried out on this subject.

This method is based on sound mathematical principles and accounts for non-local energy deposition from charged particles (i.e. electronic disequilibrium). Rather than using a database of measured data, it uses Monte-Carlo techniques to generate dose spread kernals. This method is also an opportunity for a unified theory of dose calculations for which the KERMA step is bypassed. This means a single algorithm could be developed for photon radiation as well as particle radiation.

Of the methods discussed so far, the Delta-Volume and Convolution methods show the greatest promise, but they require excessive computer processing time for routine use.

1.8.10 Monte-Carlo

This is the ultimate of dose calculation algorithms, taking into account coupled photon and charged particle transport. This method does not use any empirically measured data (except for the incident beam spectrum) but generates its own data through repetitive calculations based on interaction probabilities of individual photon and electron events.

Individual photons and charged particles are followed as they travel through the medium. To achieve a statistically reliable dose result, millions of different photon histories have to be calculated, which identifies the major drawback of this method. The amount of computer time used becomes enormous (i.e. days) and thus this method not practical for clinical use.

1.9 Why Study the Equivalent TAR Method

There are many areas in the field of dose calculation that could be studied. The Delta-Volume and Convolution approaches are actively being developed but it will be quite

some time before these methods are of practical and commercial use. The Equivalent Tissue Air Ratio method is one method which has been implemented commercially, but with limited research into the actual physics underlying the method and the many software "short cuts". As mentioned earlier there are numerous assumptions applied in order to achieve practical calculation times. Some of these assumptions are valid while others have been poorly justified and require further study. Despite all the assumptions, this method generally gives accurate dose results and is currently the commercial standard to which other methods are compared. It is for these reasons that the equivalent tissue air ratio method was chosen for study in this work.

In the following chapters the ratio of TAR's and the Equivalent TAR methods will be described in detail. The ratio of TAR's is described completely in Chapter 2. It is included for completeness because it is the starting point for the Equivalent TAR method. The Equivalent Tissue Air Ratio method will be explained in considerable detail in Chapter 3, followed by an extensive discussion in Chapter 4. Most of the assumptions will be highlighted and their implications discussed in detail.

2. The Simple Ratio of Tissue Air Ratios Method

2.1 Introduction

The ratio of TAR's method is one of the simplest pixel-based inhomogeneity correction algorithms for calculating the radiation dose distribution within a patient [4]. This method uses the pixels from an x-ray CT scan to define inhomogeneity in terms of tissue density within different slices of the patient. The method described in this chapter was implemented into the Alberta Treatment Planning (ATP) system where it was tested and made optionally available for treatment planning in January 1986.

Tests done on this method included a comparison of computer calculated values to hand calculated values for simple heterogeneous phantoms. A comparison was also made to experimental data from this laboratory [9].

2.2 Explanation of The Method

The Ratio of TAR's considers the equivalent water or radiological depth of points in a radiation field. As mentioned in the previous chapter the radiation dose at any point is composed of two separate components, the primary dose and the scattered dose. The Ratio of TAR's is only concerned with the primary component of radiation. This

method examines only the "ray" path travelled by the primary photons. The effective radiological depths along these paths are calculated and are used in the Tissue Air Ratio's replacing the normal geometric depths. The radiological depth is the line integral or ray sum of the relative electron densities along the path travelled by the primary photons (Figure 2-1). Since the actual electron densities are normalized to the electron density of water, this radiological depth can be considered to be an equivalent water depth.

$$d' = \int E(L) \, dL \qquad (2\text{-}1)$$

where,

L Path travelled by the primary photons.

E Electron density relative to that of water.

The Inhomogeneity Correction Factor is:

$$ICF = \frac{TAR(d', r)}{TAR(d , r)} \qquad (2\text{-}2)$$

where,

d' Radiological depth of calculation point.

d Geometric depth of calculation point.

r Beam radius at the calculation point.

The small size of the pixels (typically 0.1 cm.) in the CT image allows simple pixel value summation to be used to calculate the radiological depth accurately. Each pixel

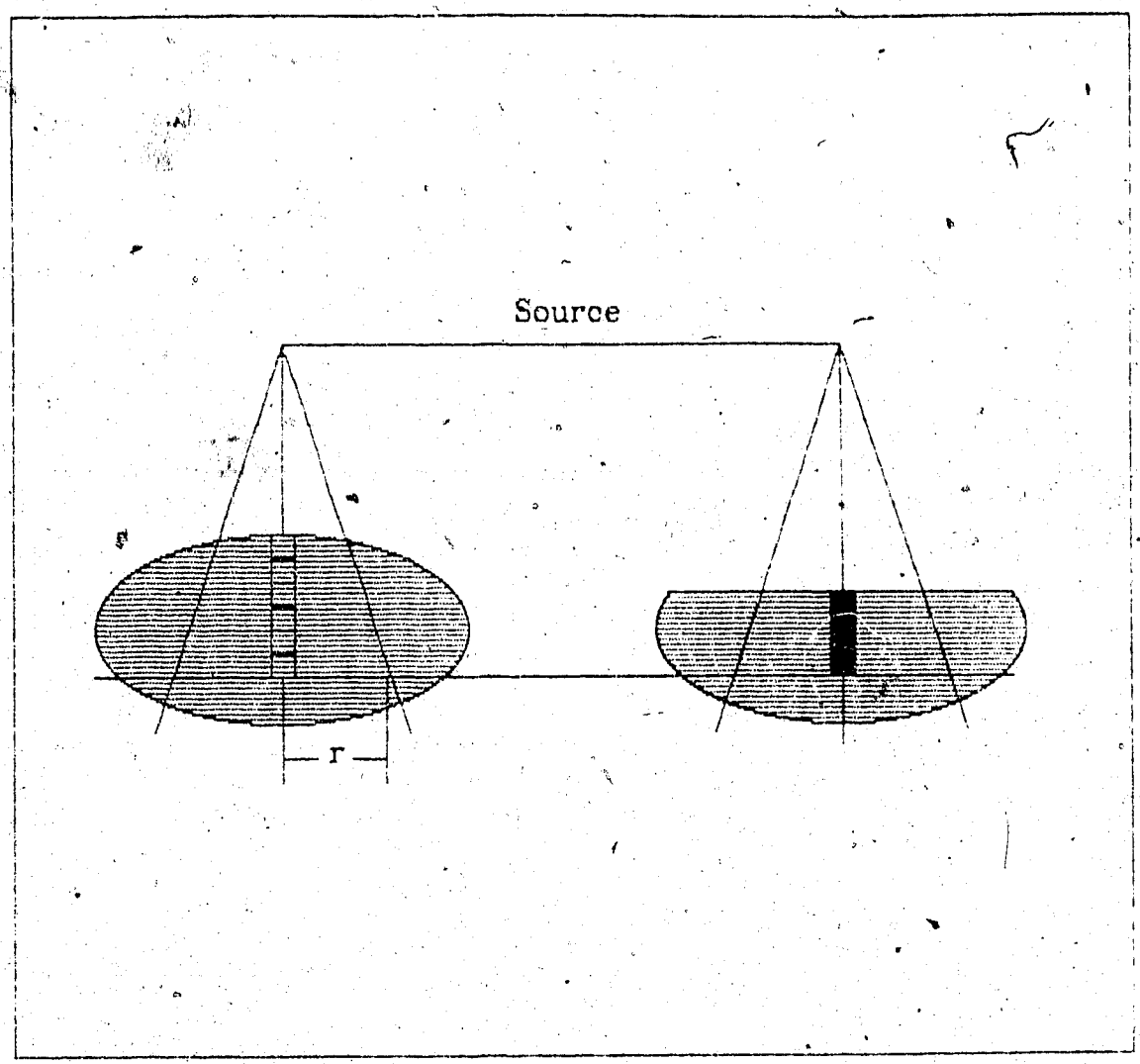

Figure 2-1

Pixel summation along ray path to give an effective radiological depth. This effective water depth is used in place of the geometric depth in the Tissue Air Ratio.

within the CT image is directly relateable to the relative electron density of the volume it represents in the patient [2].

Once the radiological depth, geometric depth, and beam radius are calculated, the algorithm then needs to calculate the TAR values for the two different depths. This is accomplished through the use of a lookup table of TAR values, and linear interpolation between the values in the table.

These TAR values are obtained from experimental data previously gathered in water phantoms (The data are stored as a function of, beam radius, depth, and incident energy). Since these data are for an all water phantom, it makes sense to use equivalent water depths in the calculation algorithm. Because of this, The Ratio of TAR's method properly accounts for the changes in the primary component of the radiation, but does not properly account for the scattered radiation. Thus it is loosely called a primary correction.

If the scaled TAR is split up into its primary and scatter components a number of assumptions are brought to light.

$$TAR(d',r) = TAR(d',0) + SAR(d',r) \qquad (2\text{-}3)$$

If the scatter term is examined it is seen that the scatter (scatter along the beam direction) is assumed to change with depth only. The geometric field size is not adjusted at all: changes in the lateral scatter are ignored.

2.3 Experimental Results

The experimental setup used to test the Ratio of TAR's method is shown in Figure 2-2. The phantom consists of layered polystyrene and cork with the source to probe distance (SPD) held constant at 100 cm. for 6-MV and 15-MV x-rays and 80 cm. for Cobalt-60 radiation. The distance from the entrance side of the cork to the probe (a), was varied to give the illusion that the cork inhomogeneity "floats" upward through the phantom past the probe. The probe to surface distance (d) was held constant at 15.5 cm. The physical densities of the cork and polystyrene were 0.30 g/cm^3 and 1.02 g/cm^3 respectively, as determined from CT scans [9].

This arrangement was used in tests for three different beam energies; 6 MV x-rays, 15 MV x-rays, and Cobalt radiation. Along with the beam energy, the field size was also varied; 5x5 cm^2 and 10x10 cm^2 fields were used. A comparison of calculated data with measured experimental data can be seen in Figures 2-3, 2-4, and 2-5.

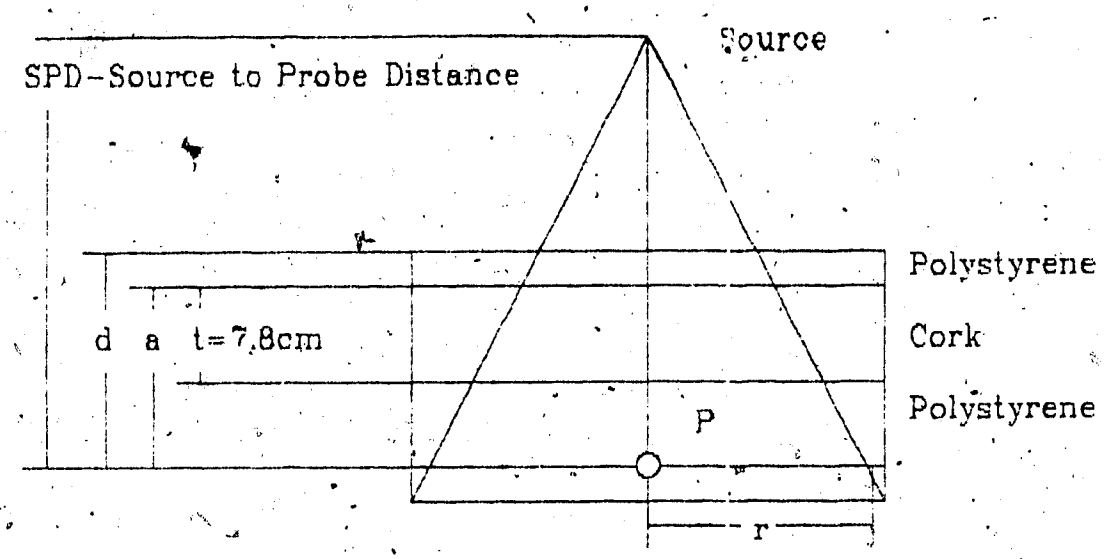

d : Surface to probe distance 15.5 cm.

t : Cork thickness 7.8 cm.

r : Beam radius at depth, d.

Polystyrene density 1.02 g/cc

Cork density 0.28 g/cc

Figure 2-2

The Slab Phantom.

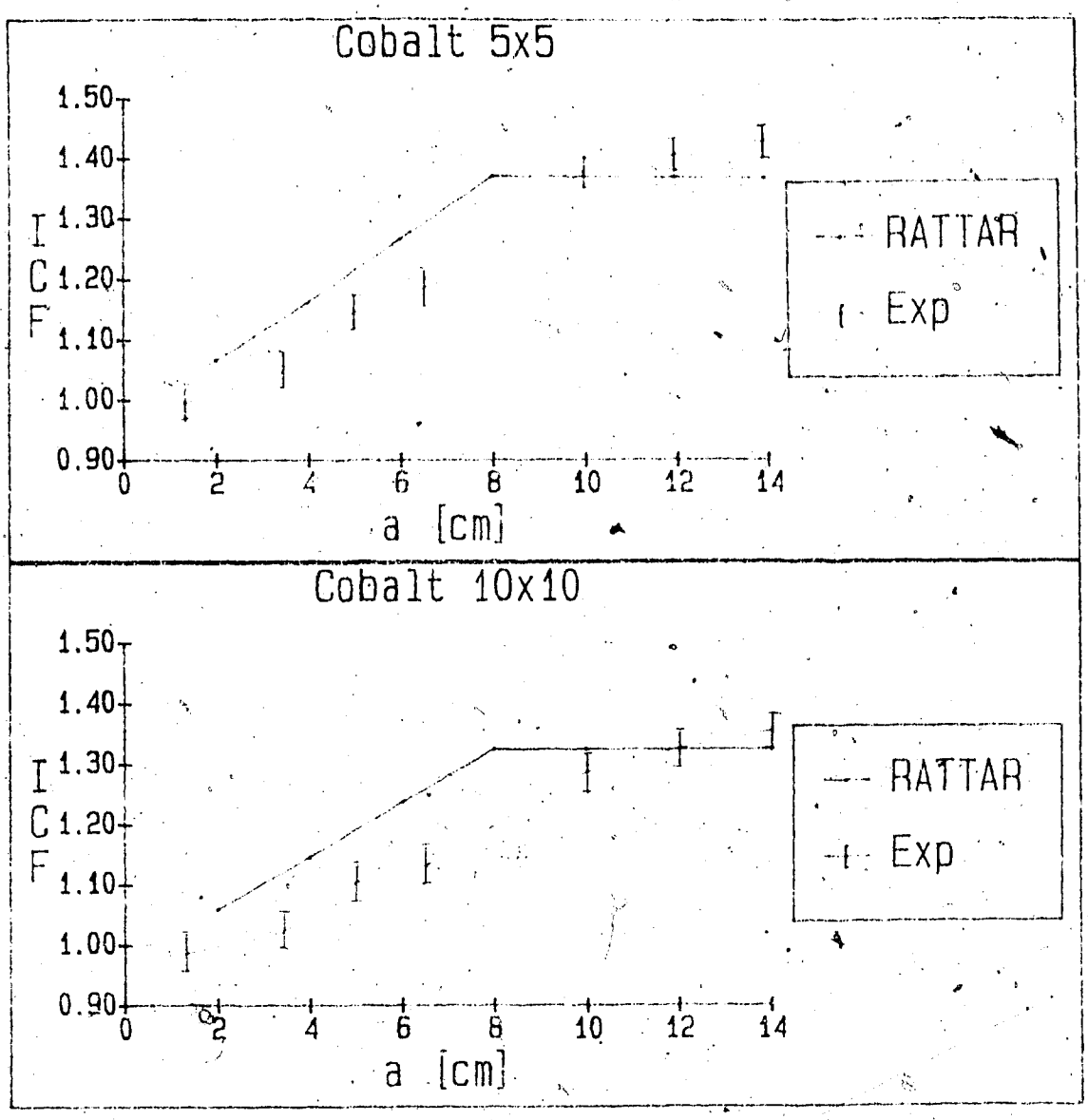

Figure 2-3
A comparison of experimentally measured values and calculations using the Ratio of TAR's method for a Cobalt beam.

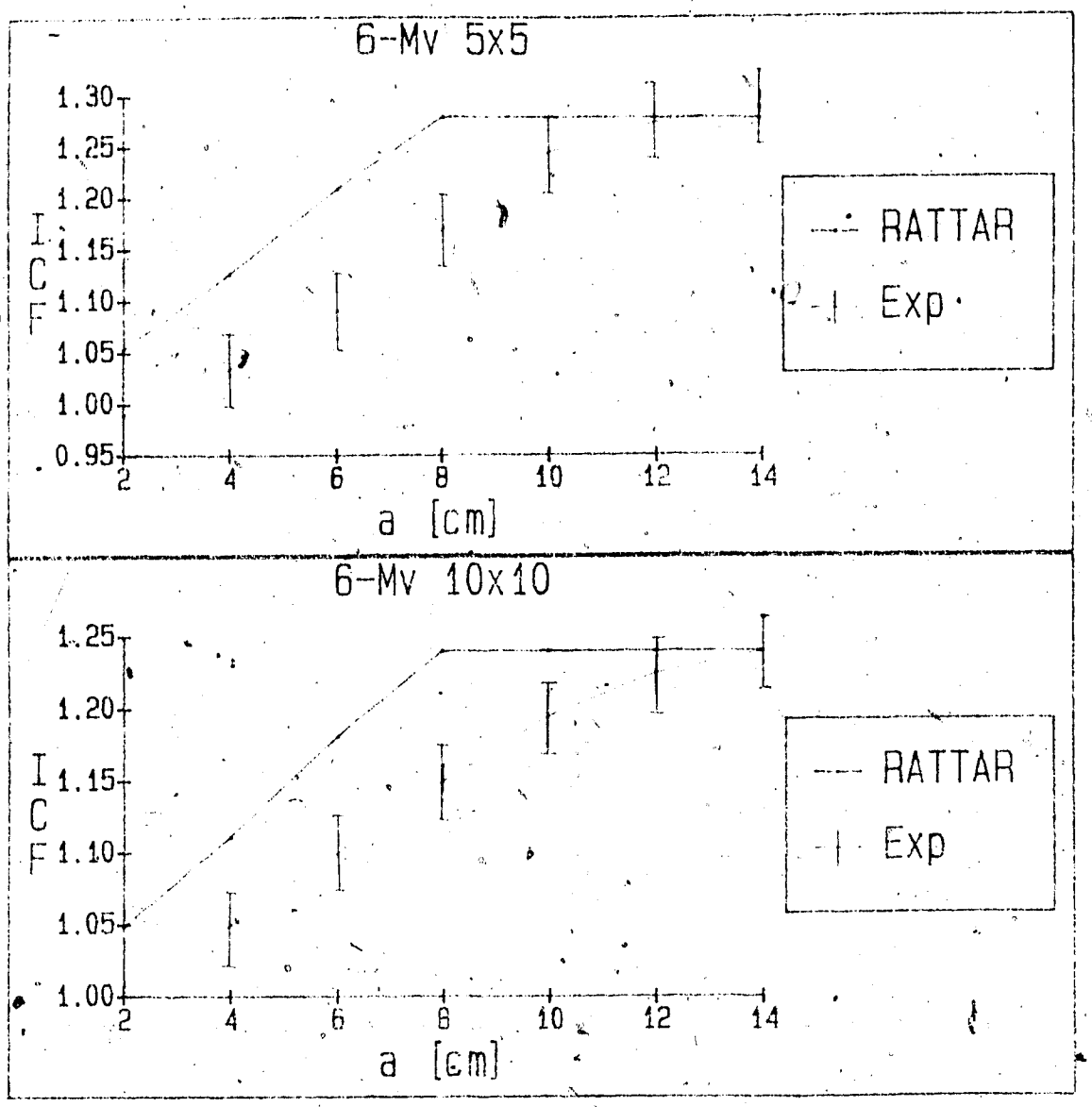

Figure 2-4
A comparison of experimentally measured values and calculations using the Ratio of TAR's method for a beam energy of 6-Mv.

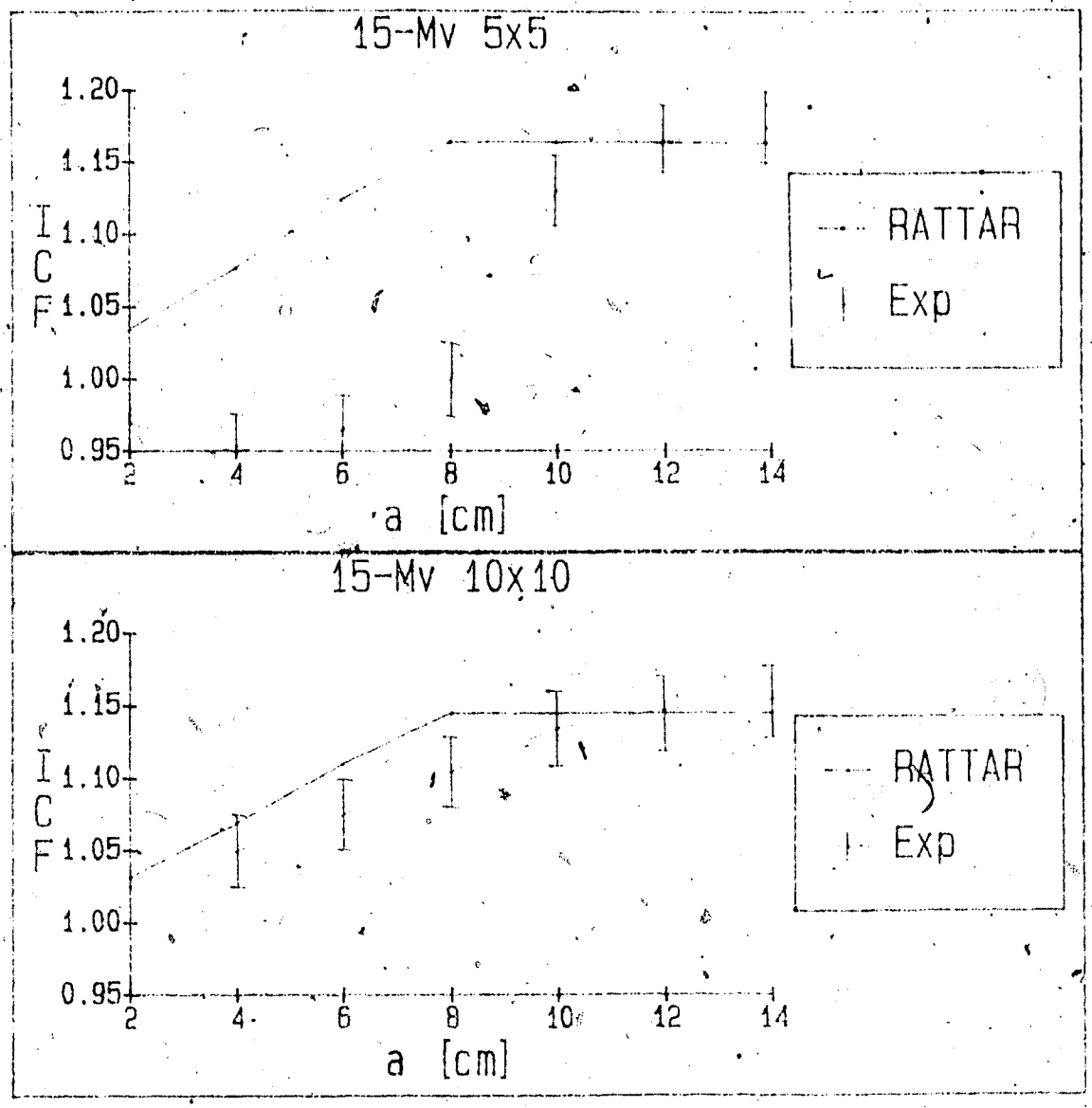

Figure 2-5
A comparison of experimentally measured values and calculations using the Ratio of TAR's method for a beam energy of 15-Mv.

The first observation is that the Ratio of TAR's method produces a plateau in the Inhomogeneity Correction Factor's for values of (a) greater than 8 cm. This observation is easily explained. Once the entire inhomogeneity (cork slab) is above the calculation point (P), the primary photons will always be attenuated by a constant radiological thickness above the calculation point. The material below the calculation point (i.e. backscattering) is ignored by the calculation algorithm because the method only looks at the primary photon path from the source to the calculation point.

The second observation is that the Ratio of TAR's method consistently overpredicts the experimental values. The method does not properly account for the scatter component of the radiation. The general reduction in scatter caused by replacing a slab of water by a slab of cork is taken into account improperly by simply varying the effective depth.

As the inhomogeneity is moved far above the calculation point, the Ratio of TAR's calculations closely approaches the experimentally obtained values. This is because the primary attenuation is the dominant component of the dose in this region. As the inhomogeneity moves closer to the calculation point the scatter component becomes increasingly

important and the Ratio of TAR's fails to accurately calculate the Inhomogeneity Correction Factor.

There is a peculiar effect for 15-MV x-rays (Figure 2-5) when the dose within the cork is reduced because of the lower density and reduced field size. This is attributed to electronic disequilibrium and is discussed in Section 4.3.3.

2.4 Advantages of This Method

The Ratio of TAR's method of dose calculation offers many advantages. It is numerically very simple which makes it easy to understand and define its limitations. It is also very easily adaptable to CT scan data. A byproduct of this numerical simplicity is that this algorithm can be executed very quickly using minimal computer time (Typically 15 to 60 seconds per beam on a VAX 11/780 processor).

As mentioned earlier, this is a pixel-based algorithm which uses CT images as its data base. The good resolution of the images allows even the smallest of inhomogeneities within the patient to be detected during calculation. The calculation algorithm uses this good resolution to sense all of the small inhomogeneities. Indeed, manual contouring of bulk inhomogeneities is rendered obsolete by this pixel based methodology, resulting in some time savings.

The strength of this method is that it corrects for the primary component of the radiation, which in may regions is the dominant component of the total dose (Section 4.3.2). It is for this reason that this method is a reasonable starting point for the Equivalent TAR method .

2.5 Disadvantages of This Method

A comparison of calculated inhomogeneity correction factors with experimental ones, showed that the Ratio of TAR's method gave consistently higher values within the cork, by as much as 15% for the simple slab geometries tested. Under such circumstances this difference is too large to make the method reliable for clinical use.

For these reasons a more accurate method of dose calculation is needed. Since this method does properly account for the primary component, it will be used as the basis for a more advanced method, called the Equivalent TAR method which "tops up" this approach with a scatter correction. This newer method is the topic of the remainder of this thesis.

3. The Equivalent Tissue Air Ratio Method

This chapter introduces the Equivalent Tissue Air Ratio Method. This will be a general explanation of the method in which the major assumptions will be highlighted. Chapter 4 will examine some of these assumptions in more detail, and asses their implications.

3.1 Introduction

Due to the inaccuracies of many dose calculation algorithms, a new algorithm was developed by Sontag [12] [13] [16], called the Equivalent Tissue Air Ratio method which also takes advantage of density information contained in digital images (eg. x-ray CT). This method uses the Ratio of TAR's as a starting point, but attempts to correct for the scatter component of the dose. This is accomplished by scaling both the depth and the beam radius in the numerator of the Inhomogeneity Correction Factor.

The Ratio of TAR's is a one dimensional method (ie. It only uses image information along a ray from the radiation source to the calculation point). The Equivalent Tissue Air Ratio method is a three dimensional algorithm (ie. It uses image information from the entire irradiated volume). For the Equivalent TAR method, numerous slices (preferably

adjacent) can be used to provide a three dimensional description of the patient (Figure 3-1).

3.2 O'Connor's Theorem

The fundamental hypothesis of the Equivalent TAR method is that O'Connor's Theorem [11] can be applied to a heterogeneous medium. O'Connor's Theorem is based on a relationship between the doses of two homogeneous media of different densities. The theorem states that the dose at a point in a homogeneous medium of relative electron density (E) can be considered equivalent to that in a homogeneous water medium (E = 1.0), provided all the linear dimensions of the non-water medium are scaled by the factor of (E). This can be seen in Figure 3-2.

$$a' = E\,a \qquad b' = E\,b \qquad (3\text{-}1a)$$

$$d' = E\,d \qquad r' = E\,r \qquad (3\text{-}1b)$$

$$dV' = E^3\,dV \qquad (3\text{-}1c)$$

This density scaling allows the Tissue Air Ratio, Primary Tissue Air Ratio, and Scatter Air Ratios to be rewritten in the following form for a homogeneous medium.

$$TAR(d,r)_E = TAR(Ed,Er)_W = TAR(d',r')_W \quad \text{Total} \quad (3\text{-}2a)$$

$$TAR(d,0)_E = TAR(Ed,0)_W = TAR(d',0)_W \quad \text{Primary} \quad (3\text{-}2b)$$

$$SAR(d,r)_E = SAR(Ed,Er)_W = SAR(d',r')_W \quad \text{Scatter} \quad (3\text{-}2c)$$

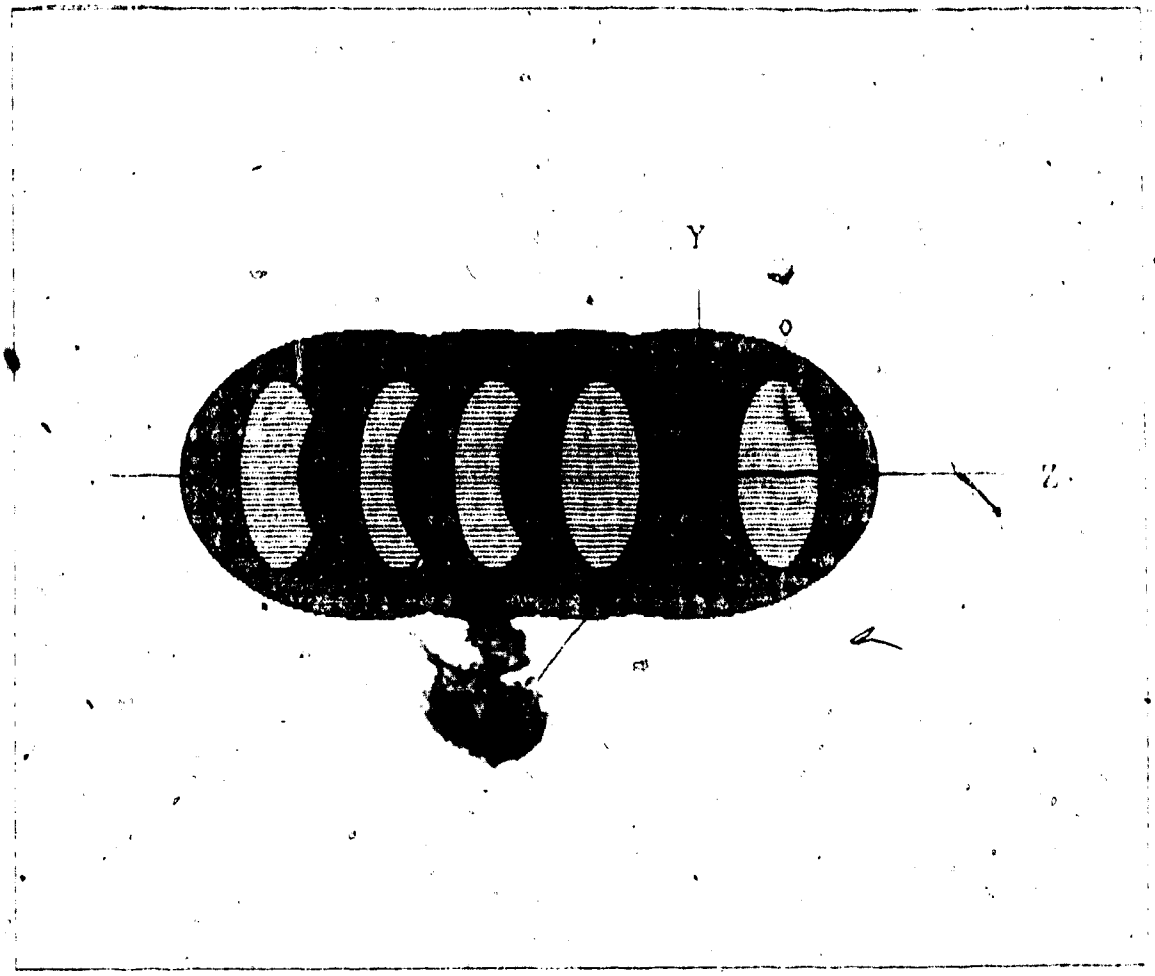

Figure 3-1

In the Equivalent TAR method, multiple CT slices may be used to produce a three dimensional description of the patient.

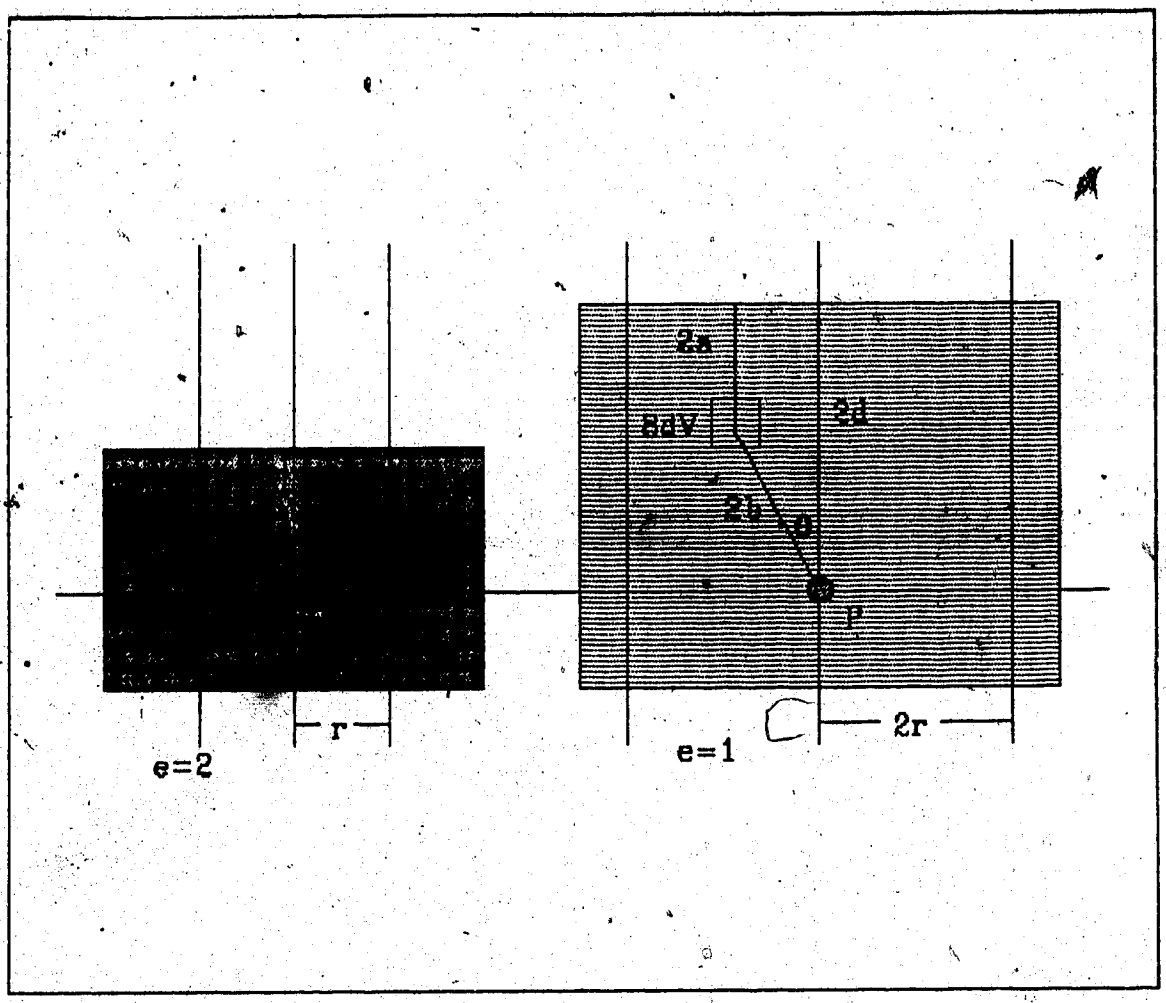

Figure 3-2

O'Connor's Theorem. A homogeneous media with arbitrary relative electron density can be considered equivalent to a water media, provided all linear dimensions are scaled properly. The dose at P is the same in both cases.

The subscripts (W) and (E) refer to water medium and non-water medium respectively. From this point on, an unsubsripted TAR or SAR refers implicitly to a water medium.

There are a number of underlying assumptions in O'Connor's Theorem.

Assumption 1: Compton interaction dominate.
It is assumed that Compton interactions are the only ones that occur between the photons and the medium.

Assumption 2: Primary and single scatter dominate.
It is also assumed that primary and single scatter account for the majority of the dose. O'Connor's Theorem can be proven analytically for the primary and first scattered photons. The multiple scatter component is assumed to act similarly, but this is not easy to prove analytically.

Assumption 3: Electronic equilibrium.
It is assumed that electronic equilibrium (Section 1.6) has been established at the point of interest in the medium.

3.3 The Inhomogeneity Correction Factor

For a heterogeneous environment, O'Connor's Theorem must be slightly modified. The modified form states that for every point within a heterogeneous medium there also exists an equivalent homogeneous water medium. Because the medium is heterogeneous an " average " relative electron density must be used to scale the linear dimensions.

$$d' = ED\ d \qquad (3\text{-}3a)$$

$$r' = ER\ r \qquad (3\text{-}3b)$$

where,

ED The average relative electron density along the primary ray to the calculation point.

ER An average relative electron density in the 3-D volume surrounding the calculation point.

The Equivalent Tissue Air Ratio method uses these density scaled quantities in the numerator Tissue Air Ratio of the Inhomogeneity Correction Factor.

$$ICF = \frac{TAR(d',r')}{TAR(d,r)} = \frac{TAR(d',0) + SAR(d',r')}{TAR(d,r)} \qquad (3\text{-}4)$$

The latter form of the correction factor uncovers further assumptions.

Assumption 4: Scatter at the Primary Depth.

The same scaled depth is used in both the primary as well as the scattered components of the Tissue Air Ratio. This assumes that the scatter (scatter along the beam direction) changes only longitudinally with depth as was the case with the simple Ratio of TAR's. The geometric field size is replaced by a scaled quantity in order to correct for lateral scatter, but perhaps at a wrong depth.

3.4 The Scaled Depth

The equivalent water depth (radiological depth) should be used for (d') in the primary term, TAR(d',0), of the correction factor, as was the case with the simpler Ratio of TAR's Method (Section 2-2).

$$d' = \int E(L)\, dL \qquad (3\text{-}5)$$

3.5 The Scaled Radius

The remainder of the problem is to derive a suitable scaling factor for the beam radius (ER). This procedure is much more complicated than that of determining the equivalent primary depth, since it must take into account the scattering in three dimensions. In a heterogeneous three dimensional medium, the relative importance of the scatter contribution from each voxel must also be considered. This

can be accomplished by assigning a weighting factor to each volume element of the medium. The scaling factor can thus be considered as a weighted average of the relative electron densities in the neighborhood of the calculation point.

$$ER = \frac{\sum\sum\sum E(i,j,k)\, W(i,j,k)}{\sum\sum\sum W(i,j,k)} \qquad (3\text{-}6)$$

where,

E(i,j,k) The relative electron density of volume element (i,j,k).

W(i,j,k) The weighting factor of volume element (i,j,k).

In order to scale the radius, the weighting factor for each volume element within the irradiated medium must be known. The relative importance to the total scatter of each volume element is dependent on a number of conditions (e.g. the energy of the irradiation, and the relative position of the scattering volume). Because of this, a different set of weighting factors must be found for every calculation point, requiring considerable computation time.

3.6 Weighting Factors

There are two different approaches that can be used to establish the weighting factors. The first approach is experimental (Wong and Andrew [21]). The process involves irradiating ring shaped concentric "air" voids submerged in

a water phantom. A differential comparison of doses at a point along the central axis, in the presence and absence of the void ring, yields information about the scatter contribution from the "air" volume in question. These measurements are very difficult to make since the dose differences are so small (typically less than 0.1%). The experimental results yield a set of weighting functions which are limited to an all water medium.

The second method for the determination of similar weighting factors is through the analytic calculation of differential Scatter Air Ratio (dSAR) values. The differential Scatter Air Ratio can be considered as the amount of scatter attributed to a small water element of volume dV. Exact values of dSAR's cannot be calculated in a heterogeneous medium because of the multiple scatter complexity, although calculation of primary, first scatter, and second scatter have been performed [20]. Thus, approximate dSAR values for an all water medium are used in determining the weighting factors.

In either the experimental or calculated approach, the weights cannot be easily determined for a heterogeneous medium. Indeed if they could be, that would be a solution to the inhomogeneity problem in itself.

Assumption 5: Weights for Water Medium.

Weights appropriate to an all water medium are assumed for each voxel in a heterogeneous medium. The different "scattering power" of each voxel is accounted for only through its density. There is no correction for attenuation to and from the voxel through a heterogeneous medium. The variance in photon attenuations along the scattered photon paths, to the calculation point (paths a and b in Figure 3-2 or 3-3) are ignored. The weights are calculated only on the basis of the geometric distances of the scattering volumes from the dose calculation point.

3.7 Determining the Weighting Factors

Approximate dSAR values for an all water medium are determined by splitting the scatter contribution into two separate components. One component is concerned with the first scattered photons while the second component involves multiply scattered photons. The sum of these two components gives the weighting factor.

$$W(i,j,k) = dSAR1(i,j,k) + dSARM(i,j,k) \qquad (3\text{-}7)$$

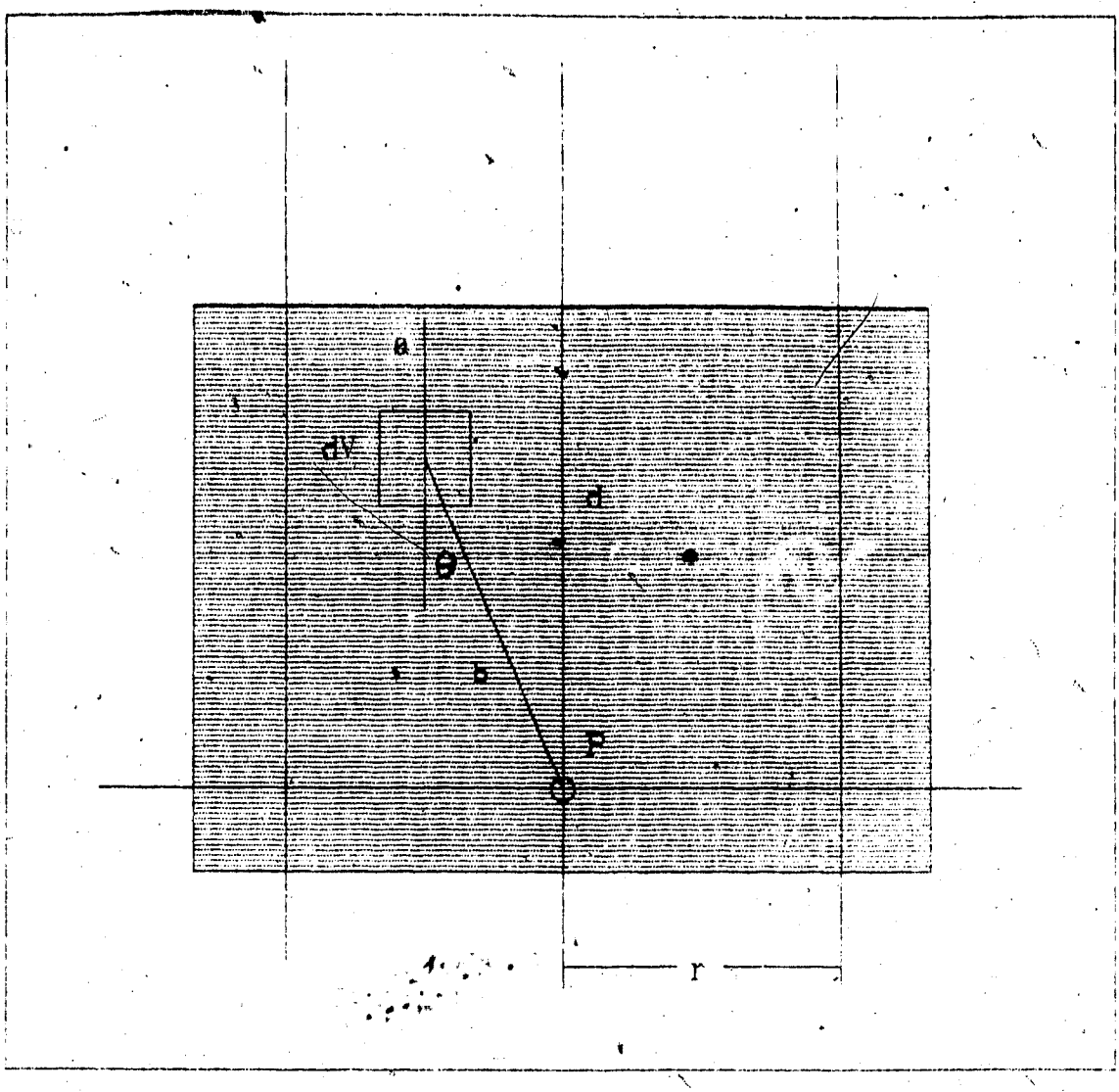

Figure 3-3

The scattering volume dV must scatter photons through an angle in order to contribute to the dose at point P. The paths a and b are assumed to be through water, and the scattering volume is also assumed to be water.

3.7.1 The First Scatter Component

The first scatter contribution can be calculated analytically by considering Figure 3-3, where,

ϕ	The photon fluence incident on the medium [photons/cm^2].
TAR(a,0)	Zero area TAR at depth (a).
SSD	Source to surface distance [cm].

The fluence reaching the scattering volume dV is given by,

$$TAR(a,0)\ [SSD/(SSD+a)]^2\ \phi \qquad (3\text{-}8)$$

where beam divergence and primary attenuation are considered. The implicit assumption here is that the medium above the scattering volume is water (Assumption 5).

The probability of a scattered photon from dV reaching the calculation point, P, is,

$$\exp(-\mu_w b)\ n_w \frac{dV}{b^2} \frac{d\sigma}{d\Omega} \qquad (3\text{-}9)$$

where,

$\frac{d\sigma}{d\Omega}$	Nishina scattering probability [probability/electron/solid angle].
n_w	Electron density for water [electrons/cm^3]
$1/b^2$	Solid angle.

$_1\mu_w$ The linear attenuation coefficient in water for the scattered photon energy [cm].

This equation takes into account the Compton scatter probability only (Assumption 1), divergence from the scattering point, and attenuation along the scatter paths. Again the implicit assumption is that the scatter path is occupied by water only (Assumption 5).

Thus the first scattered photon fluence reaching the calculation point is,

$$TAR(a,0)[SSD/(SSD+a)]^2 \Phi \exp(-{}_1\mu_w b)\, n_w \frac{dV}{b^2} \frac{dq}{d\Omega} \quad (3\text{-}10)$$

Now, this fluence must be related to the absorbed dose at the destination point, P.

$$Dose = \Phi_a \, {}_1\mu_w \, {}_1E_{a,b} / \varepsilon \quad (3\text{-}11)$$

where,

$_1E_{a,b}$ Average energy absorbed per interaction at the scattered photon energy [energy/interaction].

ε The physical density [g/cm^3].

Thus the first scatter component of the weight (dSAR1) is,

$$dSAR_1 = TAR(d,0)\,[SSD / (SSD+d)]^2\,\{\,{}_1\mu_w\,{}_1E_{ab} / \rho\, D_{AIR}\,\}\cdot \Phi \exp(-{}_1\mu_w b)\, n_w \frac{dV}{b^2}\frac{d\sigma}{d\Omega} \qquad (3\text{-}12)$$

where:

D_{AIR} The dose in air [energy/g].

This equation contains the implicit assumption of an all-water medium in which all interactions in the scattering volume occur via the Compton process only and that electronic equilibrium exists (Assumptions 1 , 3 and 5).

3.7.2 The Multiple Scatter Component

The equation used to calculate the first scatter component of the weights can be suitably modified to approximate the multiple scatter component. Instead of using the primary fluence at the scattering volume, the scattered fluence is used. This is accomplished by replacing the zero area TAR by the Scatter Air Ratio. In the first scatter component, it was assumed that the zero area TAR represents the primary photons reaching the scattering volume. Similarly the SAR represents the scattered photons reaching the scattering volume in question. The Nishina cross section is also replaced by a fraction of the total Compton cross section. The substitutions are thus as follows:

$$TAR(a,0) \equiv SAR(a,r)$$

$$\frac{d\sigma}{d\Omega} \qquad \frac{\sigma}{4\pi}$$

Assumption 6: Multiple scatter is isotropic.

The multiple scatter component of the weights assumes that multiple scatter within the medium is isotropic (hence the 4c above).

All energy dependent components of the equation (linear attenuation coefficient, average energy absorbed) use the average second scattered photon energy. Thus the multiple scatter component of the weight (dSARM) is approximated by,

$$dSAR_m = SAR(a,r)[SSD/(SSD+a)]^2 \Phi \exp(-2u_w b) \frac{dV}{b^2} \frac{\sigma}{4\pi} n_w$$

$$x \{ 2u_w 2E_{ab} / \varepsilon D_{AIR} \} \quad (3\text{-}13)$$

Again in this equation the all-water assumption is implicit and all interactions in the scattering volume are assumed to occur via the Compton process (Assumptions 1 and 5).

Thus the weighting factors are now determined, which in turn determines the scaled radius. We have a complete method for the calculation of dose in a heterogeneous medium, if we assume "water weights" are a first order approximation of the true weights in a heterogeneous medium. Before it can be

applied to any practical situations, a number of further simplifications must be made in order to exploit the format of CT scan data, accelerate the computational procedure, and reduce memory storage requirements.

3.8 The Separability of the Weighting Function

Assumption 7: The weighting function is separable.

The first practical approximation of the weighting functions, is to assume that they may be separated into two independent multiplicative components.

$$W(i,j,k) = W(i,j)\, W(k) \qquad (3\text{-}14)$$

where W(k) is the "slice weights" function and is assumed to be independent of the x and y coordinates. This weight is intended to represent the contribution, to the scatter dose, of the k'th slice. Thus from equation 3-6 the scaling factor can be written as,

$$ER = \frac{\sum\sum\sum E(i,j,k)\, W(k)\, W(i,j)}{\sum\sum\sum W(k)\, W(i,j)} \qquad (3\text{-}15)$$

$$ER = \frac{\sum\sum E(i,j)\, W(i,j)}{\sum\sum W(i,j)} \qquad (3\text{-}16)$$

where,

$$E(i,j) = \frac{\sum E(i,j,k)\, W(k)}{\sum W(k)} \qquad (3\text{-}16a)$$

This separation results in a three dimensional volume summation being "collapsed" to a two dimensional planar summation.

The W(k) weights are applied to all voxels within a particular slice to produce a modified slice. All of the modified slices are then projected into a single "effective scattering plane". The net effect of this coalescing is to reduce the entire irradiated volume into a single heterogeneous slice with appropriate "scattering power" (Figure 3-4).

3.9 Determining the Slice Weights

The W(k) weights can be considered as the relative importance of the k'th slice to the total scattered dose at the point of calculation. One method of determining the slice weights is through differential Scatter Air Ratios. Consider the SAR of a field size which includes the k'th slice. From this, subtract the SAR for a smaller field which excludes the k'th slice. This quantity now gives the amount of scatter originating within the entire k'th slice (assuming water is in the intervening space).

$$W(k) = SAR(d_{REF}, r_{LARGE}) - SAR(d_{REF}, r_{SMALL}) \quad (3\text{-}17)$$

This method of calculating the slice weights implicitly assumes a water medium and involves further simplifications.

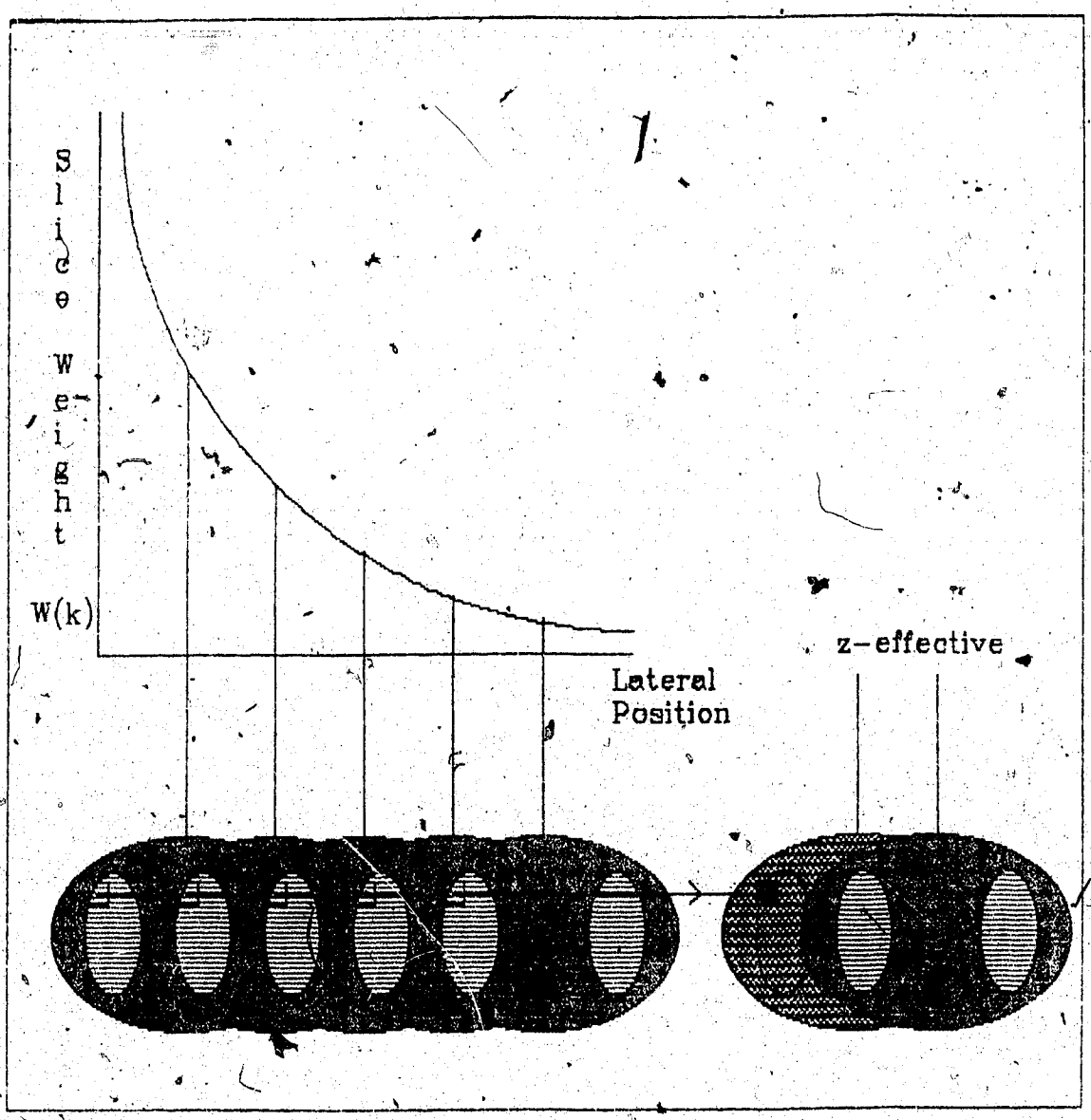

Figure 3-4

The weighting function asigns a weight to each slice. The seperate slices are then coalesced to form an effective scattering plane, which is then positioned a distance z-effective away from the calculation plane.

Assumption 8: Arbitrary reference depth.

It is assumed that the SAR values are being determined for an all-water medium at an arbitrary reference depth. The value used for the reference depth, has to be suitably chosen so that the value of the weight will be an average of all possible depths of interest within that slice.

3.10 Scatter Slice Placement

Now that the effective scattering slice has been determined, the question still remains as to where this scattering slice should be located. The relative position of the scattering slice is called the " z-effective" value. This position can be considered as the most probable position from which scatter originates. The value of z-effective is determined as a weighted average of the position, over the entire irradiated volume.

$$z_{EFF} = \frac{\Sigma \; z(k) \; W(z)}{\Sigma \; W(z)} \qquad (3\text{-}18)$$

This distance is the first moment of the weights function. (It is analogous to the mean lifetime in radioactive decay or the center of mass in mechanics).

At this point another major assumption is made. It is assumed that the material between the effective scattering slice and the calculation plane is composed of water (This is just another variant of Assumption 5).

3.11 Determining the Weights Within the Scatter Slice

The effective scattering slice has now been both determined and positioned. The pixel scattering weights W(i,j) must now be calculated at each pixel in the scattering slice. The previously derived weight equations (Equations 3-12 and 3-13) are used to calculate these weights. However, rather than calculating weights over the entire irradiated volume, the procedure is now done only for each pixel in the effective scattering slice (a direct benefit of the coalescing procedure).

Assumption 9: Scatter Grid Size.

In calculating these weights a practical assumption is made. Theoretically, the resolution of the scattering slice could be just as fine as in the original image (256 x 256). However this would require lengthy calculation times. In order to reduce the calculation time to an acceptable level, the image is "diluted" by using a coarser scatter matrix or grid. This reduces the number of weights W(i,j) which have to be calculated.

3.12 Summary of the Practical Method

With all of these simplifying assumptions, it is advantageous to list a brief "recipe" of the practical implementation.

The first step, is to determine the scaled depth. This is the radiological or equivalent water depth and is done for every calculation point, ray by ray.

The next step is to determine the effective scattering slice using the relative electron densities of each voxel and the weight of the slice in which the voxel resides. This produces a heterogeneous slice in which each pixel is an average, along a perpendicular line into neighboring slices. The scattering slice is a representation of the average inhomogeneity over the entire irradiated volume. Once this effective scattering slice is derived, its position relative to the calculation plane is determined. This is done by finding the "center of scatter" of the weights function W(k). The procedure of slice coalescing and positioning is performed only once for each beam of radiation (ie. energy and field size dependant).

Next the scatter weights W(i,j) for each voxel within the effective scattering plane must be determined. From

these weights, the average density of the volume surrounding each calculation point is determined and the radius is scaled. This process must be repeated for each pair of scattering and calculation points, and is the bulk of the computational burden.

Finally it is a simple procedure to calculate the Inhomogeneity Correction Factor for each calculation point, as a ratio of TAR's. It is evident that some of the numerous assumptions of the method should be validated individually. This is the subject of Chapter 4.

4. Results, Evaluation, and Critique of the Equivalent Tissue Air Ratio Method

4.1 Introduction

This chapter contains a more detailed evaluation and analysis of the Equivalent Tissue Air Ratio Method. In this chapter a number of experimental results will be presented. Some of the major assumptions highlighted in Chapter 3 will be investigated in detail to determine their validity.

4.2 Experimental Observations

4.2.1 The Slab Phantom

One of the phantoms used to test the Equivalent Tissue Air Ratio Method is the slab phantom [9] (Figure 4-1) already described in Section 2.3. Experimentally this phantom was used to measure the Inhomogeneity Correction Factors along the central axis for three different beam energies; Cobalt, 6-MV, and 15-MV x-rays. The experimental results are shown in Figures 4-2, 4-3, and 4-4, along with the predicted results from the simple Ratio of TAR's and the Equivalent TAR methods. Some of these results were previously discussed in Section 2.3 of Chapter 2.

The graphs generally show that the Equivalent TAR method more closely predicts the experimentally observed

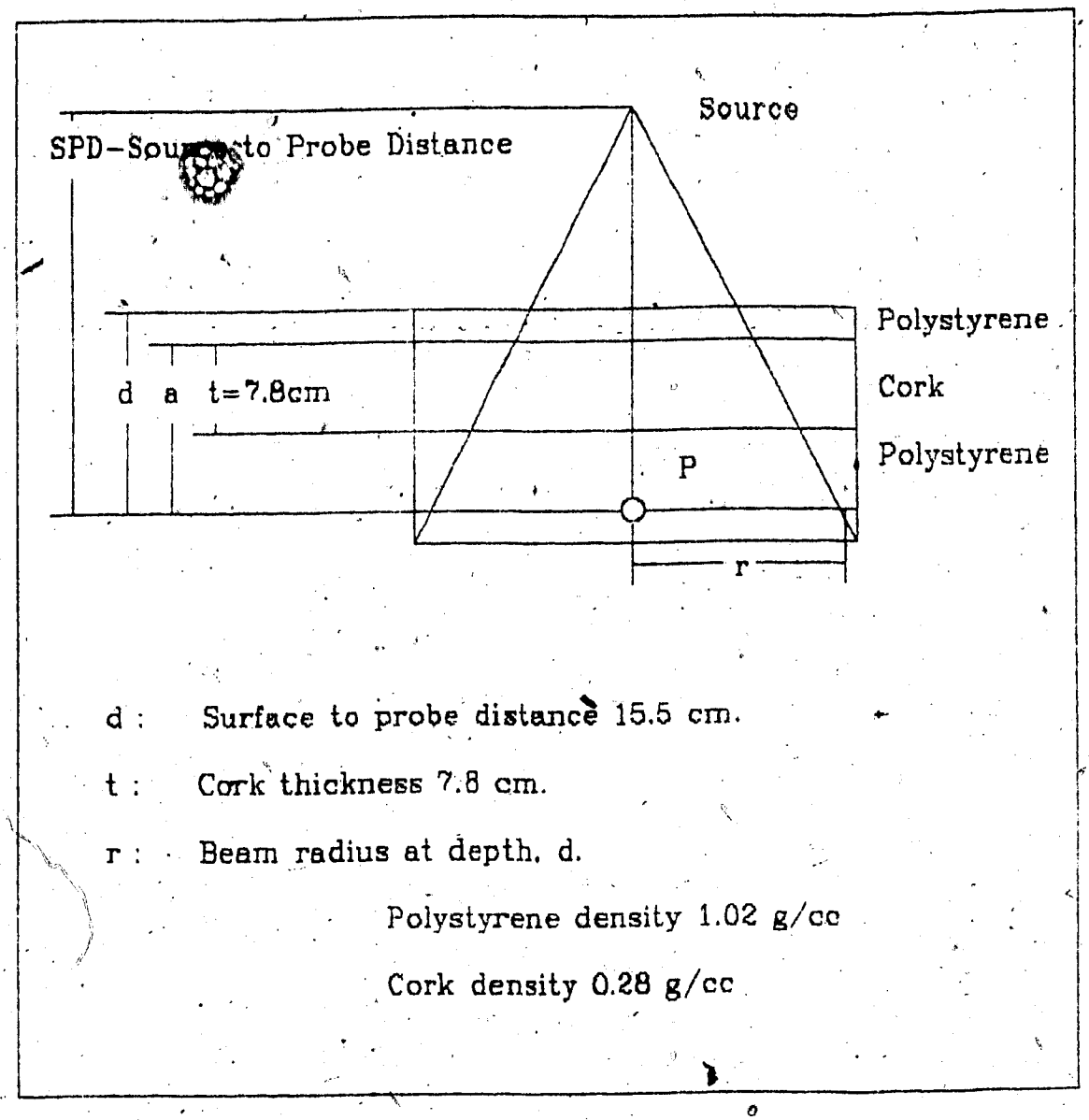

Figure 4-1

The Slab Phantom used for both experimental and calculated results.

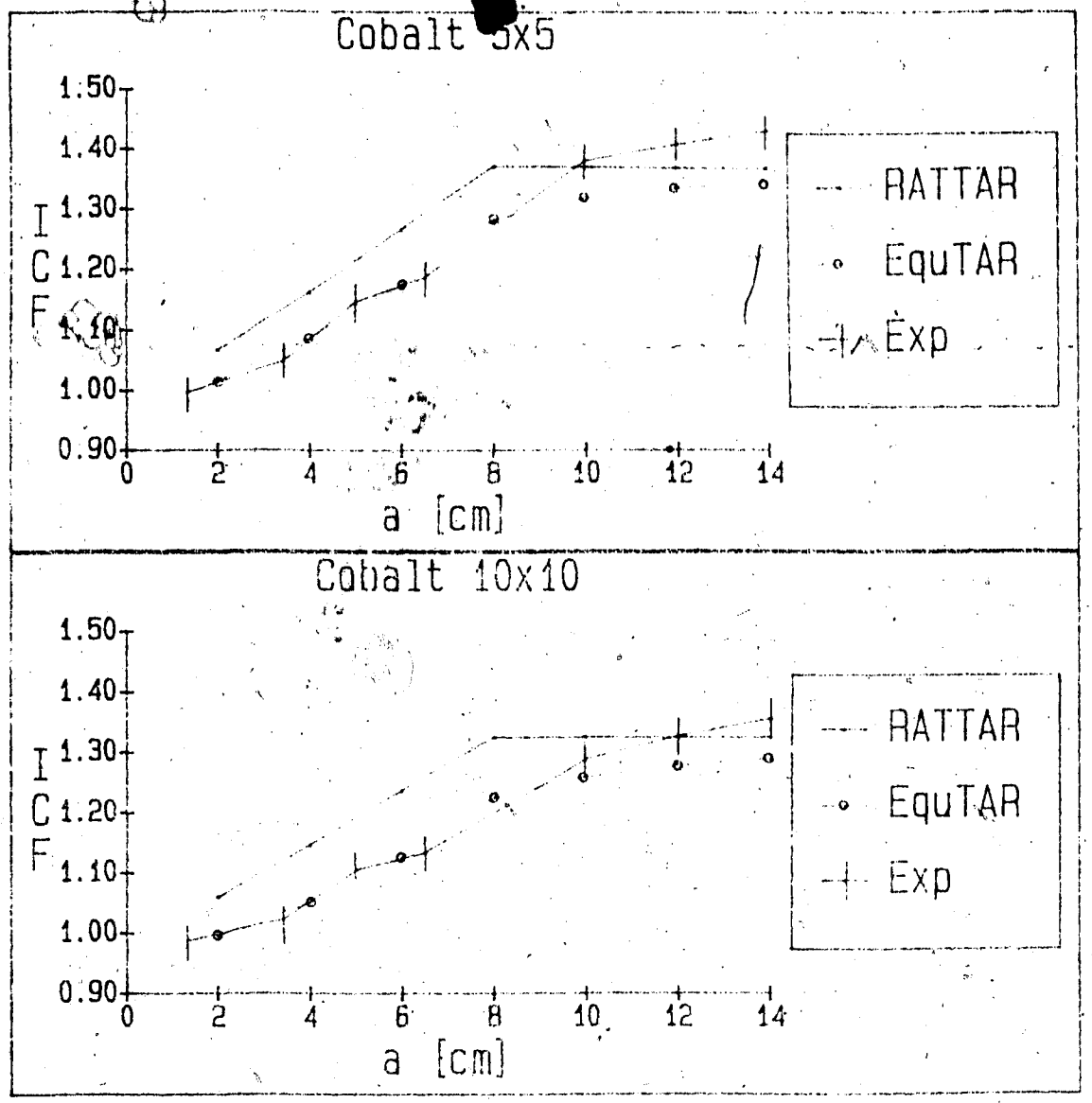

Figure 4-2

Inhomogeneity Correction Factors for Cobalt beam energy and field sizes; 5x5, 10x10. Calculated ICF's are plotted for the Ratio of TAR's and Equivalent TAR methods for comparison with experimentally measured values.

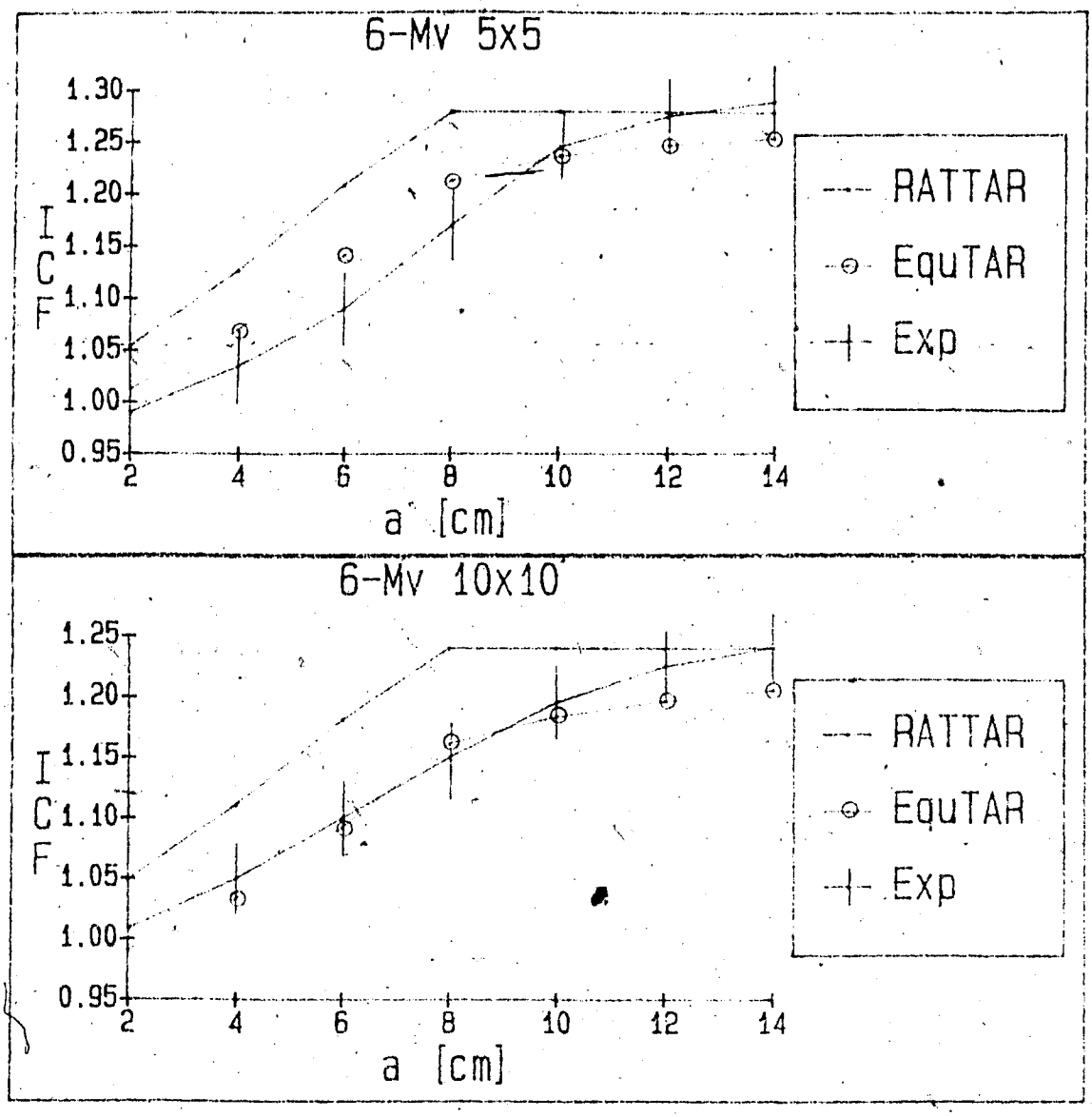

Figure 4-3

Inhomogeneity Correction Factors for a beam energy of 6-Mv and field sizes; 5x5, 10x10. Calculated ICF's are plotted for the Ratio of TAR's and Equivalent TAR methods for comparisons with experimentally measured values.

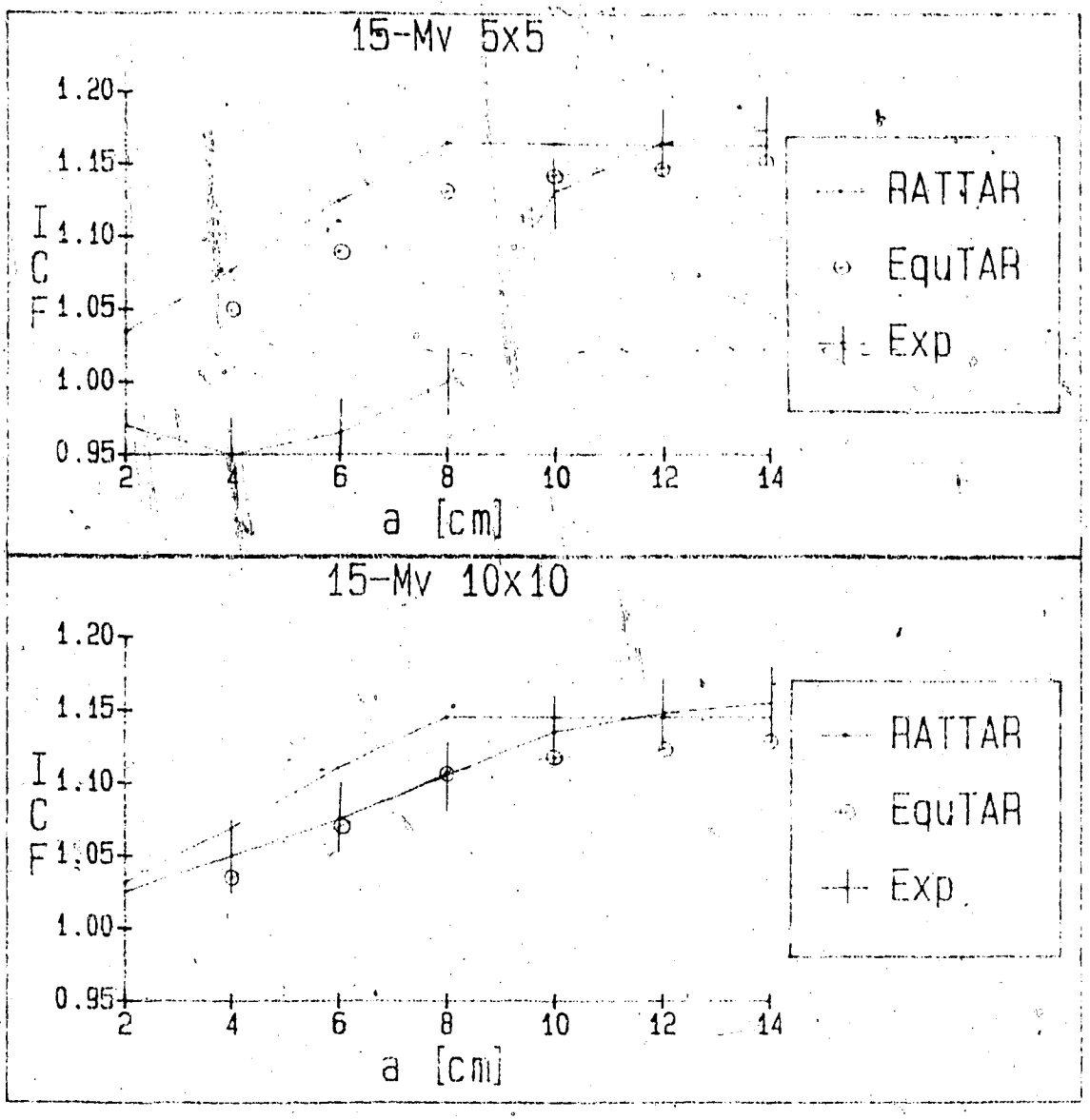

Figure 4-4

Inhomogeneity Correction Factors for a beam energy of 15-Mv and field sizes; 5x5, 10x10. Calculated ICF's are plotted for the Ratio of TAR's and Equivalent TAR methods for comparison with experimentally measured values.

values than does the simpler Ratio of TAR's method within the cork. The chief reason for this better prediction is that the Equivalent TAR method attempts to correct for the reduction in scatter originating in the cork slab.

For small beam sizes and high energies (eg. 5x5 at 15-MV) the Equivalent TAR fails to predict accurate Inhomogeneity Correction Factors. This is due to the fact that Assumption 3 (Electronic Equilibrium) becomes invalid under these circumstances.

4.2.2 The Double Lung Phantom

This phantom more closely resembles the anatomy of the mediastinum. It consists of two "lungs" embedded within a unit density (1.00 g/cm^3) material. The lungs were represented by two cork blocks (10x7x(the length of the phantom) cm^3 and density 0.30 g/cm^3). The central axis of the phantom lies directly in between the two lungs which are spaced 2.5 cm. apart (Figure 4-5). This means that there are no inhomogeneities along the central axis; thus any difference in the dose along this axis is due only to the change in lateral scatter. The simpler inhomogeneity correction algorithms (Ratio of TAR's, Batho) will predict an Inhomogeneity Correction Factor of 1.00 along the central axis, since this ray misses the lungs. The Equivalent TAR method does produce correction factors of less than unity

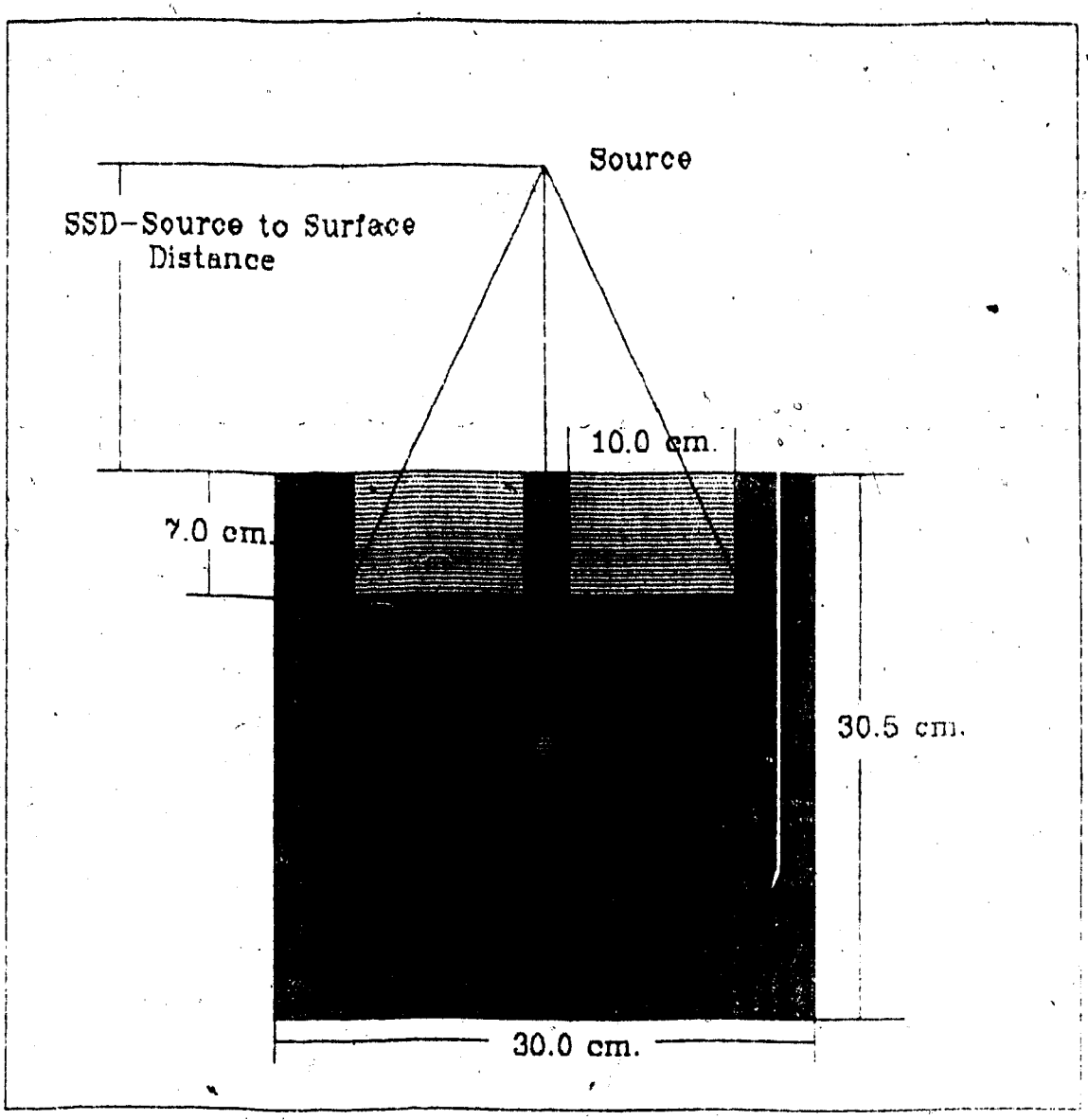

Figure 4-5

The Double Lung Phantom consists of two lungs (Density 0.30 g/cc) imbedded within a unit density (1.00 g/cc) material. The central axis does not contain any inhomogeneities thus any change in correction factor is due to scatter alone.

along the central axis, since it senses the reduction in scatter. Figure 4-6 shows the calculated correction factors obtained from the Ratio of TAR's and Equivalent TAR methods compared to previously measured experimental values [19] for a 20x20 Cobalt beam.

Figures 4-7, 4-8, and 4-9, show the effects of different field sizes and energies on the calculated correction factors for this double lung phantom. All graphs show a "well-shaped" profile. This profile is due to the change in scatter conditions as a function of depth. The deepest portion of the well is the point at which the reduction in the scatter contribution is the greatest. The lungs are less dense than the surrounding material and they produce less scatter. For deeper point, the inhomogeneity correction increases toward unity because scatter from the regions in the shadow of the cork is enhanced.

The second observation is an energy dependant effect. For each beam size, the ICF value is greater as the energy increases. For a higher energy beam the relative importance of the scatter component is reduced (Section 4.3.2). This phantom was designed to look exclusively at the scatter component, hence there will be less of an effect when the scatter is less important.

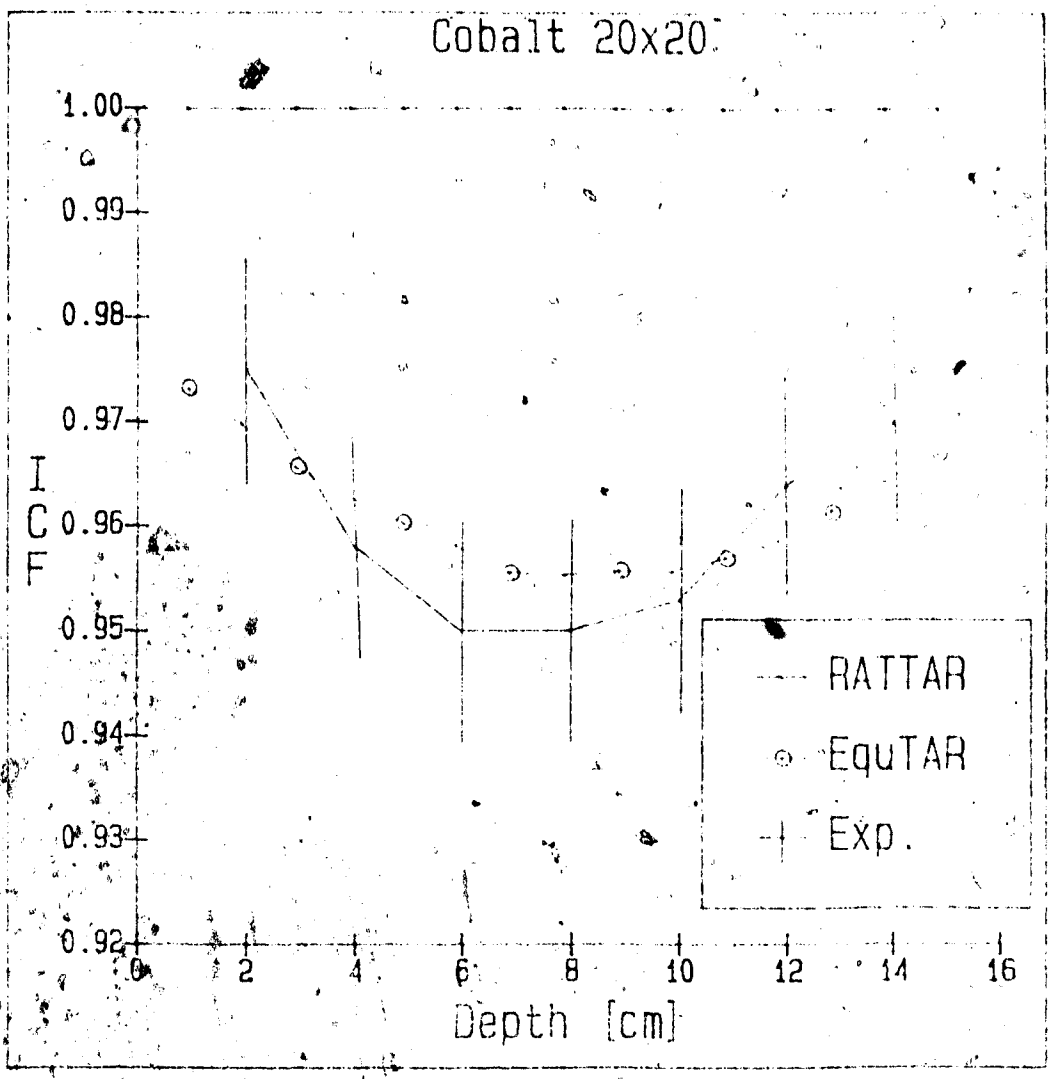

Figure 4-6

The Inhomogeneity Correction Factor as a function of central axis depth within the double lung phantom for a 20x20 Cobalt beam.

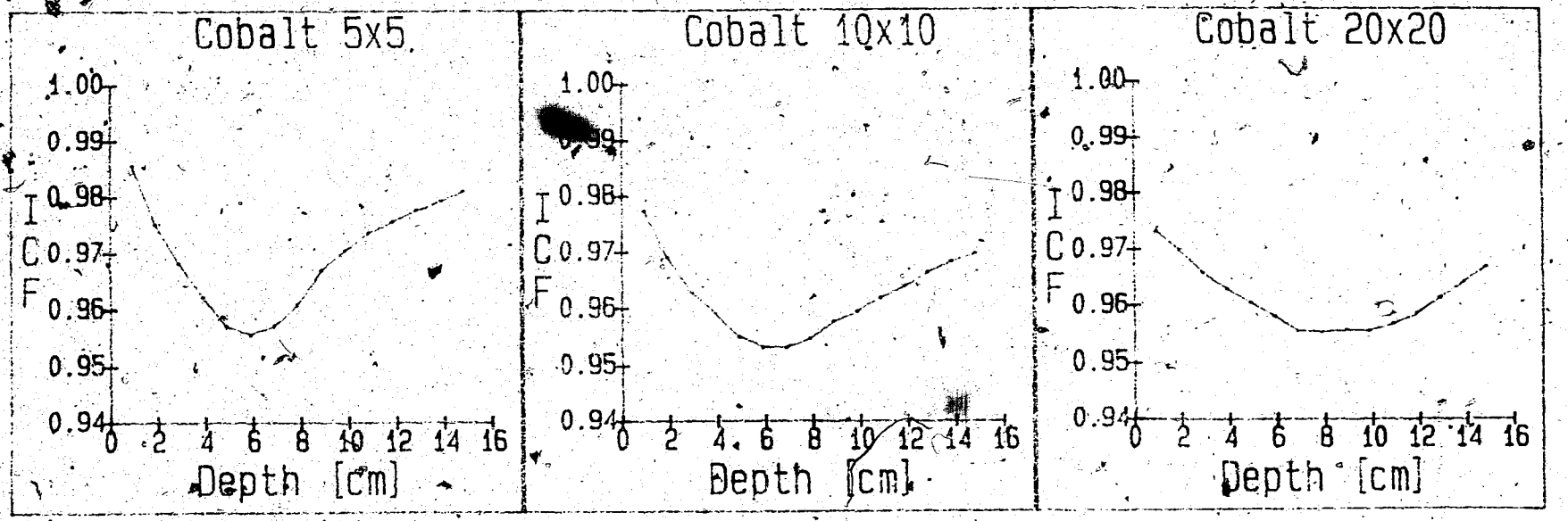

Figure 4-7

Central axis Inhomogeneity Correction Factors for the double lung phantom using a number of different Cobalt beam sizes.

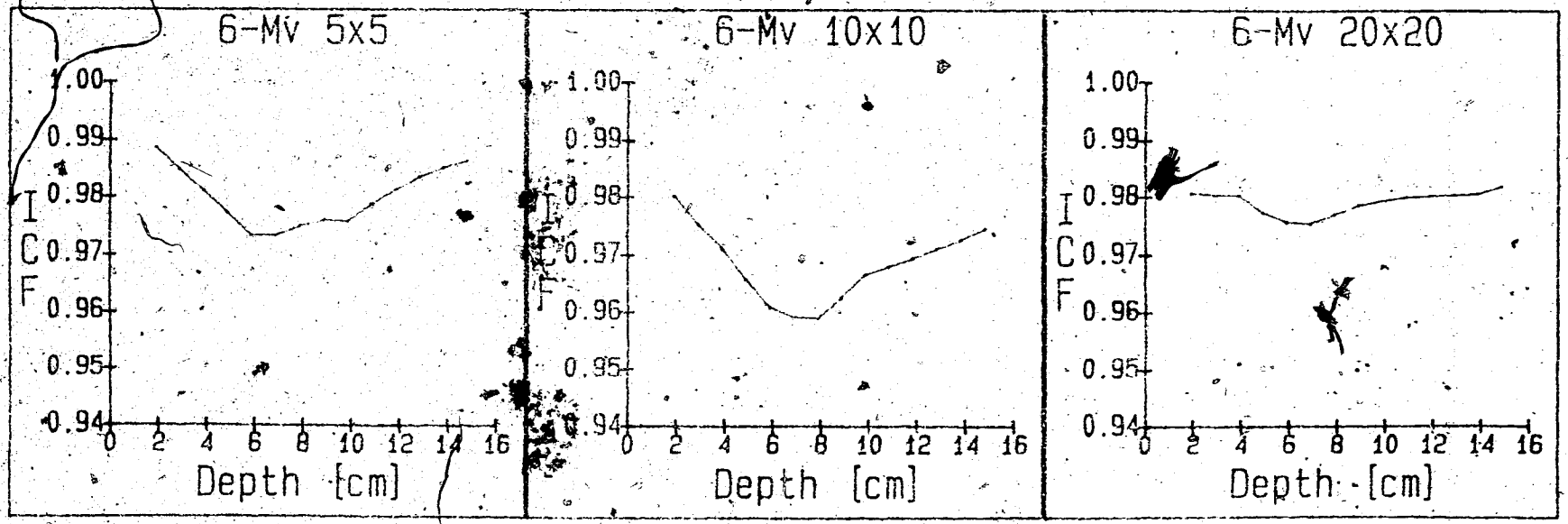

Figure 4-8

Central axis Inhomogeneity Correction Factors for the double lung phantom using a number of different 6-Mv beam sizes.

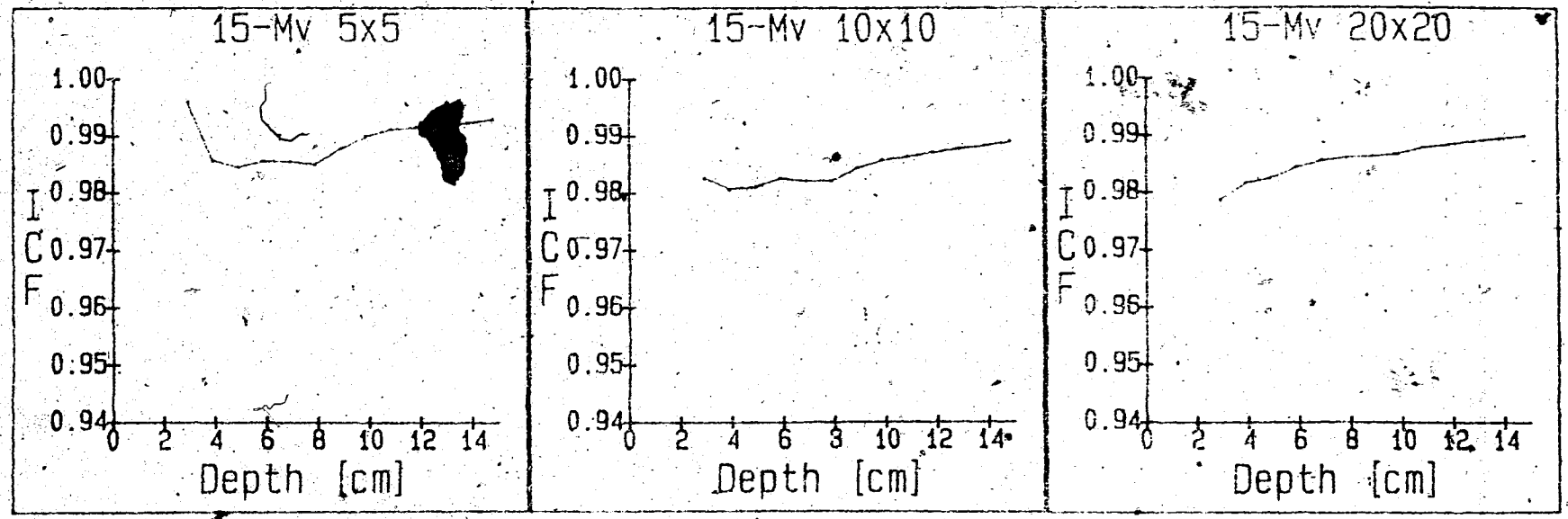

Figure 4-9

Central axis Inhomogeneity Correction Factors for the double lung phantom using a number of different 15-Mv beam sizes.

The density of the lungs is also very important. The low density lungs are seen to decrease the Inhomogeneity Correction Factor because less scatter originates from them. If the density of the lungs were increased above unity, they would contribute more scatter than the surroundings and the ICF should rise above unity instead of fall. This was indeed observed. Figure 4-10 shows an interesting result when the lungs are unequal (one with high density and the other with low). The lack of scatter from the one lung was compensated by the other lung, thus giving the net impression that both lungs were of unit density.

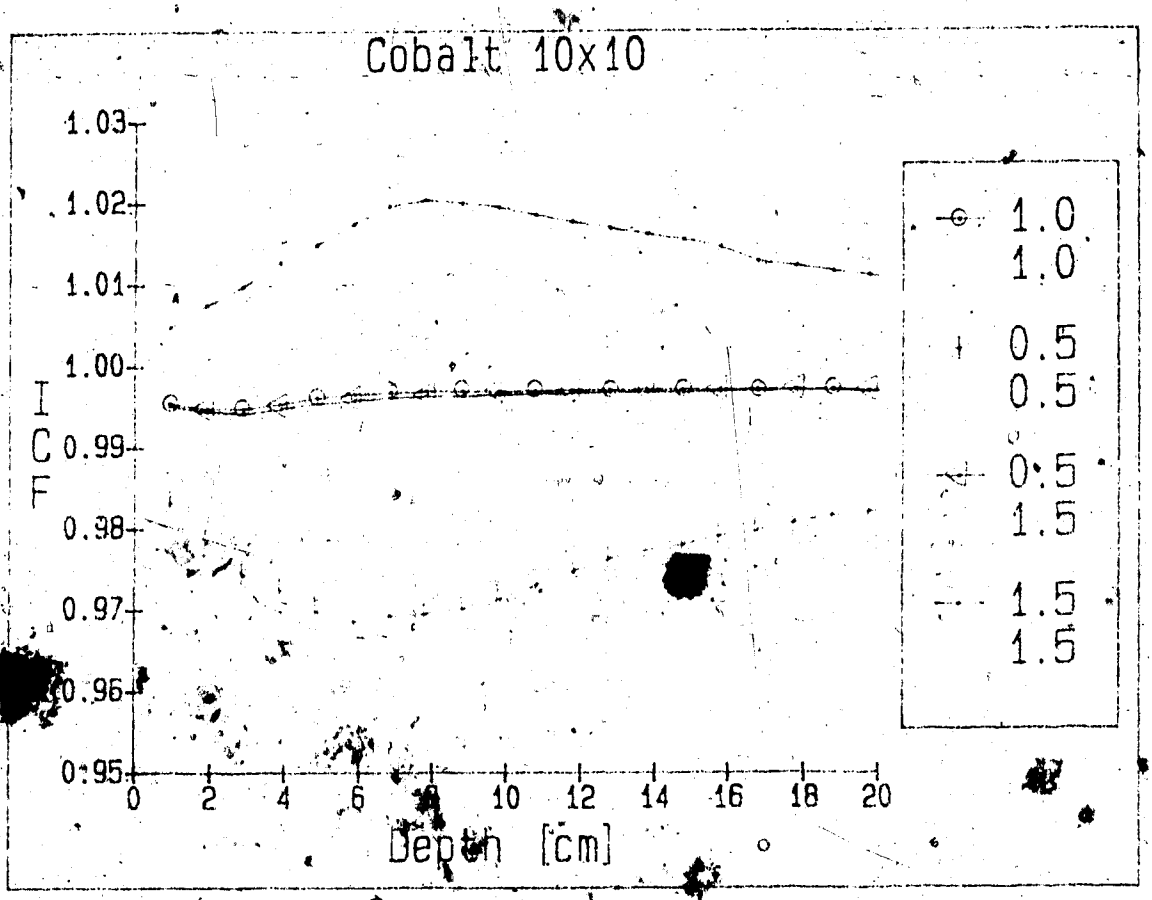

Figure 4-10.

The effect of varing the lung density, in the double lung phantom. The numbers in the legend refer to the relative electron densities of each lung.

4.3 Assumptions

4.3.1 Assumption 1: Compton Dominance

As stated in Section 3.2, the first and most important assumption in the Equivalent Tissue Air Ratio Method is that the Compton process is the dominant interaction between photons and tissue. From Figure 4-11 [6] it can be seen that the Compton process accounts for more than 50% of the interactions between the energy range of 10 keV and 5 Mev. If the Equivalent TAR Method is used within this energy range, then indeed the Compton process is dominant and O'Connor's Theorem is applicable. At the energy of Cobalt (1.17 and 1.33 Mev) the Compton process accounts for 99.8% of the primary interactions, and at this energy the assumption is definitely a valid one. The Equivalent TAR method was developed initially and tested for Cobalt-60 radiation.

As the beam energy increases, it must be kept in mind that the Compton process becomes less dominant and that the errors in the methods results will be due, in some part, to the break down of this assumption. For 15-MV x-rays, the effective photon energy is approximately 5 Mev [8], for which there remains a 95 % dominance in water. In other tissues of higher atomic number (i.e. bone), the assumption will break down further [6].

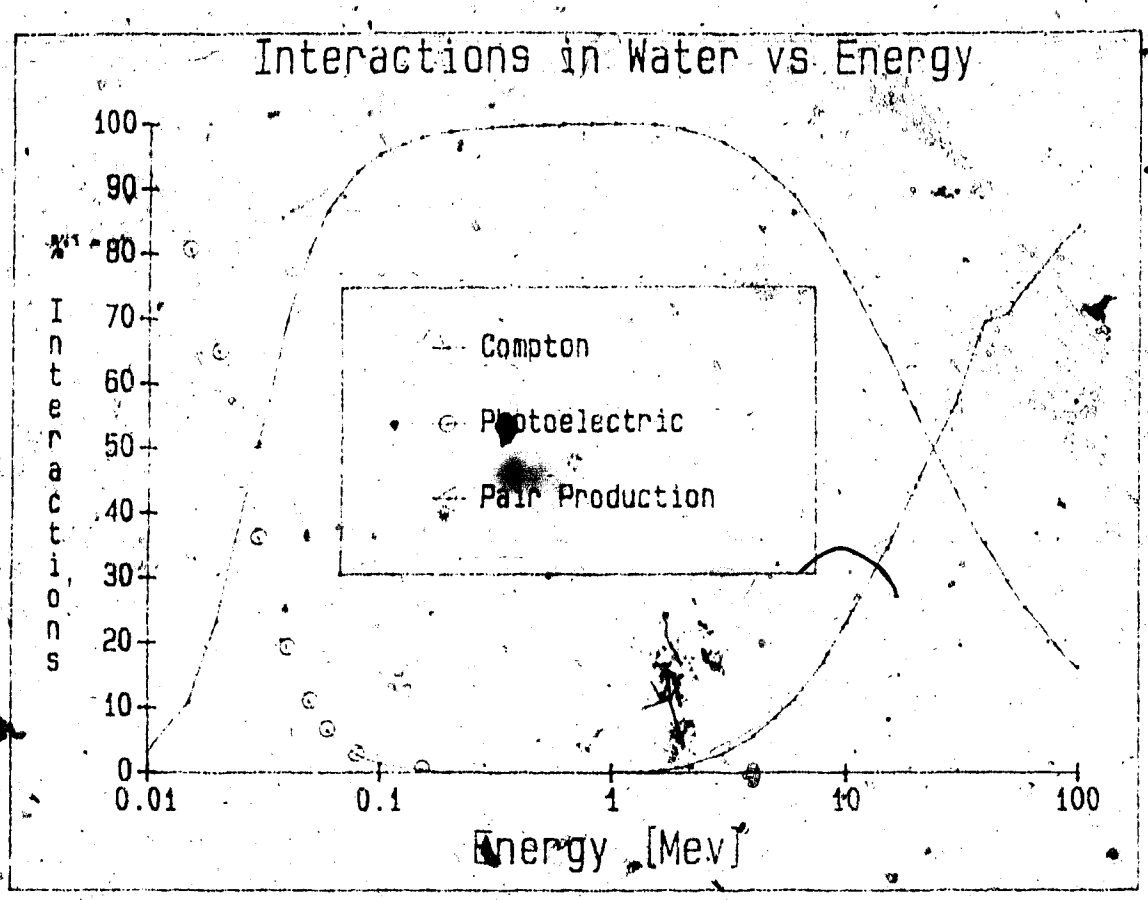

Figure 4-14

The percentage of photon interactions in water as a function of energy. The Compton process is dominant at the intermediate energies studied in this work, 1.17, 1.33 Mev (Cobalt), 2 Mev (6-Mv), 5 Mev (15-Mv).

4.3.2 Assumption 2: Primary and First Scatter Dominance

The primary component of the radiation field is the most important component in delivering the absorbed dose. The primary component is directly related to the zero-area Tissue Air Ratio, which corresponds to a pencil beam of radiation. The percentage of the dose due to the primary component at a point can be calculated by considering a ratio between the zero-area TAR and the total Tissue Air Ratio. Similarly, a ratio between the Scatter Air Ratio and the Tissue Air Ratio will yield the percentage of dose due to the overall scatter component of the field. Figures 4-12 and 4-13 show the percentage of the dose due to the primary and the scatter components of the radiation field as a function of different beam sizes for Cobalt and 15 MV energy. These data are for an all water medium at a reference depth of 10 cm.

These graphs show that as the field size increases the fractional primary component decreases while the scatter component becomes increasingly more important. For a typical field size of 10x10 cm^2, the primary component is responsible for 80 % of the absorbed dose at a depth of 10 cm. for Cobalt radiation. As the energy increases, the relative importance of the primary component also increases. This means that the scatter corrections will be less

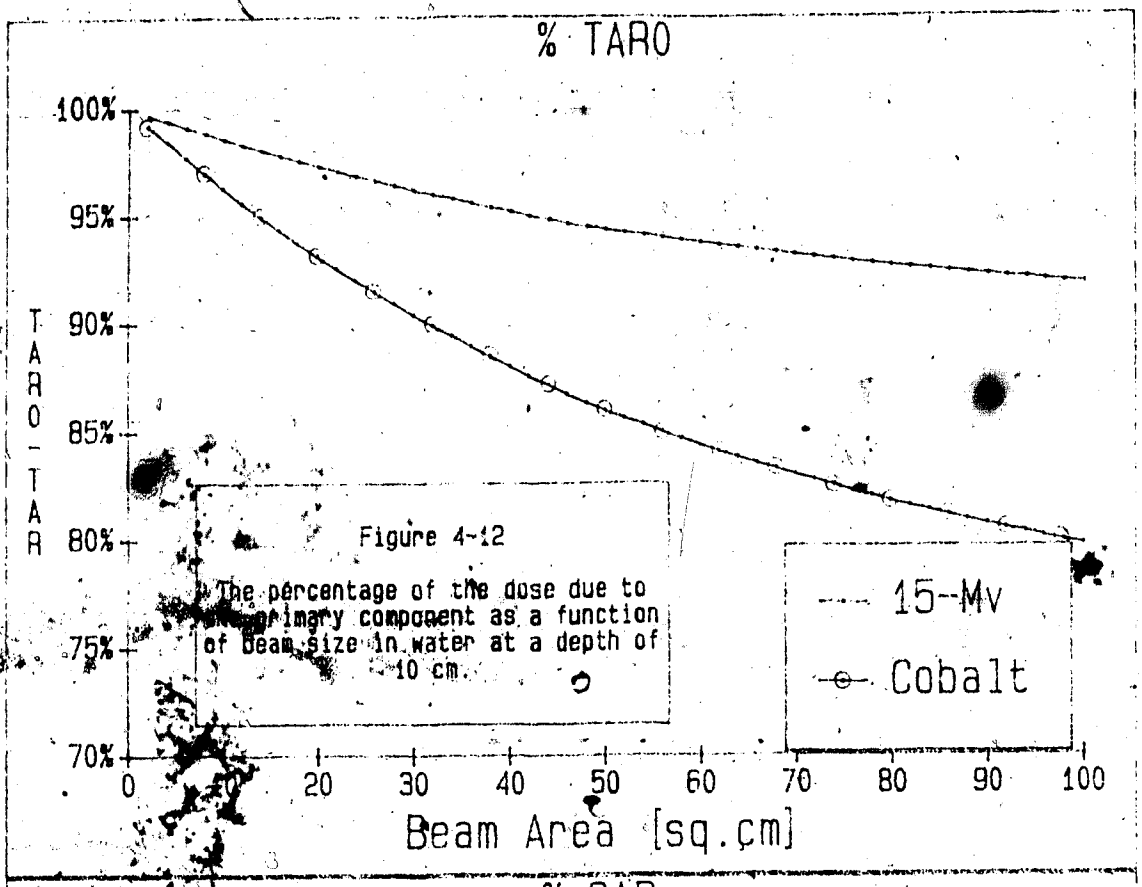

Figure 4-12

The percentage of the dose due to the primary component as a function of beam size in water at a depth of 10 cm.

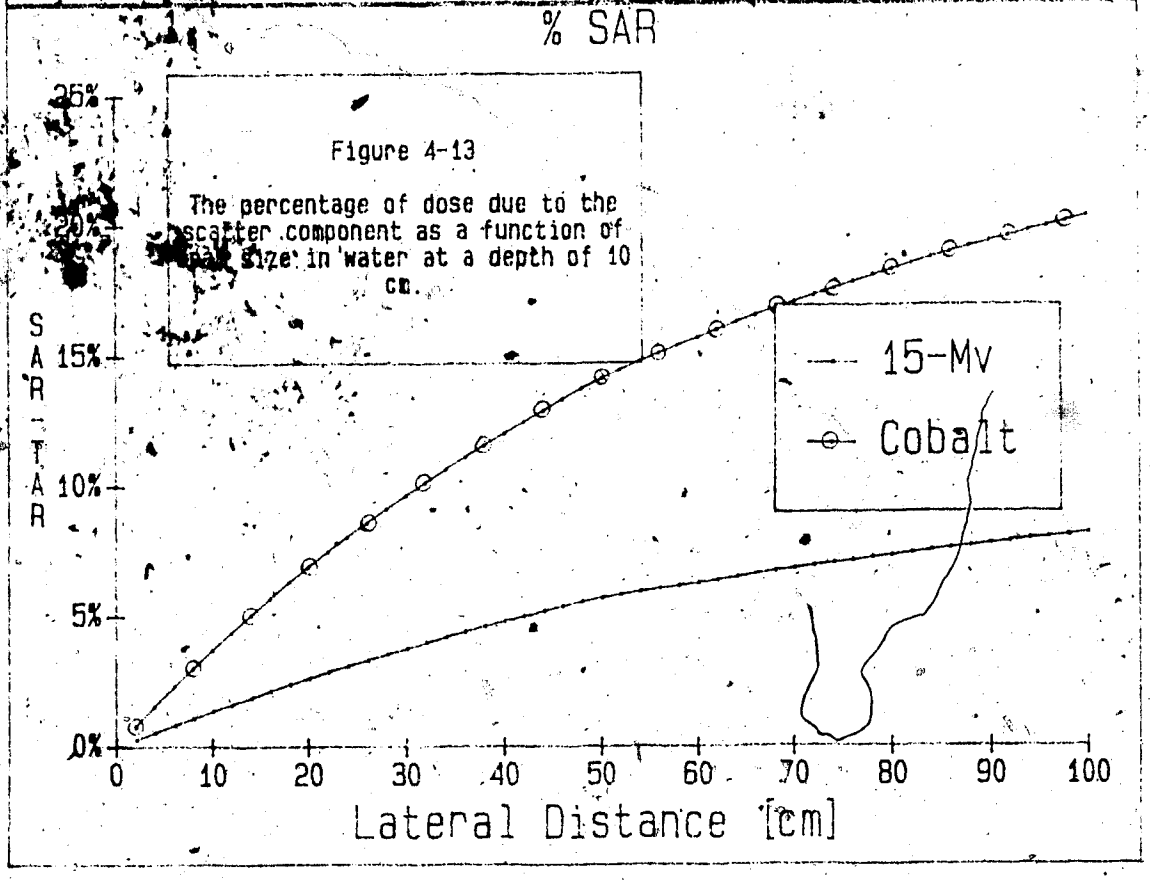

Figure 4-13

The percentage of dose due to the scatter component as a function of beam size in water at a depth of 10 cm.

important (compared to the primary) at higher energies than at lower energies.

The zero-area Tissue Air Ratio by definition, is independent of field size, but relative to the total TAR, its importance decreases with increased field size; because more scatter is contributing to the total dose. As the field size increases the volume of irradiated material increases, thus yielding more scatter.

If the field size is held constant and the depth is varied, it can be seen in Figure 4-15 that the scatter component of the dose increases with depth. Scatter is generally directed in the forward direction so that as the depth increases there is more irradiated material above the point in question. Thus there is more scatter reaching the points at moderate depths. For deeper points, the gain in scatter is offset by attenuation losses.

It is difficult to fragment the total scatter into the single and multiple scatter components. The Equivalent Tissue Air Ratio Method attempts to correct for single and multiple scatter through the use of weighting factors that calculate each component separately. Wong investigated the difference between first and second scatter dose contributions [20] for Cobalt radiation. He, used semi-analytic and direct numerical integration to study the

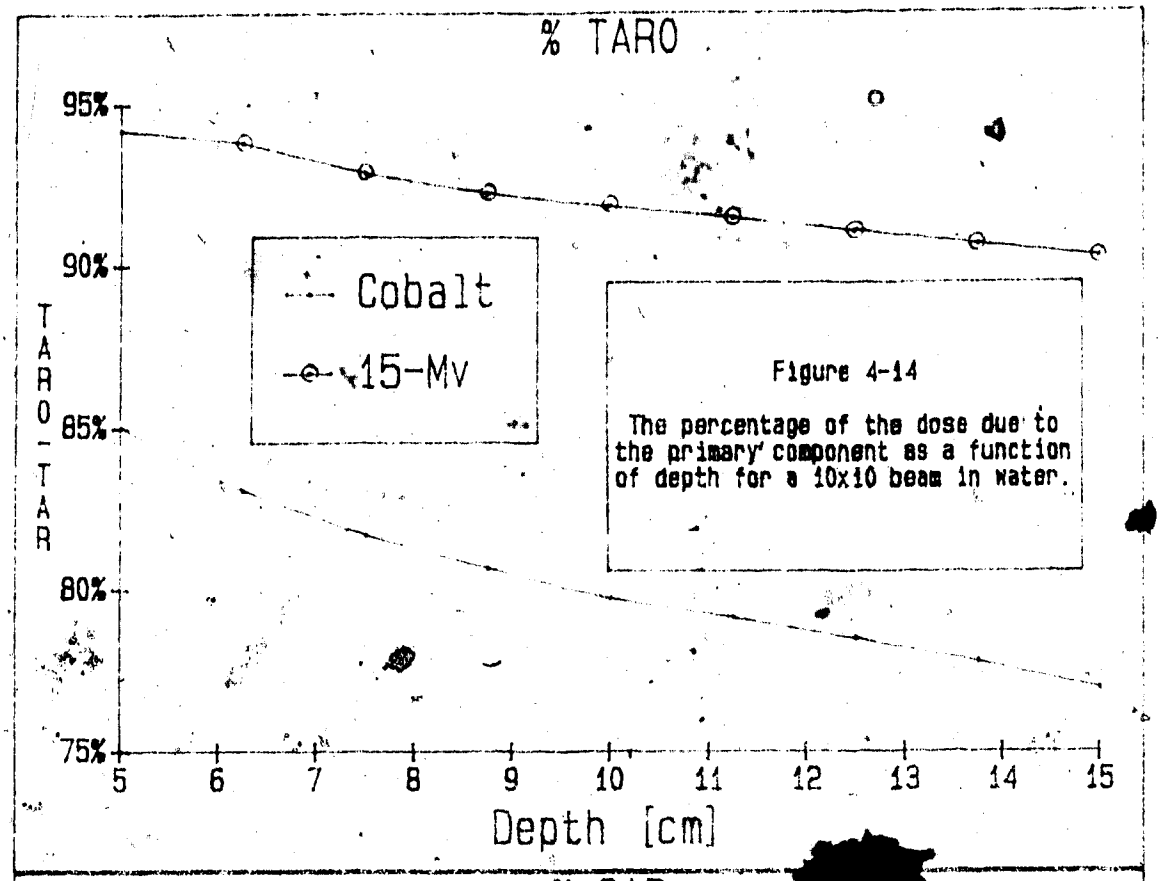

Figure 4-14

The percentage of the dose due to the primary component as a function of depth for a 10x10 beam in water.

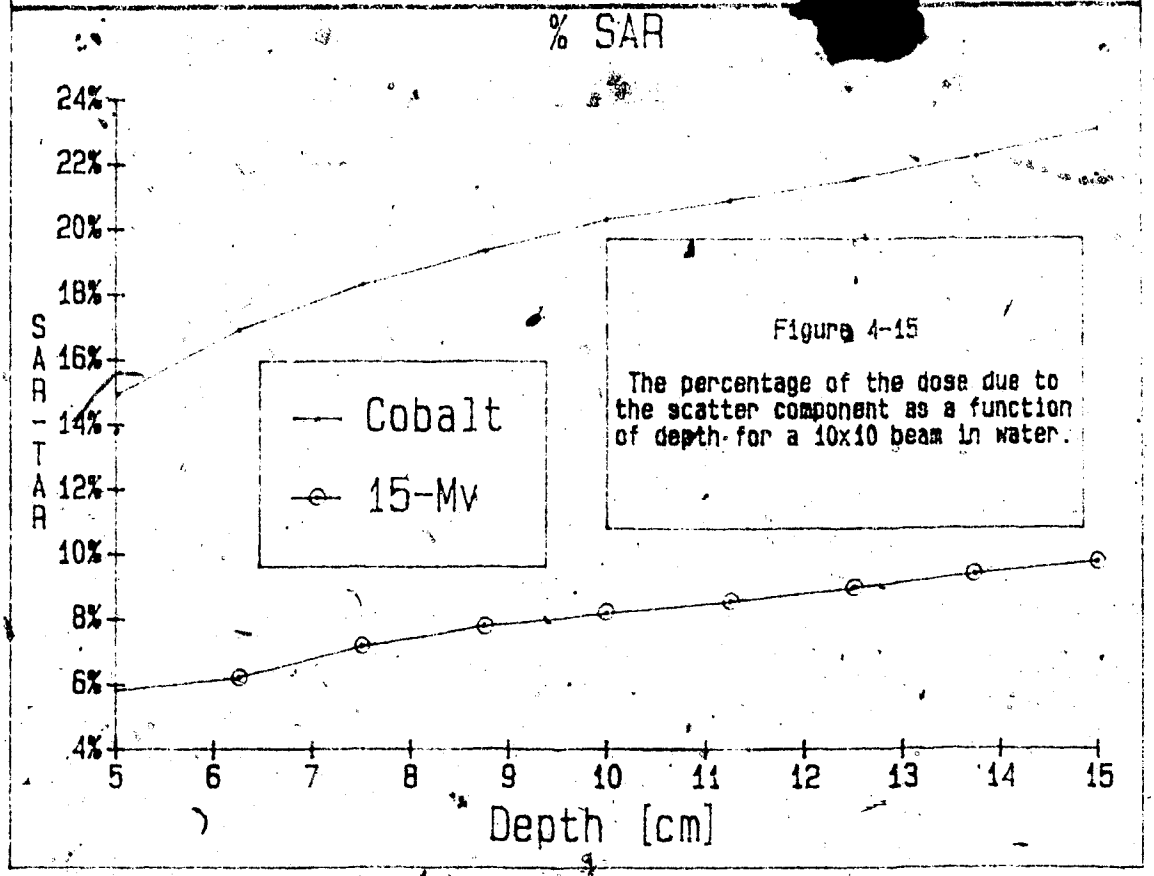

Figure 4-15

The percentage of the dose due to the scatter component as a function of depth for a 10x10 beam in water.

contribution of doubly scattered photons. He showed that the first scatter contribution is generally greater than the second scatter contribution, and that the second scatter appears more isotropic.

A simple calculation was performed in which equation 3-7 was modified. The multiple scatter components of the weights were excluded from the calculation, and only the first scatter component was considered as follows:

$$W(i,j,k) = dSAR1(i,j,k) \qquad (4\text{-}1)$$

Figure 4-16 presents the results from these calculations for a homogeneous water tank. The Inhomogeneity Correction Factor using the first and multiple scatter components is consistently higher than that using the single scatter alone. This is an expected result since multiple scatter can only add to the total dose. Figure 4-17 shows the percent difference between the single and total scatter models. The average difference between the two different models was 0.10 %. This shows that the multiple scatter calculation in the Equivalent Tissue Air Ratio algorithm has minimal effect on the end dose results obtained, at least in this all water situation.

It has been shown that the primary and first scatter components of the radiation are the most important

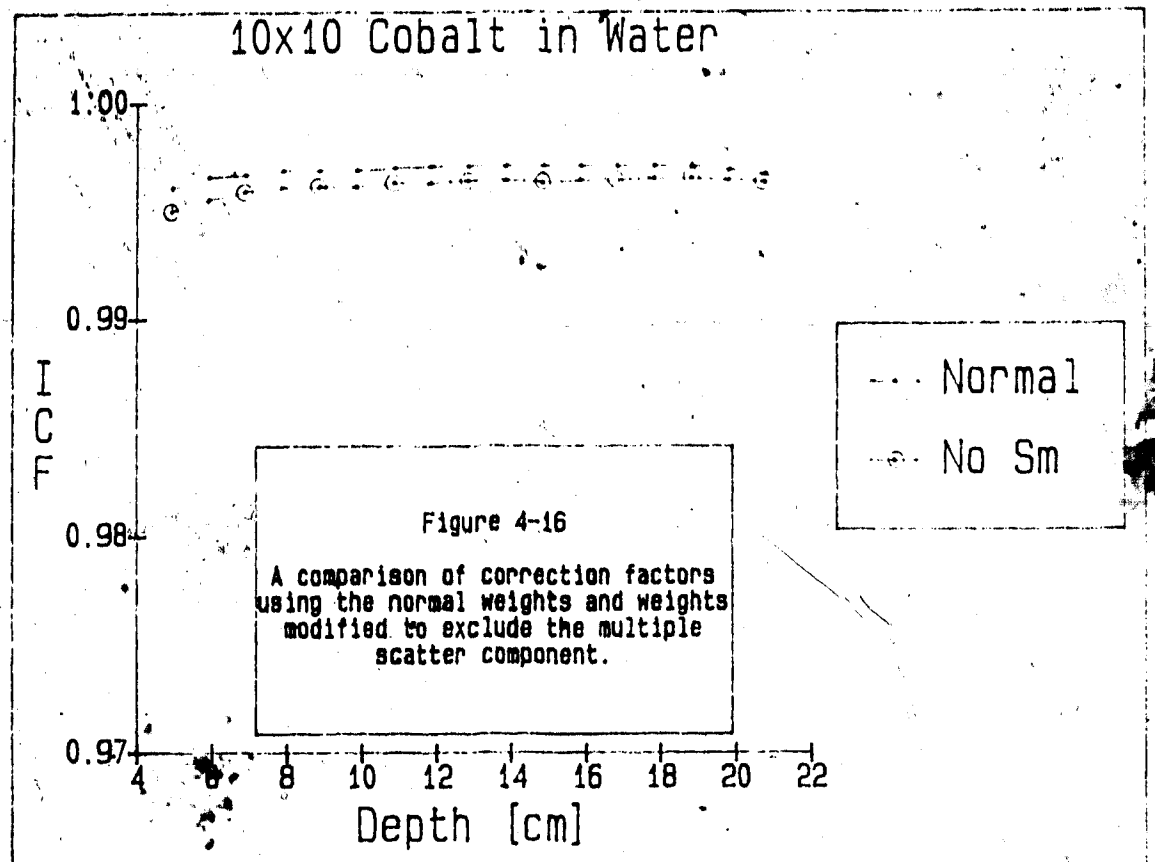

Figure 4-16

A comparison of correction factors using the normal weights and weights modified to exclude the multiple scatter component.

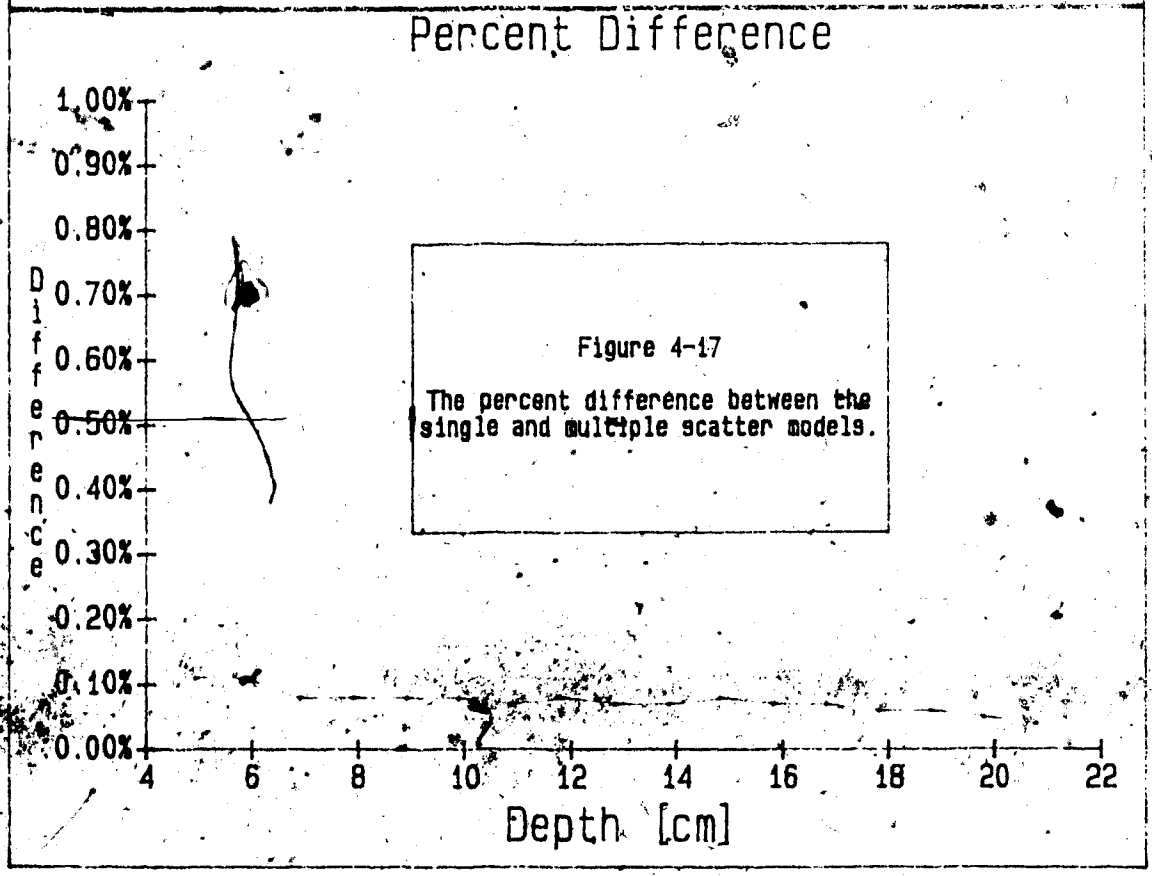

Figure 4-17

The percent difference between the single and multiple scatter models.

contributions to the dose. Thus the assumption that primary and single scatter are dominant (Assumption 2) is a valid one.

4.3.3 Assumption 3: Electronic Equilibrium

In Section 1.6 the concept of electronic equilibrium was introduced. Assuming that electronic equilibrium is present allows the problem of dose calculation to be reduced to a problem of photon transport. The Equivalent TAR method assumes that electronic equilibrium is always present. Under most circumstances this is a valid assumption.

There are circumstances in which this assumption breaks down, and the calculated correction factors differ greatly from those that are actually observed [9] [10]. The case of high energy and small beam size is one such case. In Figure 4-4 lateral electronic disequilibrium is seen to occur for a 5x5 field using 15-MV x-rays. In this case, differences of more than 10 % are observed. For a 5x5 6-MV field (Figure 4-3) electronic disequilibrium is suspected to occur but it is not as pronounced as in the 15-MV case.

If electronic disequilibrium is thought to be present, then extreme care must be taken when using any form of inhomogeneity correction algorithm. Suspect regions include beam boundaries, tissue interfaces, and regions occluded with beam blocks.

4.3.4 Assumption 4: Primary Depth Scatter

The Equivalent TAR method assumes that the same scaled depth can be used in both the primary and scatter components of the Tissue Air Ratio (Equation 3-4). This assumes that the scatter changes mainly with depth as does the zero area Tissue Air Ratio. This is difficult to check, but could be done through Monte-Carlo calculations in which the scatter components, at different depths, could be scored separately from the primary. It was felt that this was beyond the scope of this project.

4.3.5 Assumption 5: Attenuation in the Weights

In calculating the scatter weights W(i,j) it was assumed that the material above the scattering volume was water (Assumption 5 and Figure 3-3). Thus only the geometric depth of the scattering volume was used. It would have been more appropriate to use the radiological depth (along paths a and b) because this would have taken into account the attenuation changes caused by the inhomogeneities along the scatter pathways. This assumption was relatively easy to test since one of the computer subroutines developed during this work calculates both the geometric and the radiological depths.

The geometric depths (a) to the scattering volume were replaced with their corresponding radiological depths. Then both versions of the algorithm were used to calculate the doses within an inhomogeneous phantom (a CT slice of a patient). A comparison of the two different dose distributions was then made using an isodose difference map. There were dose differences of less than 1 %. The use of geometrical depths is fundamentally incorrect but the impact appears to be minimal for practical situations.

Most biological tissues have a density near that of water, thus the radiological depth will be close to the

geometric depth of these scattering volumes. It has been previously shown than scatter typically contributes about 20 % to the total dose, at Cobalt energy (less at higher energies). Thus a 20 % difference in the depths used, should produce less than a 4 % difference in the total dose contribution from that scattering volume, taking exponential attenuation into account. Furthermore, the total scatter contribution is the sum of contributions from all of the volumes that are irradiated. It is likely that some volumes may have radiological depths that are greater than their geometric depths while others may be less. There is a resultant balancing that could decrease the difference value down to the 1 % that was observed.

Primary attenuation in the scatter weights appears to have a minimal effect on performance. A similar argument would hold for secondary attenuation along path b (Figure 3-3). Thus, using the geometric depths appears to be adequate, and offers the opportunity for enhancing the speed of the computation.

4.3.6 Assumption 6: Isotropic Multiple Scatter

The Equivalent TAR method assumes that multiple scattering is isotropic within the medium. It is very difficult to test the validity of this assumption since it is difficult to separate the different components of the scatter experimentally. One approach is to use Monte-Carlo calculations in which each photon is followed through a cascade of individual multiple interactions (Section 1.8.10). Figure 4-18 shows the dose spread function [22] for Cobalt-60 due to multiple scattering alone. The primary interaction point (I) is at the center of the curves . The dose deposition due to a million photons (having a first interaction at I) was then recorded after it had been multiply scattered (≤ 3). The figure shows that the multiple scatter is only slightly forward directed. Moreover, the multiple scatter component is relatively small so that for most practical purposes the assumption of isotropy is defensible.

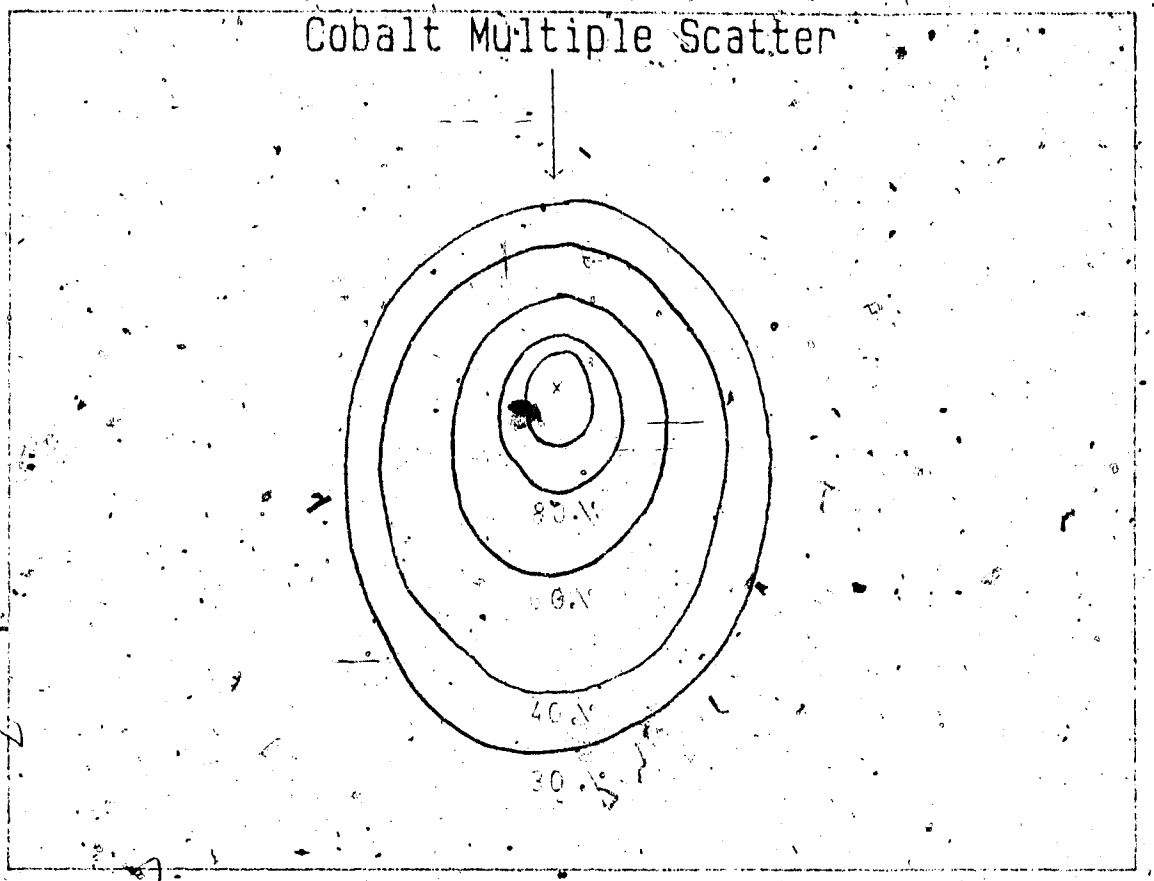

Figure 4-18

Isodose curves for the multiple scatter contribution to the total dose at the energy of Cobalt.

4.3.7 Assumption 7: Weighting Function Separability

To make the Equivalent TAR method practical, the three dimensional weights W(i,j,k) are separated into two independent components (Equation 3-14). This assumption is very difficult to validate and was not done in this work. This would require a true three dimensional weighting function. To do this a three dimensional ray tracing program would have to be used in order to calculate the primary and secondary attenuations along the paths travelled by the scattered photons. Once this weight for a specific volume is obtained, it could be compared to the product of the slice weight W(k) and pixel weight W(i,j).

4.3.8 Assumption 8: Arbitrary Reference Depth

In calculating the individual slice weights W(k), an arbitrary reference depth was used for the SAR values. As mentioned previously, the W(k) weights can be considered as the relative importance of the k'th slice to the total scattered dose, for a point located at this reference depth. This weight is determined as a difference of SAR's, assuming that all the intervening slices scatter as though they were composed entirely of water. Figure 4-19 shows these SAR values as a function of lateral distance (LD) from the calculation plane. The SAR value for a lateral distance of 2.5 cm. is the SAR for a beam that irradiates all material up to 2.5 cm. away from the calculation plane (This is a 10x5 cm^2 beam since it irradiates 2.5 cm. on each side of the central axis). This graph can then be used in determining the weight of a slice. The weight is essentially the derivative of the SAR curve at the point of interest (Equation 3-17).

Figure 4-20 shows a curve of unnormalized slice weights as a function of lateral distance away from the calculation plane. This curve is derived by using SAR values for a specific reference depth (10 cm.). Similar curves are obtained by using other reference depths. Figure 4-21 shows a three dimensional plot of slice weight as a function of both lateral distance and reference depth.

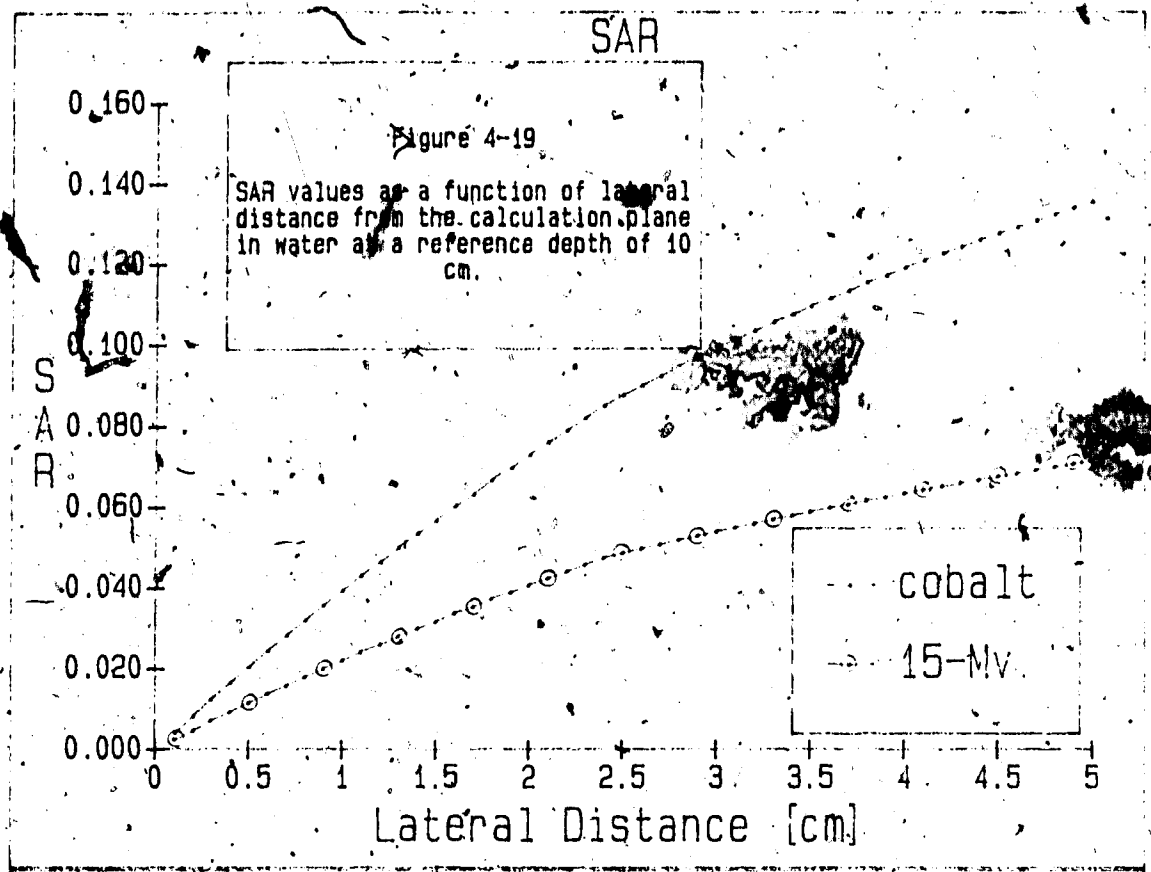

Figure 4-19

SAR values as a function of lateral distance from the calculation plane in water at a reference depth of 10 cm.

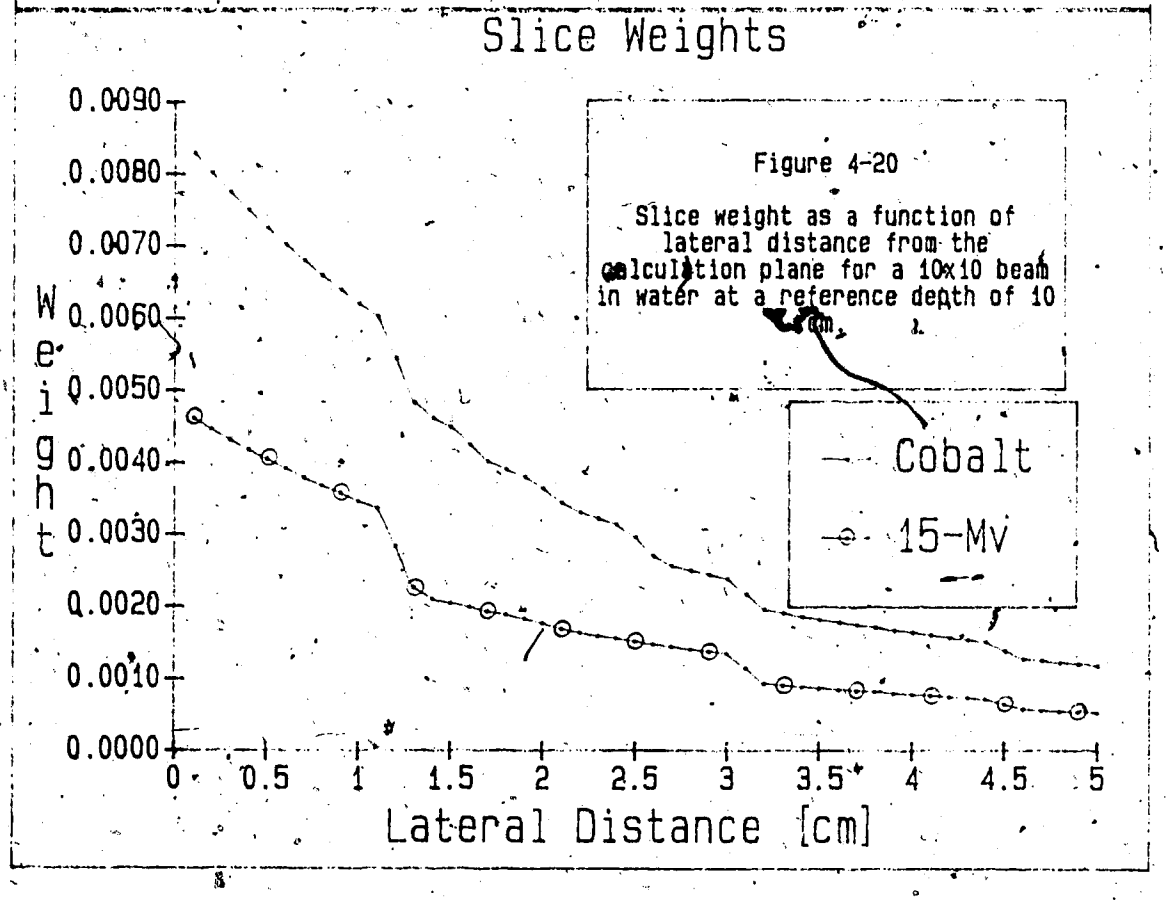

Figure 4-20

Slice weight as a function of lateral distance from the calculation plane for a 10x10 beam in water at a reference depth of 10 cm.

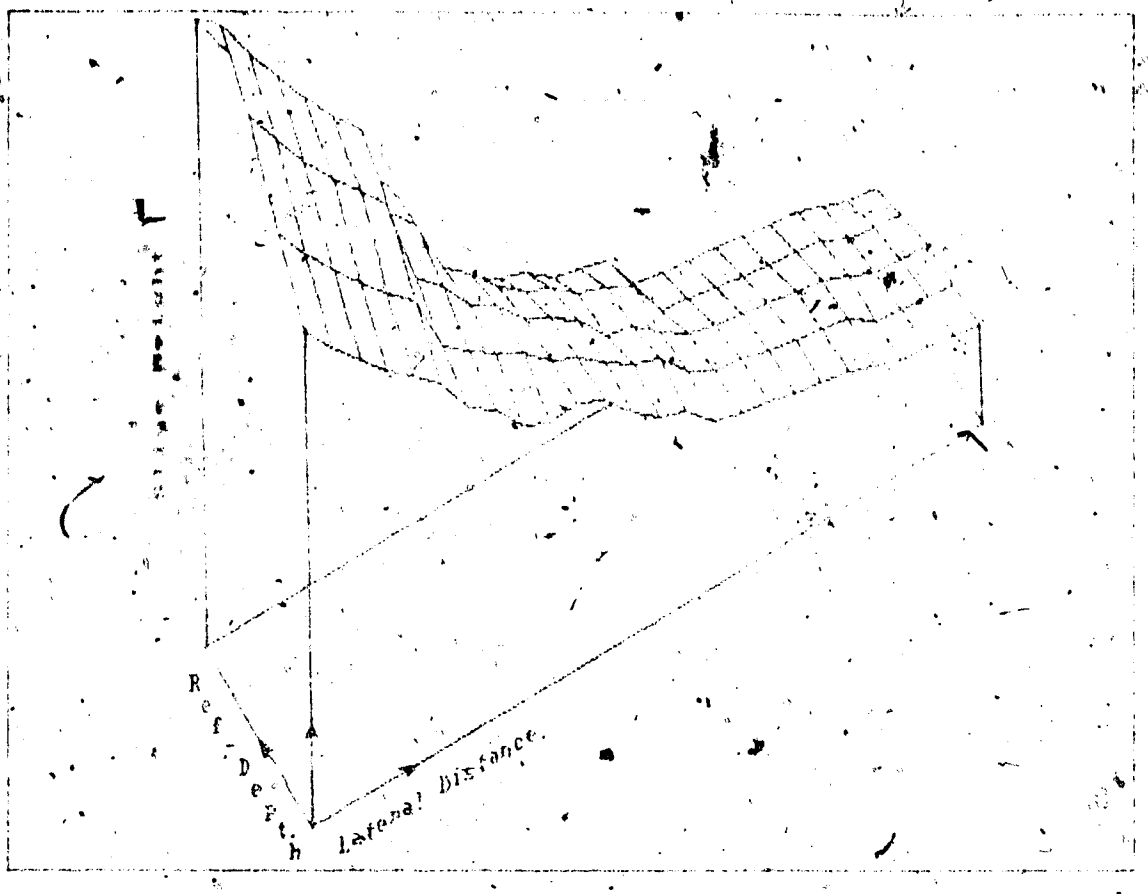

Figure 4-21

Effect of reference depth on the weights.

The "noise" in the weights graphs is due mainly to calculation and experimental inaccuracies. The original SAR values used in the weights, are linearly interpolated for intermediate values. When the derivatives of these values are numerically calculated, inaccuracy occurs because of the resulting small values, compared to the scatter from individual slices. More accurate measurements of SAR values are required, as well as improved data interpolation.

The slice weights W(K) are used in determining the position of the effective scattering slice (z-effective). Recall that this value is the most probable lateral position from which scatter originates. Thus changes in the weights will also produce changes in the z-effective values. Figures 4-22, 4-23, and 4-24, show the effect of reference depth and field sizes on the z-effective values at different energies. From the figures it is observed that the reference depth has little effect on the z-effective values for small field sizes. As the field size increases the z-effective value increases almost linearly with the reference depth used.

Another small effect is that as the energy increases the z-effective value decreases for all field sizes. As the energy increases, the scatter becomes more forward directed with less lateral dispersion. Hence the most probable position for the scatter to originate is closer to the

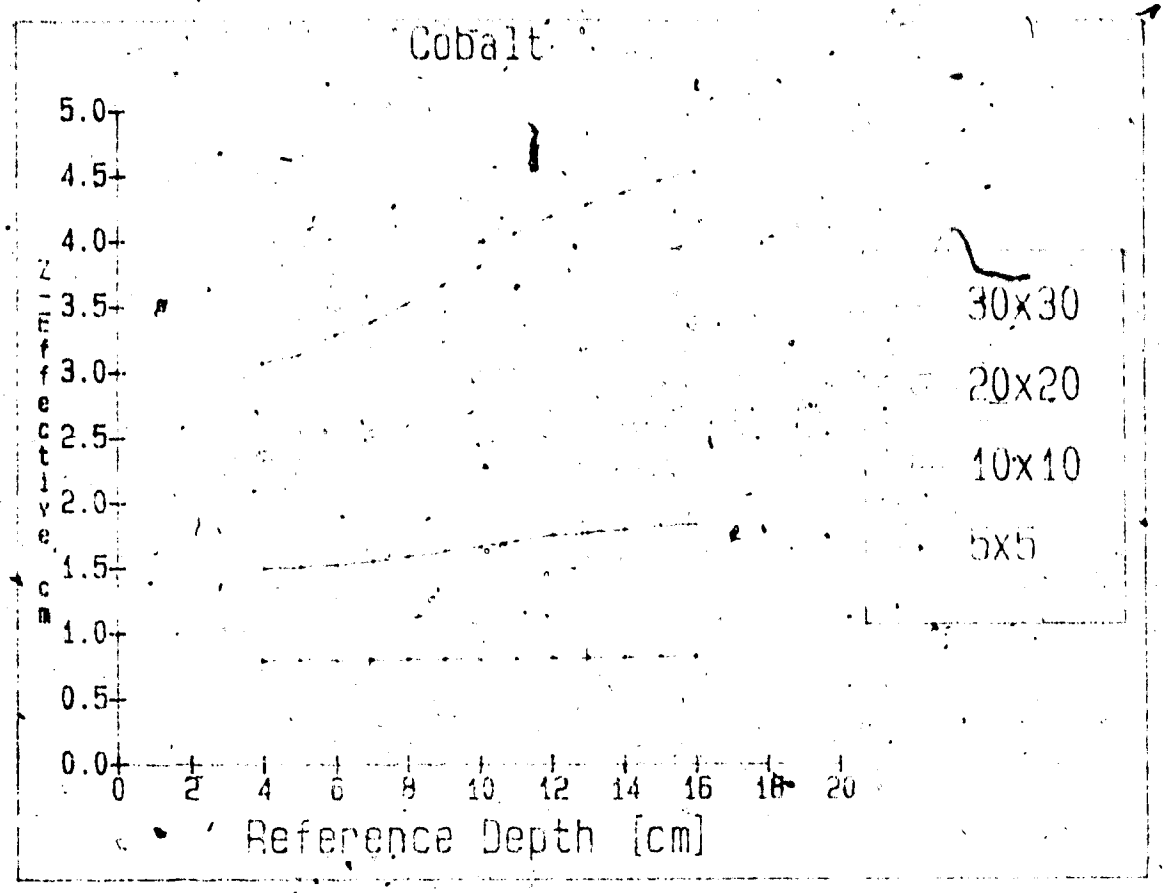

Figure 4-22.

The z-effective value as a function of reference depth for a number of different beam sizes at the energy of Cobalt.

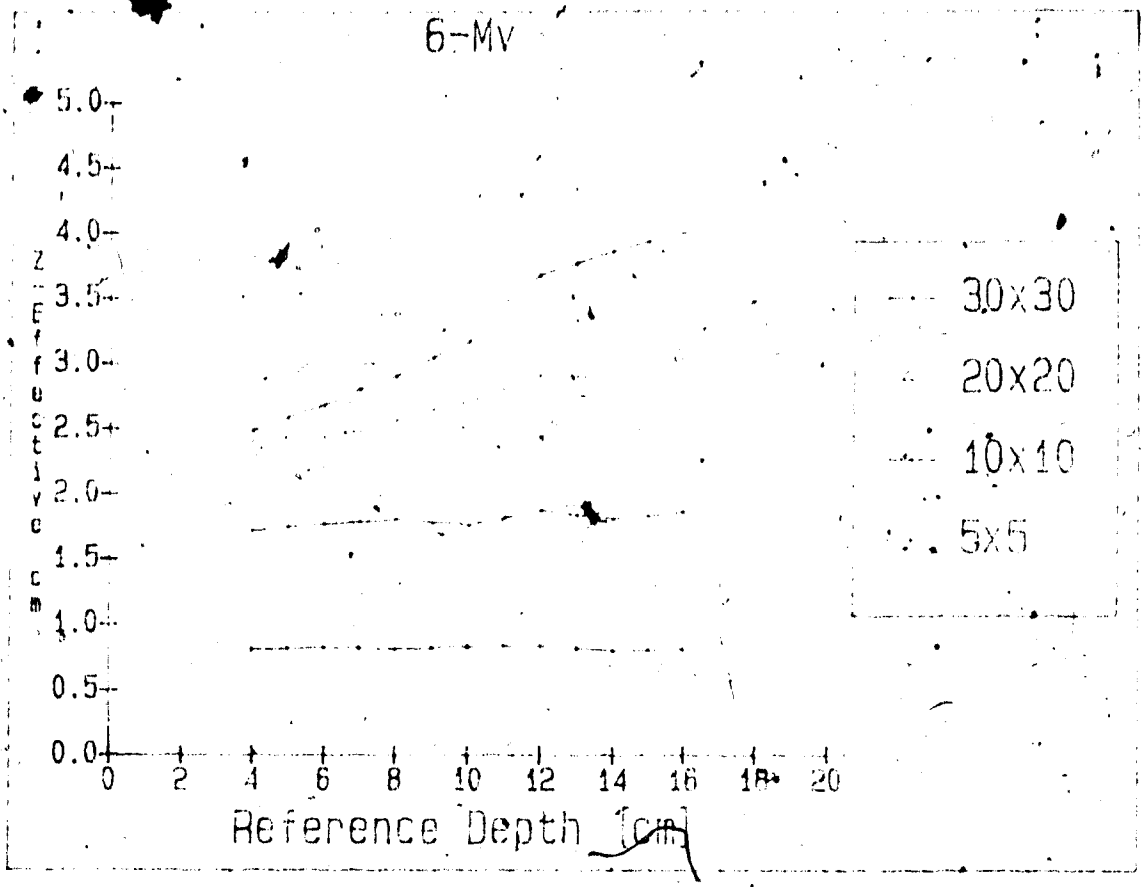

Figure 4-23

The Δ-effective value as a function of reference depth for a number of different beam sizes at an energy of 6-Mv.

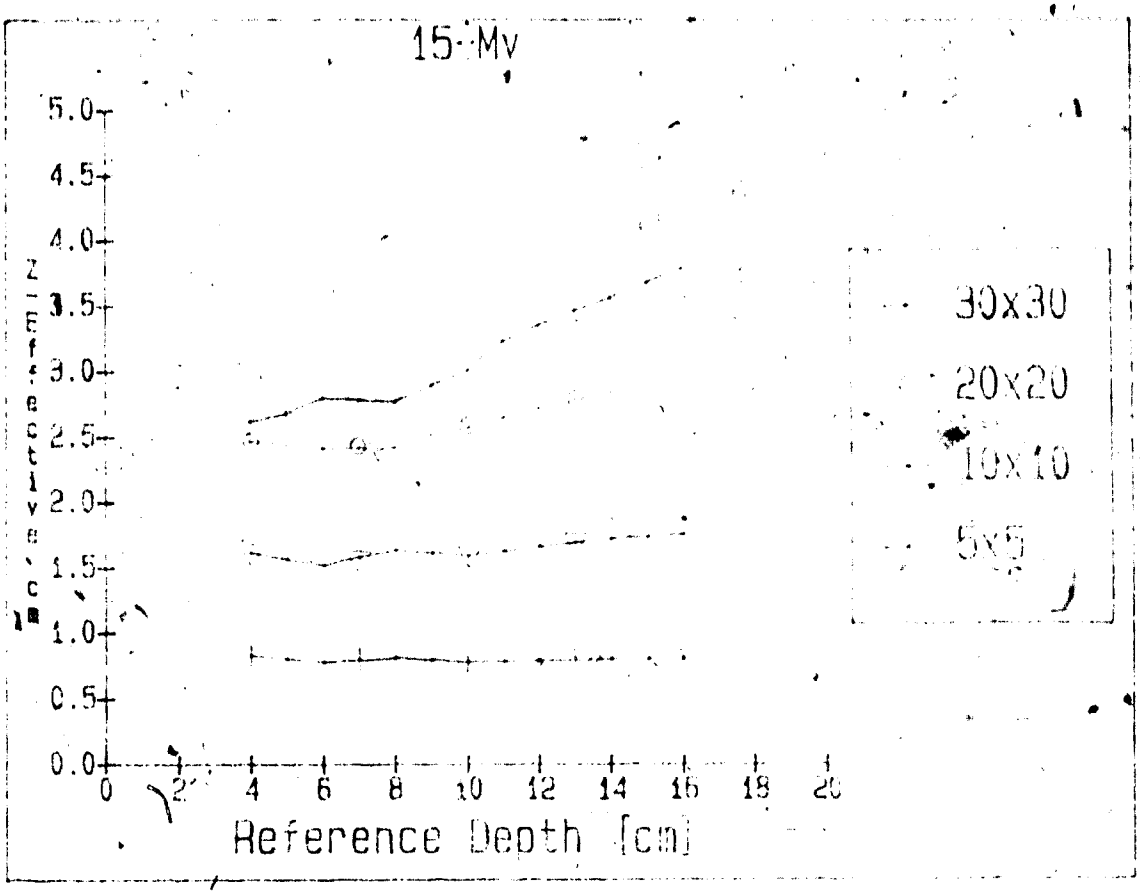

Figure 4-24

The z-effective value as a function of reference depth for a number of different beam sizes at an energy of 15-Mv.

calculation plane; This is also evident in the weights profiles of Figure 4-20.

The slice weights W(k) are used in the coalescing procedure. Thus any variation in the weights due to the reference depth will be observed in the electron densities of volumes within the effective scattering slice. To investigate this problem a three dimensional phantom was composed of five slices, spaced 1 cm. apart (Figure 4-25). Each slice was homogeneous in the x-y plane but the electron densities of the slices were varied for each phantom. The coalescing procedure was performed using different reference depths.

Effective Slice Densities

Reference Depth	5 cm	10 cm	15 cm
Phantom 1	0.85	0.83	0.80
Phantom 2	0.93	0.92	0.90
Phantom 3	1.00	1.00	1.00
Phantom 4	1.07	1.08	1.10
Phantom 5	1.15	1.17	1.20

If all the slices are identical in density (i.e. Phantom 3), then the coalesced density will be independent of the weights function (The density will come out of the summation in Equation 3-16a). However when the density of

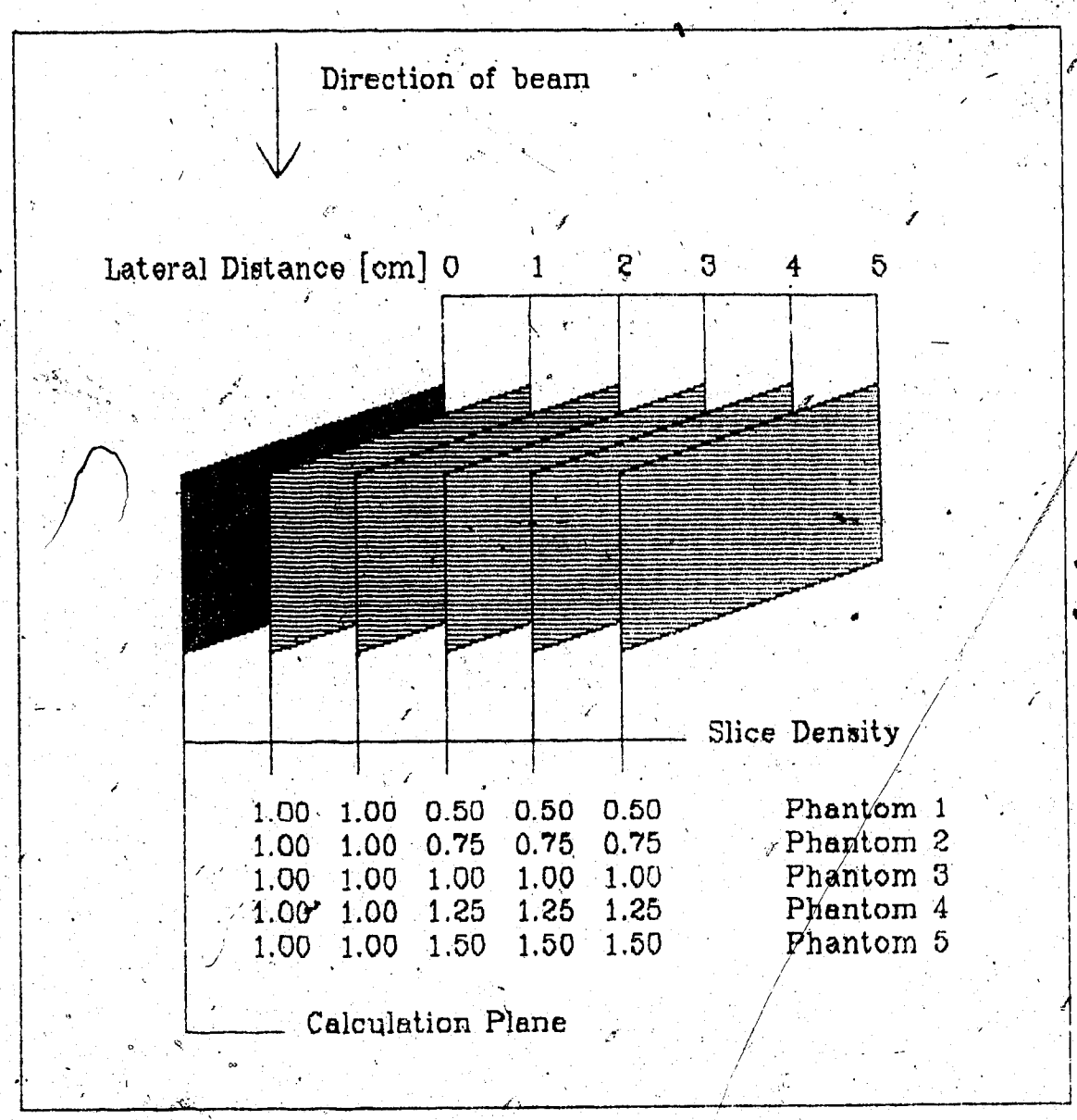

Figure 4-25

The three dimensional phantom used to test the effect of reference depth on slice coalescing.

the slices changes, the coalesced density is a weighted average of the densities and the weighting function is more important.

As the reference depth was increased the relative weight of the more distant slices also increased (ie. they become more important in determining the average). This can be understood qualitatively by considering a shallow point in the phantom. It receives scatter from nearby scattering volumes, along a path which defines a scattering angle. If the point is then moved deeper within the phantom, then the lateral distance of the scattering volume must be increased to maintain the same scattering angle or "weight". Thus the distant slices are being sensed and their importance is increased.

The density of the scattering slice is observed to vary only slightly with reference depth. The reference depth is usually chosen so that the slice weights used will be an average of all possible depths of interest within that slice. The original Equivalent TAR algorithm assumes a reference depth of 10 cm., which would be about the midpoint of a patient under most circumstances.

4.3.9 Assumption 9: Scatter Grid Size

Choosing a scatter grid size has a major influence on the dose calculation time required. To test the influence of this selection, data was generated for two different phantoms. The phantoms used were the slab and double lung phantoms that were previously described (Sections 4.2.1 and 4.2.2).

It is theoretically possible to have the effective scattering slice with the same resolution as the original image (256x256). However doing so would result in calculation times of more than 1000 minutes per beam on a VAX-11/780 processor. In order to reduce these times for practical use (minutes instead of hours), the size of the scatter grid is reduced. The physical area covered by the grid is still the same, but the voxel size is greater.

Timing measurements were made of the calculation algorithm for different scatter grid sizes (Figure 4-26). It takes approximately 15 seconds to multiply the Inhomogeneity Correction Factors by the dose in water to yield the dose distribution in the heterogeneous medium, regardless of the scatter grid size. Once this offset time is subtracted from the total time, the resulting net time shows a quadratic relation to scatter grid size (i.e. a

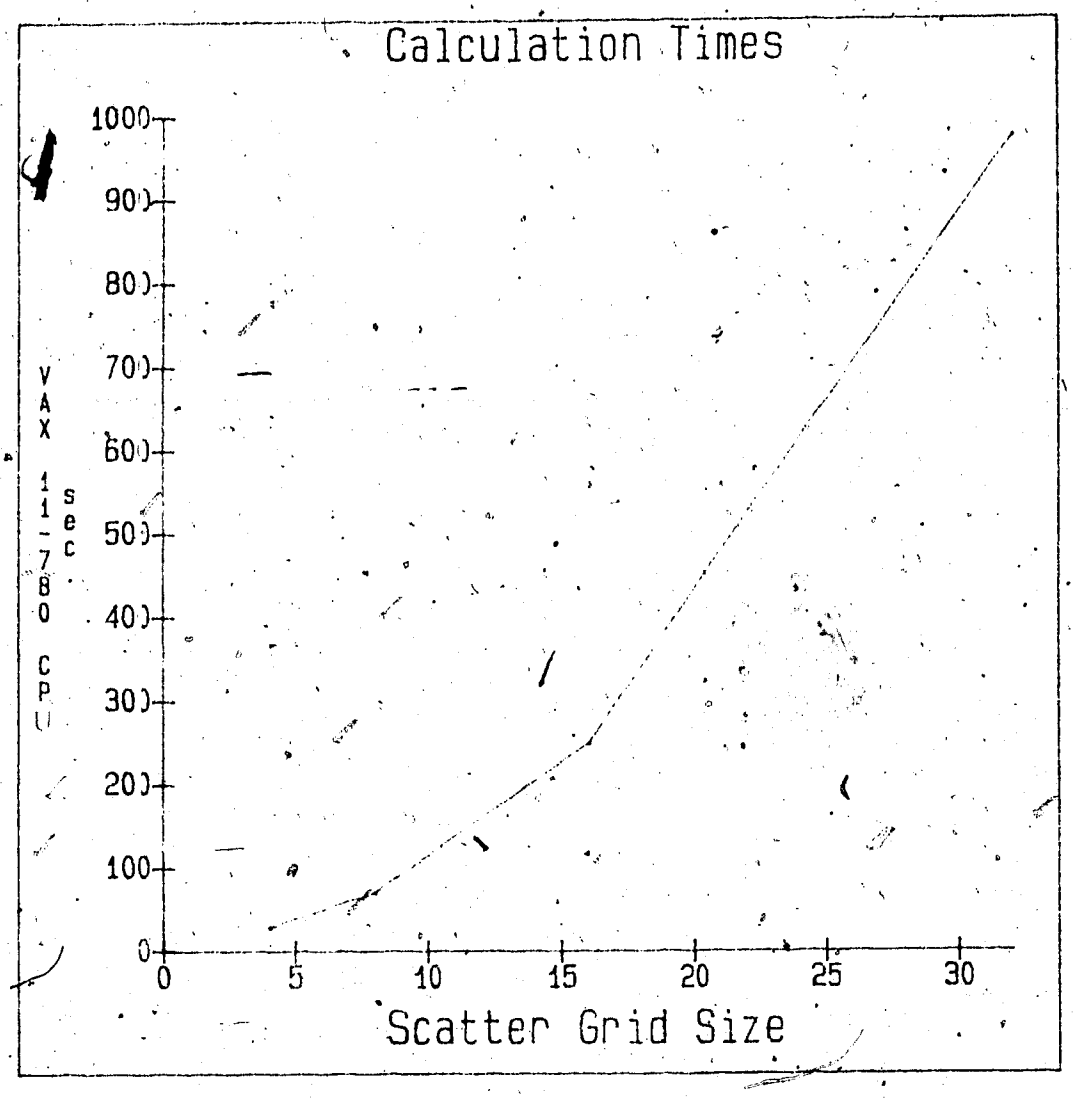

Figure 4-26

Calculation time as a function of grid size. The grid size given is the number of pixels along each axis (ie. a grid size of 16 means 16x16).

linear relation to the number of pixels). If the scatter grid size is doubled the calculation time is quadrupled.

Scatter Grid Size	Net Time
4x4	1/4 minute
8x8	1 minute
16x16	4 minutes
32x32	16 minutes

By minimizing the time (ie. using a smaller scatter grid) the error introduced in the ICF increases. Thus a compromise must be achieved in which both calculation time and error are balanced. To investigate this, the slab phantom (Figure 4-1) was used with the (a.) parameter set to 4 cm. The Inhomogeneity Correction Factor was then observed as a function of central axis depth and scatter grid size as shown in Figure 4-27. The most accurate results use a scatter grid size of 32 , judging from the agreement with measured data. The 4x4 grid showed a maximum difference of 12 % while the 8x8 grid gave differences of 4 %. The 16x16 grid showed only a 1 % maximum difference. It is difficult to see the effects of these differences in Figure 4-27, so an isodose difference map was produced comparing the different calculated doses in two dimensions (Figure 4-28).

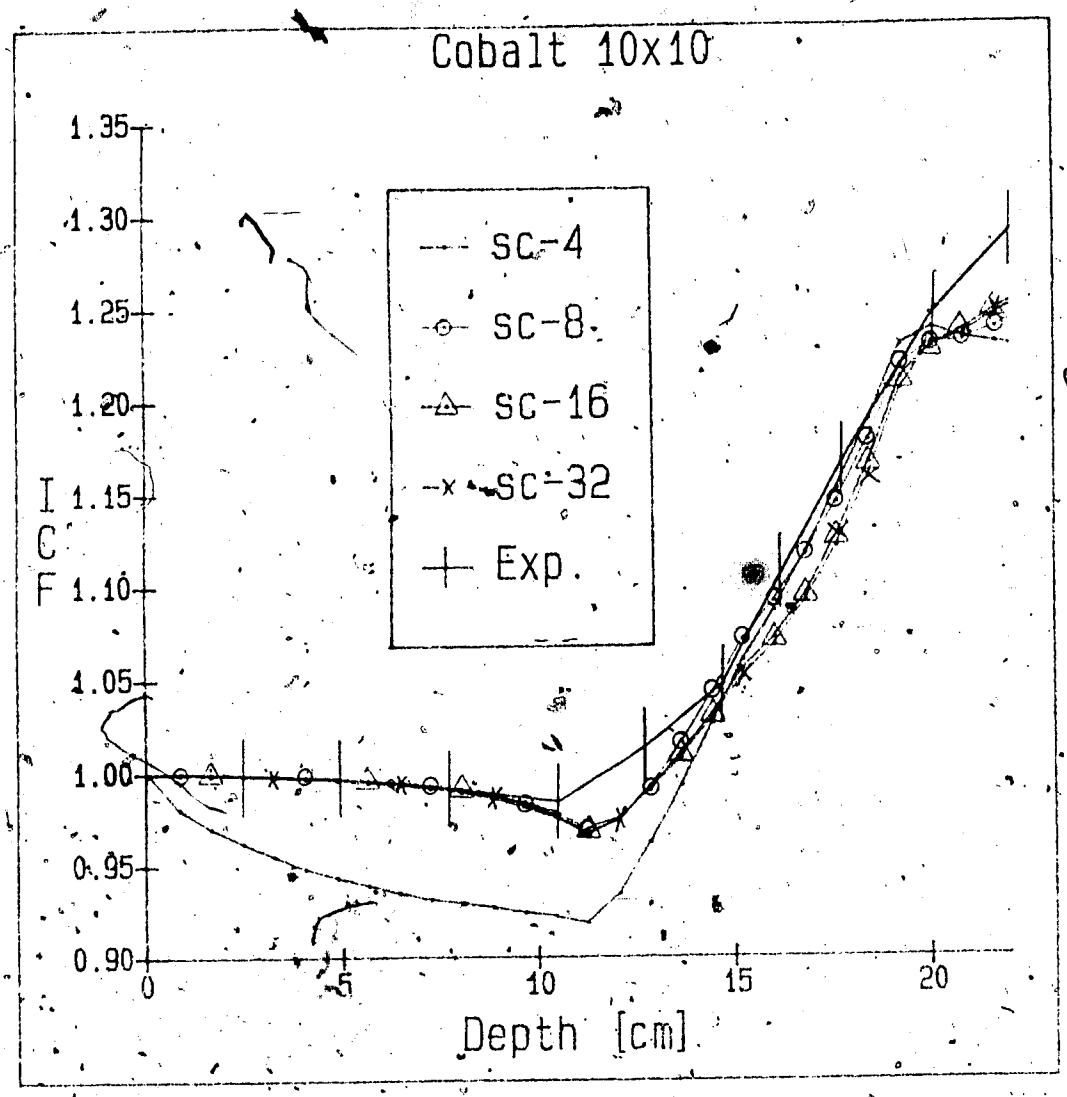

Figure 4-27

The Inhomogeneity Correction Factor as a function of central axis depth within the slab phantom for a 10x10 Cobalt beam. Different scatter grid sizes were used to calculate the ICF factors.

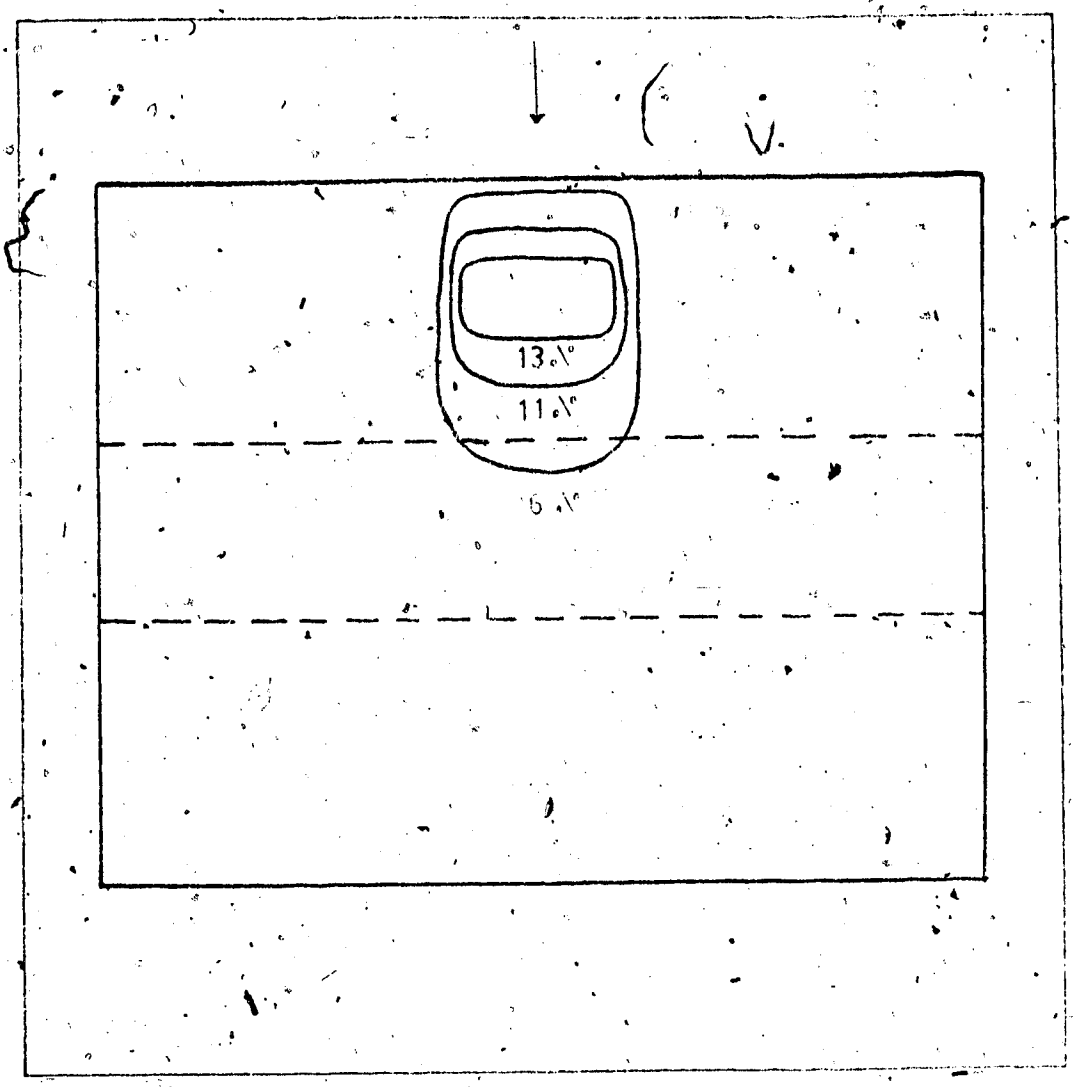

Figure 4-28

Isodose values for the differences between the 4x4 and 32x32 scatter grids in the slab phantom for a 10x10 Cobalt beam.

The maximum differences occurred above the inhomogeneity with relatively good agreement within and below it. Deep within the phantom most of the scatter comes from above because forward scattering is more dominant than lateral scattering. At shallower depths there is very little overlying material, but there is still a similar amount of scattering material laterally. Hence the relative importance of the lateral scatter is greater for shallower depths. As the grid size decreases the volume of each voxel increases and the scattering centers are further apart. If the center of a scattering voxel does not lie within the beam area, then the scatter from that voxel is discarded, even though a partial voxel may be within the beam, resulting in a loss of scatter. This is more important at the beam boundaries near the top of the phantom because portions of the major source of lateral scatter are lost. As the grid size is increased the spatial resolution at the beam boundaries increases and less of the scatter is lost, thereby increasing the dose.

As the energy is increased all of the above effects are similar but decreased in magnitude. As the energy is increased the scatter contribution to the total dose becomes less (Figure 4-13). Thus at higher energies, greater error in the weights, effective z, scattering slice, and grid size is tolerable in calculating the scatter correction. For 15-

MV x-rays a grid size of 8x8 appears to be adequate for most circumstances.

The second phantom used to investigate the scatter grid size was the double lung phantom. Again the ICF was examined as a function of central axis depth. The results can be seen in Figures 4-29, 4-30, 4-31, and 4-32. Because the central axis of this phantom was unit density, any variations in the Inhomogeneity Correction Factor are due solely to the scatter contribution. It is observed that the curves converge as the scatter grid size increases. The maximum difference of 3 % was observed to occur between the 4x4 and 32x32 size grids for a 10x10 Cobalt beam. These differences are again attributed to the loss of resolution in the scattering slice which "blurrs" the sharp borders of the adjacent lung. With greater spatial resolution, the lower density of the lung is sensed more accurately. This explains the deeper "wells" of the ICF profiles for dilute scatter matrices.

Figure 4-29 compares experimental values [19] of ICF's with those calculated using different scatter grid sizes for a 20x20 Cobalt beam. At the center of the well, a scatter grid size of 8x8 more accurately predicts the values. However near the surface and below the well, the 32x32 grid more closely predicts the observed values. The 16x16 grid size appears to be an acceptable compromise.

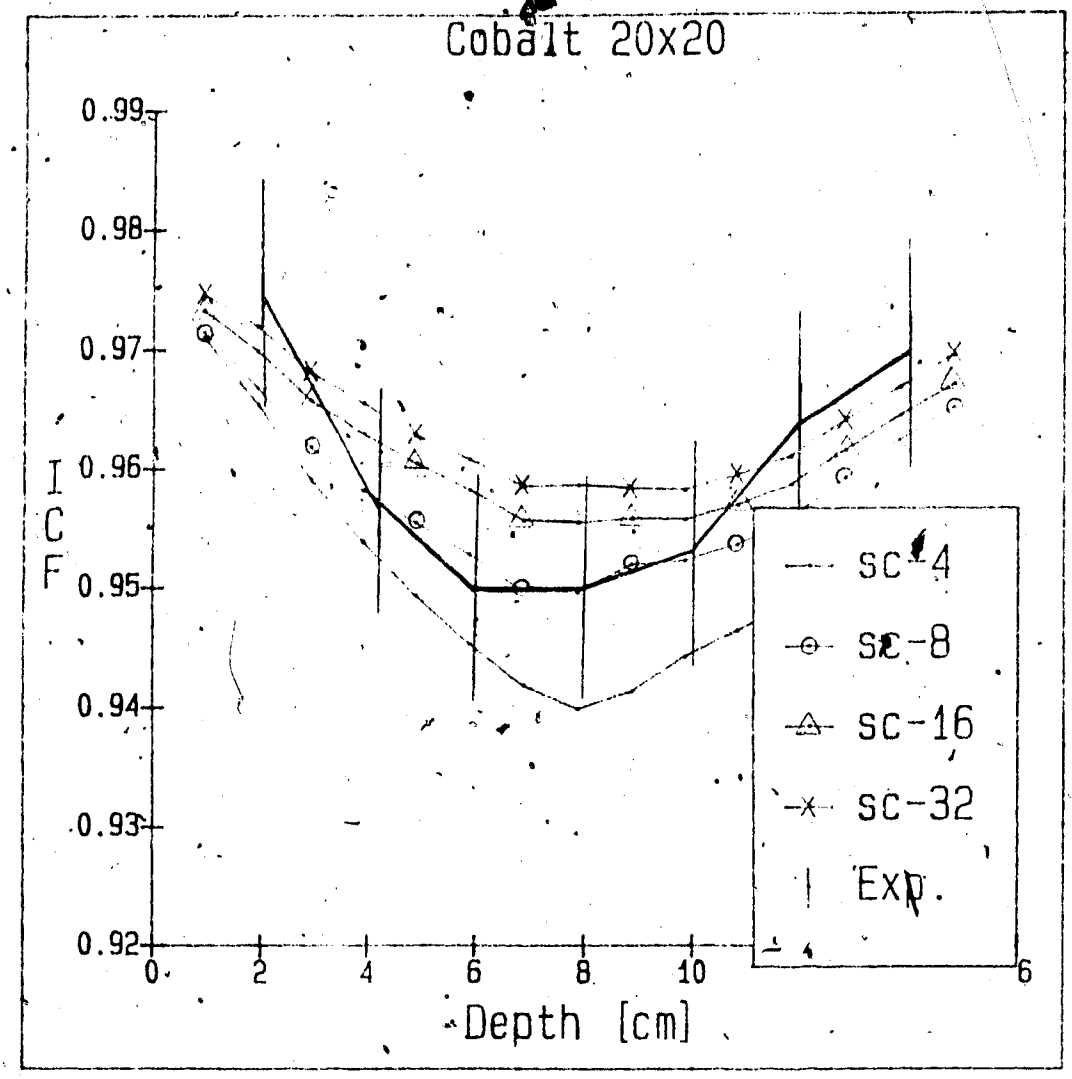

Figure 4-29

The Inhomogeneity Correction Factor as a function of central axis depth within the double lung phantom for a 20x20 Cobalt beam and a number of different scatter grid sizes.

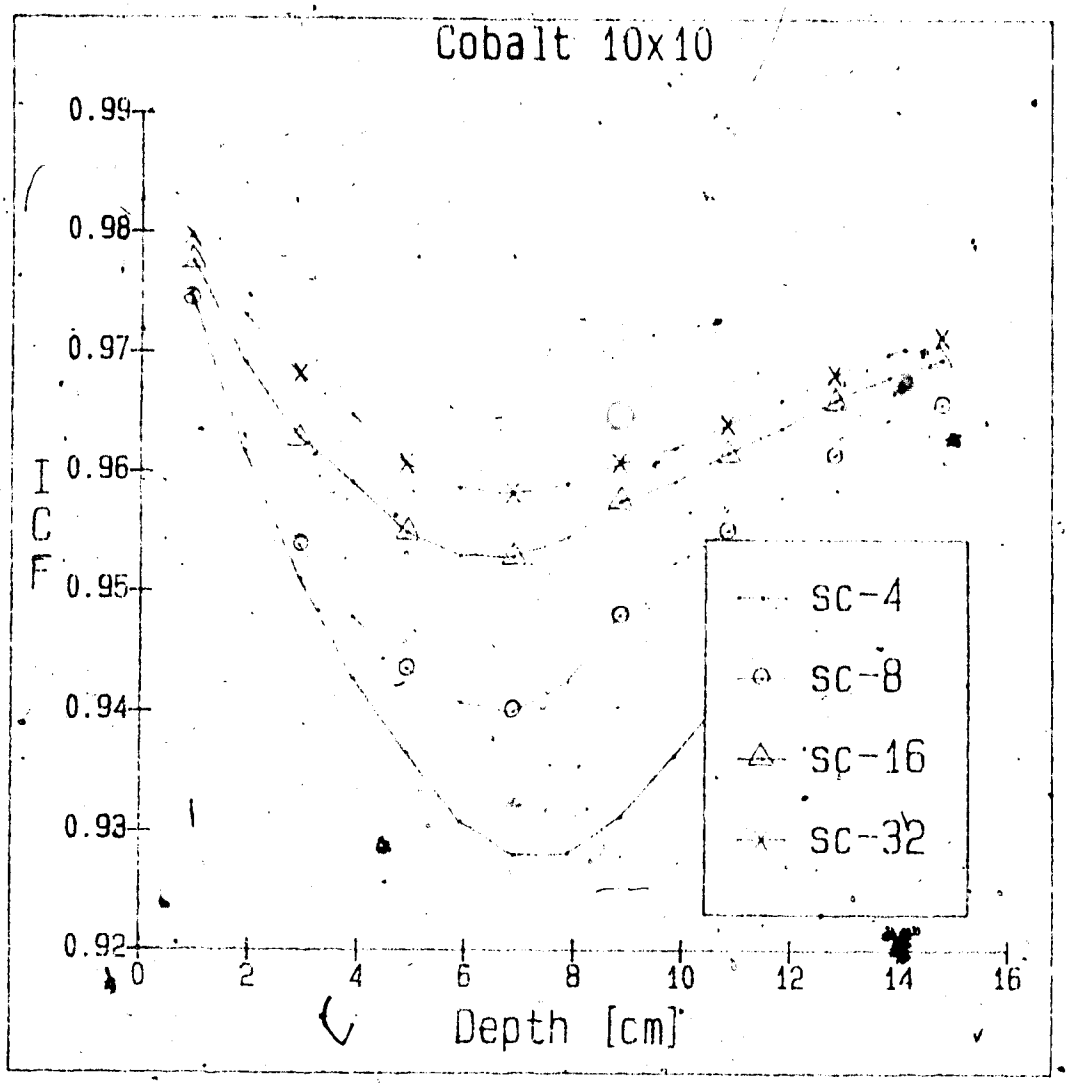

Figure 4-30

The Inhomogeneity Correction Factor as a function of central axis depth within the double lung phantom for a 10x10 Cobalt beam and a number of different scatter grid sizes.

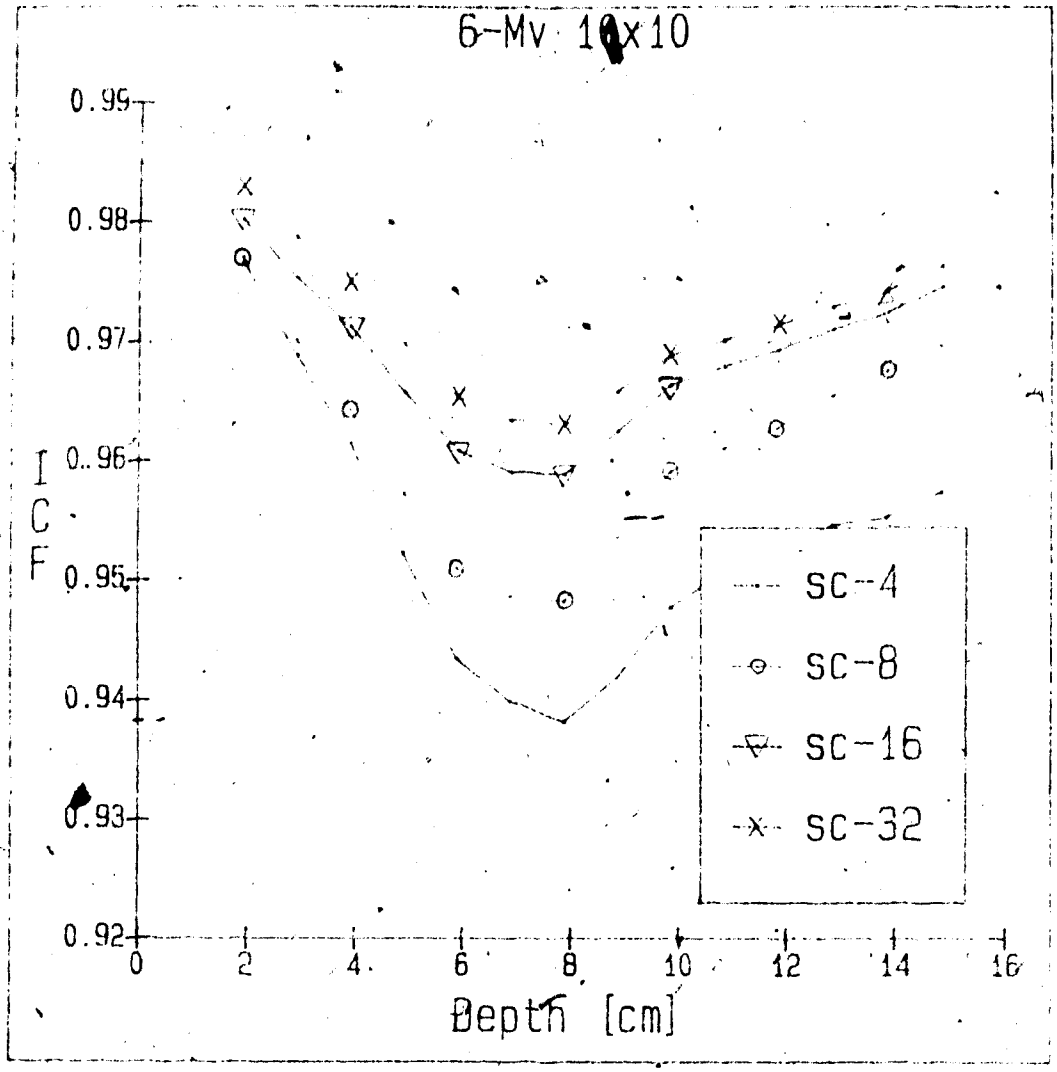

Figure 4-31

The Inhomogeneity Correction Factor as a function of central axis depth within the double lung phantom for a 10x10 6-Mv beam and a number of different scatter grid sizes.

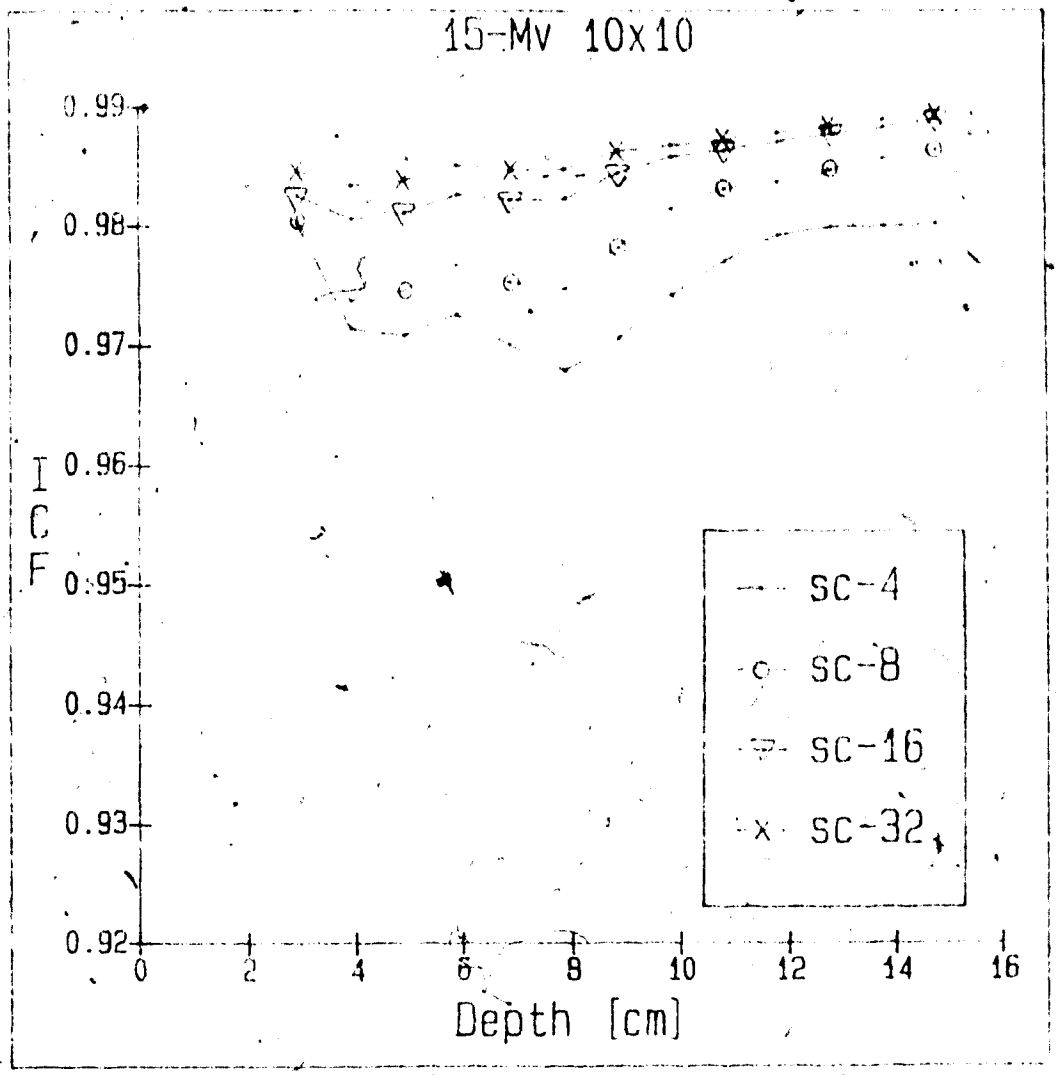

Figure 4-32

The Inhomogeneity Correction Factor as a function of central axis depth within the double lung phantom for a 10x10 15-Mv beam and a number of different scatter grid sizes.

It was also observed that as the energy increases the differences decrease. Again this is due to the decreased relative importance of the scatter at the higher energies.

From these results a number of recommendations can be made. For the phantoms tested a practically acceptable scatter grid size is 16x16. This gives calculation times of about four minutes on a VAX 11/780 processor and acceptable accuracy for Cobalt-60 radiation. Increasing the scatter grid size by a factor of two would quadruple the calculation time to an unacceptable level and only yield a one percent gain in the dose accuracy. As the energy increases (eg. 15-MV) the scatter grid size may be decreased (to 8x8), due to the decrease in sensitivity to scatter. The calculation time then approaches one minute per beam, which is very competitive with simpler but less accurate algorithms (e.g. Simple Ratio of TAR's).

4.4 Sensitivity of the Weights Function

It has been shown that, in general, scatter will contribute less than 20 % of the total dose to a typical point in the patient. The Equivalent TAR method accounts for this small scatter component through the calculation of scatter weights which requires the majority of the calculation time. If a less complicated weighting scheme could be used, there would be a considerable savings in computation time. To investigate this, some artificially set weights were used, and thus produced surprising results in simple phantoms.

Three versions of the Equivalent TAR method were used on the slab phantom for a 10x10 Cobalt beam (Figure 4-33). The normal version in which weights were calculated via Equation 3-7 was used as a reference for comparison. In the second version, the weights W(i,j,k) were set equal to 1.0, and in the third version, weighting factors were randomly chosen between 0.0 and 1.0 were used. The results from the random weights were surprisingly close (within 4 %) to the results using the correct weights. However, the shape of the curves more closely resembled those computed by the Ratio of TAR's method. This is because the Ratio of TAR's can be considered as the Equivalent TAR method with the weights set equal and a unit density scattering slice. The curve for random weights falls very close to that for the 1.0 weights.

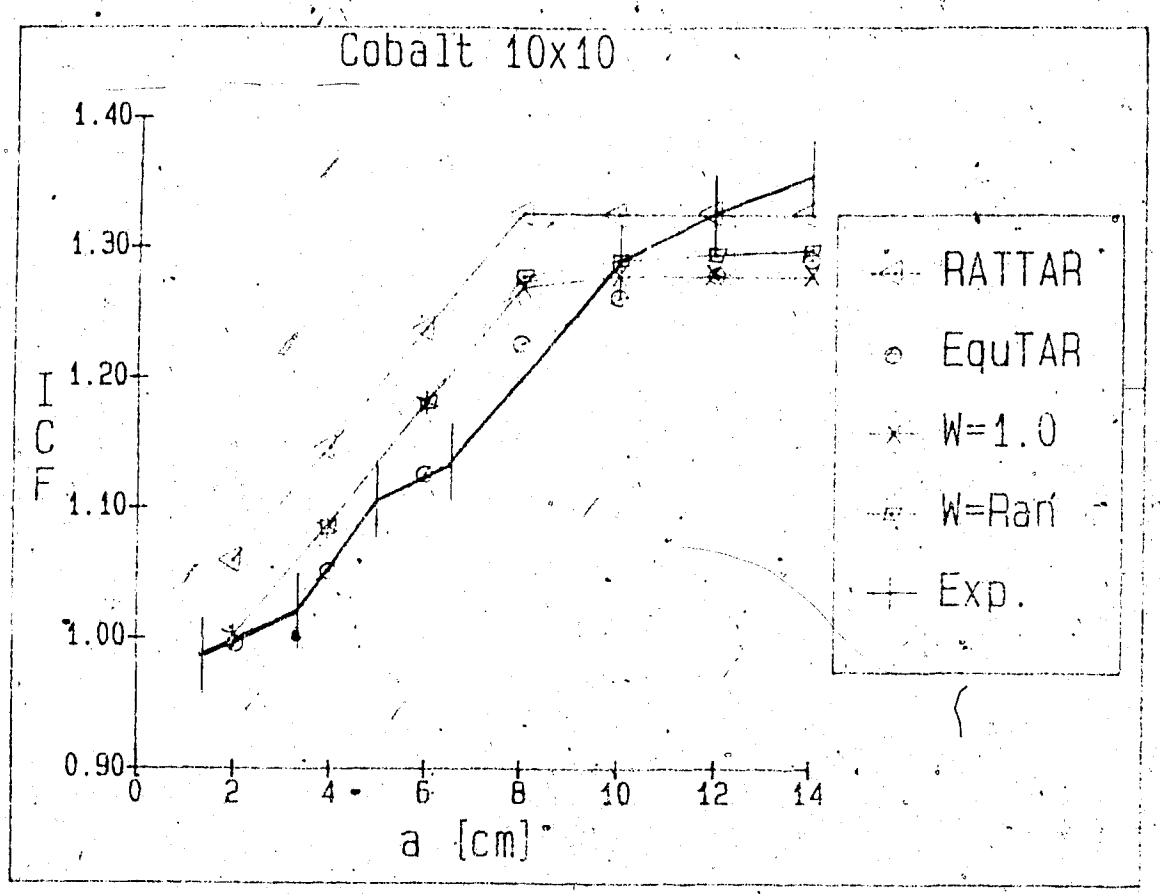

Figure 4-33

The effects of different weighting functions on the Inhomogeneity Correction Factors for the slab phantom.

Even though the individual weights were random, their combined average approaches a uniform distribution . These approaches, including the simple Ratio of TAR's, fail to consider the changes in lateral scatter caused by the cork slab.

These results would suggest that the weights are relatively unimportant, at least for a simple phantom. This is expected since the effective scattering slice is expected to be the same as the calculation slice (Equation 3-16a). For a more complicated phantom (the double lung phantom), Figure 4-34 shows the effects of different weighting schemes for a 20x20 Cobalt beam. From this figure, it is obvious that the artificial weights do not give acceptable results, when compared to the experimentally observed [19] values.

With the weights set equal to 1.0 a decreasing ICF curve was obtained. Again the random weight curve lies between the Ratio of TAR's and the curve for unit weights. With uniform weights, the method assigns equal importance to all scatter volumes within the medium. Points below the calculation point will be weighted more than they should while points above will be weighted less than they should . Because all points are weighted the same, the weighted average density (Equation 3-6) becomes that of an "average phantom". Thus the phantom appears to be uniform with a density equal to the spatial average. This produces the

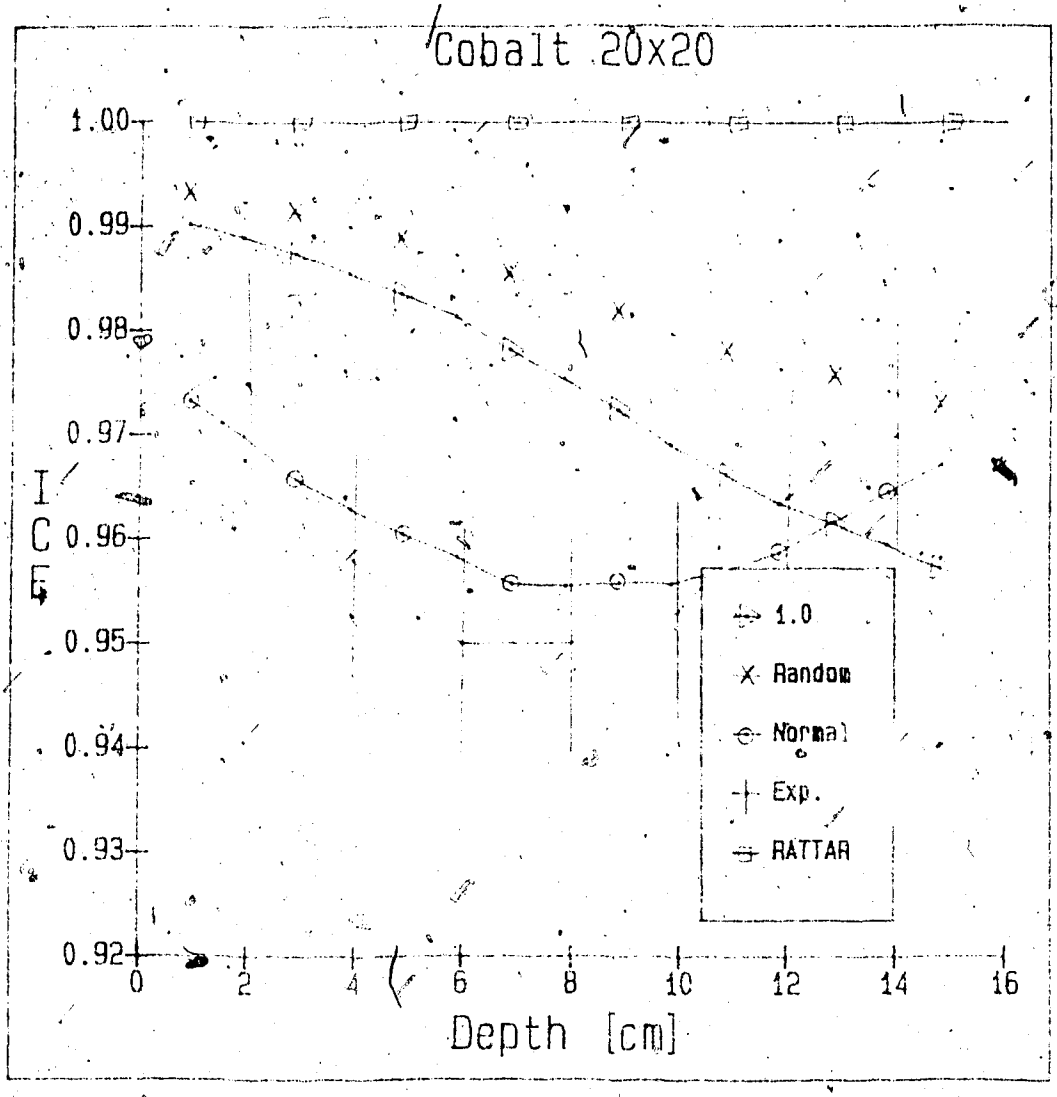

Figure 4-34

The Inhomogeneity Correction Factor as a function of central axis depth within the double lung phantom for a 20x20 Cobalt beam with artificially set weights.

monotonically decreasing graph observed, as observed in depth dose curves in a uniform medium.

The higher beam energy (15-MV) produces similar results, but the effects are not as pronounced, as expected. This is again due to the decreased relative importance of the scatter.

The weights may be complicated and difficult to calculate, but they do produce results that are more accurate, especially for complex heterogeneous phantoms.

5. Conclusions

At first sight the Equivalent Tissue Air Ratio method appears to be a very good inhomogeneity correction algorithm. It correctly predicts the Inhomogeneity Correction Factors, as confirmed by comparisons with measured data.

Secondary investigation of the method proves to be disheartening. There are many implicit assumptions made throughout the method, some of which are not physically valid. The assumption of an all water medium appears throughout the method, even though we are solving a problem in an inhomogeneous medium. For simple phantoms the weights appear to have minimal effects, and for such cases it would be more efficient to arbitrarily set the weights. When more complicated phantoms (e.g. patients) are examined, the set weights produce results that are not acceptable. A more complicated calculated weighting procedure must be used.

Thus, upon more in-depth analysis, the assumptions turn out to be acceptable in practice. The water assumption is obviously invalid, but it must be remembered that most tissues within the patient have water densities and a form of averaging takes place naturally . Some tissue densities are less than that of water while others are greater, and some of the effects tend to cancel each other out. Of

course, the user must be careful not to use the method in situations that would contradict some of the major assumptions. The energy must be kept within a suitable range in order to assure that the Compton process dominates. Care must also be taken if the inhomogeneities differ dramatically from that of water (e.g. hip prosthesis).

5.1 Future Work

For many of the assumptions investigated, much more work could have been done examining their effects and implications, particularly with more measurements or Monte-Carlo simulations. Future work could eliminate some of the computational simplifications. With the speed of modern computers the question of coalescing must be re-examined. A true three dimensional algorithm would eliminate some of the "2-D" assumptions in the present coalescing procedure.

Electronic equilibrium must also be examined since there is a tendency to use higher energy x-rays. Linear accelerators are gradually replacing Cobalt-60 units, and the temptation to use this new technology is evident. Finally, experimental validation of dose computation algorithms for contemplated clinical application remains paramount.

6. References

[1] H.F. Batho,
Lung corrections in Cobalt-60 beam therapy,
Journal of the Canadian Association of Radiologists,
15:79-83, 1964.

[2] J.J. Battista, W.D. Rider, J. Van Dyk,
Computed tomography for radiotherapy planning,
International Journal of Radiation Oncology, Biology,
and Physics, 6:99-107, 1980

[3] M. Cohen, D.E.A. Jones, D. Greene, eds.,
Central axis depth dose data for use in radiotherapy,
British Journal of Radiology, Supplement 11, 1972.

[4] J.R. Cunningham, ed.,
Determination of absorbed dose in a patient irradiated
by beams of x and gamma rays in radiotherapy
procedures, International Commission on Radiation Units
and Measurements Report 24, Washigton D.C., 1976.

[5] R.A. Geise, E.C. McCullough,
The use of CT scanners in megavoltage photon beam
therapy, Radiology, 124:133-141, 1977.

[6] H.E. Johns, J.R. Cunningham,
The Physics of Radiology, 4th edition,
Charles C. Thomas, Springfield Ill., 1983.

[7] H.E. Johns, G.F. Whitmore, T.A. Watson, F.H. Umberg,
A system of dosimetry for rotation therapy with typical rotation distributions,
Journal of the Canadian Association of Radiologists, 4:1, 1953.

[8] T.R. Mackie,
PhD thesis, University of Alberta,

[9] T.R. Mackie, E. El-Khatib, J. Battista, J. Scrimger,
Lung dose corrections for 6- and 15-MV x-rays,
Medical Physics, 12(3):327-332, 1985.

[10] T.R. Mackie, J. Scrimger, J. Battista,
A convolution method for calculating dose for 15-MV x-rays, Medical Physics, 12(2):188-196, 1985.

[11] J.E. O'Connor,
The variation of scattered x-rays with density in an irradiated body, Physics in Medicine and Biology, 1:352-369, 1957.

[12] N.J.Schroeder,
A system for the calculation of dose produced by external photon beams,
MSc thesis, University of Saskatchewan, May 1983.

[13] M.R. Sontag,
Photon beam dose calculations in regions of tissue heterogeneity using computed tomography,
PhD thesis, University of Toronto, April 1979.

[14] M.R. Sontag, J.Battista, M.J.Bronskill, J.R.Cunningham,
Implications of computed tomography for inhomogeneity corrections in photon beam dose calculations,
Radiology, 124:143-149, 1977.

[15] M.R. Sontag, J.R.Cunningham,
Corrections to absorbed dose calculations for tissue inhomogeneities, Medical Physics, 4(5):431-436, 1977.

[16] M.R. Sontag, J.R.Cunningham,
The Equivalent Tissue Air Ratio Method for making absorbed dose calculations in heterogeneous medium,
Radiology, 129:787-794, 1978.

[17] T.D. Sterling, H. Perry, L. Katz,
Automation of radiation treatment planning,
British Journal of Radiology, 37:544, 1964.

[18] M. Tatcher, S. Palti,
Evaluation of Density Correction Algorithms for Photon Beam Dose Calculations,
Radiology, 141(1):201, 1981.

[19] J.W. Wong, R.M. Henkelman,
A new approach to CT pixel-based photon dose calculations in heterogeneous media.
Medical Physics, 10(2):199-208, 1983.

[20] J.W. Wong, R.M. Henkelman, A. Fenster, H.E. Johns,
Second scatter contribution to dose in a Co-60 beam,
Medical Physics, 8(6):775-782, 1981.

[21] J.W.Wong,R.M.Henkelman,J.W.Andrew,J.Van Dyk,H.E.Johns,
Effect of small inhomogeneities on dose in a
Cobalt-60 beam,
Medical Physics, 8(6):783-791, 1981.

[22] C. Field,
Private communication.

[23] F. Buschke, R.G. Parker,
Radiation Therapy in Cancer Management,
Grune and Stratton, New York, 1972.

[24] S.W. Young,
Nuclear Magnetic Resonance Imaging, Basic Principles,
Raven Press, New York, 1984.